UNIVERSITY OF BIRMINGHAM

DRIVER-ORIENTED INTELLIGENT CONTROL METHODOLOGY FOR SERIES-PARALLEL HYBRID ELECTRIC VEHICLES

BY

JI LI

A THESIS SUBMITTED TO

THE UNIVERSITY OF BIRMINGHAM FOR THE DEGREE OF

DOCTOR OF PHILOSOPHY

DEPARTMENT OF MECHANICAL ENGINEERING

SCHOOL OF ENGINEERING

UNIVERSITY OF BIRMINGHAM

AUGUST 2020

ABSTRACT

Rapid development in informatics enables optimization of hybrid electric vehicle (HEV) systems with a fusion of external dynamics, e.g. driver and traffic. This thesis studies the driver-oriented energy management problem of a series-parallel HEV for promoting a paradigm shift to more sustainable mobility. The objective of this research is to characterize human driving behaviour and maximize personalized energy economy for real-world driving. Driver-oriented intelligent control methodology is proposed to tailor a family of control strategies for minimizing energy consumption of HEVs. The research uses emerging 'mediums' computational intelligence and Internet of the Things to create an accessible human-machine interaction system for energy management personalization. The research work is carried out in four parts with distinctive contributions.

Firstly, a novel approach that uses personalized non-stationary inference is proposed to increase the robustness of the rule-based vehicle control system through real-time driving behaviour monitoring for vehicle energy economy improvement. On the basis of the personalized non-stationary inference, the author aims to transfer driving style classification methods from continuous indexing towards discrete classes and expand the human-related factors from velocity and acceleration only towards velocity, gas pedal, brake pedal, and steering wheel angle. Secondly, the concept of the driver-identified supervisory control system is introduced, which forms a novel architecture of adaptive energy management for HEVs. As a man-machine system, the proposed system can accurately identify the human driver from natural operating signals and provides driver-identified globally optimal control policies as opposed to mere control actions. To better acclimate to stochastic driving condition,

the author considers elevating HEV energy management into an online level. Thirdly, a novel back-to-back competitive learning mechanism is proposed for a fuzzy logic supervisory control system for HEVs. This mechanism allows continuous competition between two fuzzy logic controllers during real-world driving. Not only the optimizer, but also the predictor is considered to promote for synchronous online update. Fourthly, an online predictive control strategy for series-parallel plug-in HEVs is investigated, resulting in a novel online optimization methodology named the dual-loop online intelligent programming that is proposed for velocity prediction and energy-flow control.

All work is demonstrated via customized experimental plans which are designed based on a hardware-in-the-loop testing bench and a driving simulator platform. This allows a deeper insight into each control strategy in the driver-oriented intelligent control methodology, exposing strengths and drawbacks that have not been noticeable from past work.

ACKNOWLEDGMENTS

First and foremost, I would like to thank my supervisor Professor Hongming Xu, who has offered timely support and guidance whenever needed. He showed me what truth-seeking and perseverance are. He encouraged me to explore a wide range of research interests, which has been expanding in stimulating conversations, contributing greatly to my work efficiency and enjoyment of research.

It has also been a privilege to work with Professor Huw Williams, whose immense practical knowledge of automotive engineering has been invaluable to me. As a Fellow of the Royal Statistical Society, he is passionate and rigorous about mathematics that always invigorates me to move forward. There is no doubt that working and publishing with him made me a better researcher and made me appreciate my research more widely.

I would like to thank my colleague and also my friend Dr Quan Zhou who gave me inestimable support in the academic. As a good team player, he is always willing to share his insights on new things in the first place for me. Sometimes he is more like my tutor leading me to explore my own research route. It was also he who showed me the true meaning of friendship.

I need to thank my secondary supervisor Dr Raya Al-Dadah for supporting me in administrative work. Also, many great memories with Ziyang, Yunfan, Haoye, Carlo, Lewis, Aawishkar, Scott, Olalere, Yinglong, and Bin throughout the research days, always providing perspective.

Finally, I am genuinely grateful for my family and their unqualified love and encouragement. Distinct thanks to my wife Zhongcanzhu who intertwined my soul. She decorated our simple life in the alien land and brought us a little fairy Emma and follow-up fantastic adventures.

This thesis was partly proofread for the conventions of language, grammar, and spelling by Janet's Proofreading Service.

TABLE OF CONTENTS

LIST OF FIGURES

LIST OF TABLES

LIST OF PUBLICATIONS

Journal papers contributed to the thesis

[1] **Li, J.**, Zhou, Q., Li, Z., Zhang, Y., He, Y., Shuai, B., Williams, H., Xu, H., & Lu, G. Online Driver-oriented Energy Management of Connected Hybrid Electric Vehicles with Personalized Non-stationary Inference. Submitted to *IEEE Transactions on Systems, Man, and Cybernetics: Systems*.

[2] **Li, J.**, Zhou, Q., He, Y., Williams, H., & Xu, H. (2020). Driver-identified Supervisory Control System of Hybrid Electric Vehicles using Spectrum-guided Fuzzy Feature Extraction. *IEEE Transactions on Fuzzy Systems*. vol. 28, no. 11, pp. 2691-2701.

[3] **Li, J.**, Zhou, Q., Williams, H., & Xu, H. (2020). Back-to-back Competitive Learning Mechanism for Fuzzy Logic based Supervisory Control System of Hybrid Electric Vehicles. *IEEE Transactions on Industrial Electronics*. vol. 67, no. 10, pp. 8900-8909.

[4] **Li, J.**, Zhou, Q., He, Y., Shuai, B., Li, Z., Williams, H., & Xu, H. (2019). Dual-loop online intelligent programming for driver-oriented predict energy management of plug-in hybrid electric vehicles. *Applied Energy*, 253, 113617.

Other Journal papers

[5] **Li, J.**, Li, Z., Zhou, Q., Zhang, Y., & Xu, H. (2018). Improved scheme of membership function optimisation for fuzzy air-fuel ratio control of GDI engines. *IET Intelligent Transport Systems*, 13(1), 209-217.

[6] Zhou, Q., **Li, J.**, Shuai, B., Williams, H., He, Y., Li, Z., Xu, H. & Yan, F. (2019). Multi-step reinforcement learning for model-free predictive energy management of an electrified off-highway vehicle. *Applied Energy*, 255, 113755.

[7] Li, Z., **Li, J.**, Zhou, Q., Zhang, Y., & Xu, H. (2018). Intelligent air/fuel ratio control strategy with a PI-like fuzzy knowledge–based controller for gasoline direct injection engines. *Proceedings of the Institution of Mechanical Engineers, Part D: Journal of Automobile Engineering*, 0954407018779180.

[8] Shuai, B., Zhou, Q., **Li, J.**, He, Y., Li, Z., Williams, H., Xu, H., & Shuai, S. (2020). Heuristic Action Execution for Energy Efficient Charge-sustaining Control of Connected Hybrid Vehicles with Model-free Double Q-learning. *Applied Energy*.

[9] Li, Z., Zhou, Q., Zhang, Y., **Li, J.**, & Xu, H. (2019). Enhanced Intelligent PI-like fuzzy knowledge based controller using chaos-enhanced accelerated particle swarm optimization algorithm for transient calibration of air/fuel ratio control system. *Proceedings of the Institution of Mechanical Engineers, Part D: Journal of Automobile Engineering*.

[10] Zhang, Y., Zhou, Q., Li, Z., **Li, J.**, & Xu, H. (2018). Intelligent transient calibration of a dual-loop EGR diesel engine using chaos-enhanced accelerated particle swarm optimization algorithm. *Proceedings of the Institution of Mechanical Engineers, Part D: Journal of Automobile Engineering*, 0954407018776745.

[11] Zhou, Q., Zhang, Y., Li, Z., **Li, J.**, Xu, H., & Olatunbosun, O. (2018). Cyber-physical energy-saving control for hybrid aircraft-towing tractor based on online swarm intelligent programming. *IEEE Transactions on Industrial Informatics*, 14(9), 4149-4158.

[12] Zhou, Q., He, Y., Zhao, D., **Li, J.**, Li, Y., Williams, H., & Xu, H. (2020). Modified Particle Swarm Optimisation with Chaotic Attraction Strategy for Modular Design of Hybrid Powertrains. *IEEE transactions on Transportation Electrification*. Early Access.

[13] He, Y., Zhou, Q., Makridis, M, Mattas, K., **Li, J.**, Williams, H., & Xu, H. (2020). Multi-objective Optimization of V2V-based Cooperative Driving and Hybrid Energy Management. *IEEE transactions on Transportation Electrification*. 6(1), 346-355.

[14] He, Y., Wang, C., Zhou, Q., **Li, J.**, Makridis, M., Williams, H., Lu, G., & Xu., H. (2020). Multi-objective component sizing of a hybrid ethanol-electric vehicle propulsion system. *Applied Energy*.

[15] **Li, J.**, Zhou, Q., Williams, H., Xu, H., and Du, C. Control Optimization of Plug-in Hybrid Electric Vehicles via Cyber-physical Surrogate-assisted Strength Pareto Evolutionary Algorithm. Submitted to *IEEE Transactions on Industrial Informatics*.

[16] **Li, J.**, Gu, Y., Wang, C., Liu, M., Zhou, Q., Lu, G., Pham, D.T., & Xu, H. Pedestrian-aware Supervisory Control System Interactive Optimization of Hybrid Electric Vehicles via Fuzzy Adaptive Cost Map and Bees Algorithm. Submitted to *IEEE Transactions on Fuzzy Systems*.

Conference papers

[17] Zhou, Q., **Li, J.**, He, Y., Shuai, B., Williams, H., Xu, H., Li, Y., and Yan, F. (2020). K-fold Fuzzy Learning for Implementation of Dynamic Programming Results in Realtime Energy Management of the Plug-in Hybrid Vehicle. *Applied Energy Symposium*. Accept.

[18] He, Y., Ciuffo, B., Zhou, Q., Makridis, M., Mattas, K., **Li, J.**, Li, Z., Yan, F., & Xu, H. (2019). Adaptive cruise control strategies implemented on experimental vehicles: A review. *IFAC-PapersOnLine*, 52(5), 21-27.

Conference attendance

[1] Intelligent Vehicle Dynamics and Control, FISITA Online Conference. 05/2020.

[2] Artificial Intelligence: transforming the economy, transforming society - MICRA Showcase, University of Warwick, Coventry, UK. 09/2019.

[3] Conference of Sino-UK Collaboration in Development of Advanced Manufacturing and Automobile, PHBS UK Campus, Oxford, UK. 10/2018.

[4] Engine Combustion, Transient Performance and Control - UnICEG, University of Birmingham, Birmingham, UK. 09/2018.

[5] Connected & Autonomous Vehicles Conference, University of Salford, Manchester, UK. 05/2018.

[6] Challenges Test Rigs for Power, Electronics, Motors & Drives - IET Birmingham, Austin Court, Birmingham, UK. 11/2017.

LIST OF ABBREVIATIONS

APSO	Accelerated Particle Swarm Optimization
A-ECMS	Adaptive Equivalent Consumption Minimization Strategy
AI	Artificial Intelligence
BCLM	Back-to-back Competitive Learning Mechanism
BP	Battery Package
CAPSO	Chaos-enhanced Accelerated Particle Swarm Optimization
CD/CS	Charge Depleting and Charge Sustaining (strategy)
CI	Computational Intelligence
CASE-V	Connected and Autonomous Systems for Electrified Vehicles
DOIP	Dual-loop Online Intelligent Programming
DP	Dynamic Programming
EMS	Energy Management System
ECMS	Equivalent Consumption Minimization Strategy
ECF	European Climate Foundation
FEP	Fuzzy Encoding Predictor
FL	Fuzzy Logic
HiL	Hardware-in-the-Loop
HEV	Hybrid Electric Vehicle
ISG	Integrated Starter-Generator
ICE	Internal Combustion Engine
ITAE	Integral Time Absolute Error
IT-2	Interval Type-2
LSTM	Long Short-Term Memory
MPC	Model-based Predictive Control
NNP	Nearest Neighbour Predictor
NEDC	New European Driving Cycle

NN	Neural Network
ODEM	Online Driver-oriented Energy Management
PSO	Particle Swarm Optimization
RM	Research Module
SFFE	Spectrum-guided Fuzzy Feature Extraction
SoC	State of Charge
TD	Temporal Difference
T-S	Takagi-Sugeno
V2X	Vehicle-to-Everything (network)
V2I	Vehicle-to-Infrastructure (network)
WLTP	Worldwide harmonized Light-duty vehicles Test Procedure

DEDICATION

This thesis is dedicated to

My wonderful parents who have raised me to be the person I am today

My wife who believes in the richness of learning

My daughter who made me keep on learning

CHAPTER 1

INTRODUCTION

Optimal energy management strategies are critical for hybrid electric vehicles (HEVs) to achieve the best performance and greatest energy efficiency through power-split control. The human driver is another primary element that affects the energy consumption, emissions, and driving safety of a road vehicle. They have a large impact on electrified vehicles' fuel consumption; however, the driver is often ignored during the development of control strategies due to uncertainty and complexity. This thesis provides a systematic computational-intelligence methodology for supervisory controlling of hybrid electric vehicles, where the system is composed of vehicle dynamics and driver behaviours. In this chapter, the background section introduces: 1) the current progress in vehicle electrification; 2) driving behaviour in modern energy management; and 3) government thrust. This is followed by the scope and objectives of the thesis, and then the outline is presented in the final section.

1.1. BACKGROUND

Persistent environmental issues and periodic energy crises are major concerns for the automobile industry. [1] As an emerging trend, vehicle electrification aims to investigate alternative powertrain technologies and offer potentially fuel-efficient solutions in propulsion systems, traffic strategies and urban studies. [2] Hybrid technology is a good transition solution to environmental pollution that makes it possible to both improve the fuel economy and reduce the exhaust emissions of vehicles. [3, 4] For hybrid and electric vehicles,

developing optimal energy management strategies is critical to achieving the best performance and energy efficiency through power-split control. As another primary element, the driver plays a significant role in safety and eco-driving. [5] Most of the literature in developing control strategies currently ignores the effect of human drivers on errors in eco-driving, leading to further errors in tracking the recommended velocity profiles. Also, the industry thinks the application of such control strategies in real-world driving is extremely limited due to implementation complexity and the demand for large computational resources. Thus, the author was able to see there may be a beneficial way to organically integrate the vehicle and the driver into a whole system to achieve a highly optimized performance.

1.1.1. CURRENT PROGRESS IN VEHICLE ELECTRIFICATION

HEVs have inherited the benefits of conventional internal combustion engine (ICE) vehicles and battery electric vehicles. From the perspective of energy-flow, these two power machines, ICEs and motor machines, can be combined in series, parallel or series-parallel layouts. In series drivetrains, a motor machine provides the mechanical energy required for the wheels. In parallel drivetrains, both a motor machine and an ICE provide the mechanical energy required for the wheels.

Liquid fuel is still the energy resource for HEVs. The ICEs are the main energy converter and supply all the energy required for a whole vehicle. Using ICEs to extend the mileage of vehicles can effectively overcome the mileage inadequacy of pure electric vehicles. The duty of motor machines is to improve the efficiency of HEV systems and reduce energy consumption. During

real-world driving, motor machines help optimize operation points of ICEs by coordinating the torque and rotation speed of the ICEs. They also enable the recovery of kinetic energy through regenerative braking.

Degree of hybridization - Currently, a new concept concerning the degree of hybridization has entered the public perspective. It is regarded as an effective assessment to reflect the power level of the main traction motor in HEVs. From the aspect of the degree of hybridization, HEVs can be assigned into four categories: micro hybrid, mild hybrid, full hybrid, and plug-in hybrid. The vehicles classed as micro hybrid operate at about 12 volts and can automatically stop/start the engine in stop-and-go traffic. The mild hybrid vehicles, operating normally above 48 volts, use regenerative braking and an electric motor to aid a combustion engine. Inheriting the functionalities of mild hybrid vehicles, the full hybrid vehicles also drive at times using only the electric motor. To increase the pure electric range, the plug-in vehicles were eventually designed to encompass an electric drivetrain as the primary source of energy and traction.

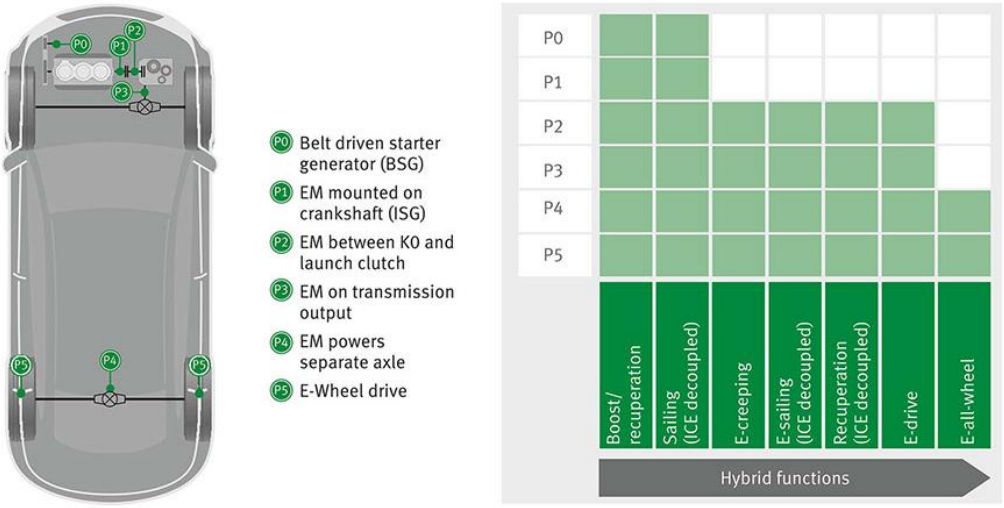

Fig. 1-1. Various mild hybrid architectures and the associated functionalities [6]

Fig. 1-1 summarises various paths for incorporating the electric motor in the powertrain. All architectures can be used to achieve the basic functions of boost and recovery when the ICE is engaged, and navigation when disengaged; to disengage operation here, an automatic launch clutch is mandatory. The arrangements of P2 to P5 have the following in common: when the ICE is disengaged, they allow the recovery of braking energy (different from the arrangement of P0 and P1 related to crankshaft speed), and the performance of the 48-volt system makes pure electric driving possible. The P4 and P5 architectures also make available a 48V-based all-wheel drive.

Series hybrid drivetrains - Series hybrids are also referred to as extended-range electric vehicles [7] or range-extended electric vehicles. Initially, it was common for diesel-electric locomotives and ships to be connected in series (the Russian inland vessel Vandal launched in 1903 was the world's first diesel-powered ship). Ferdinand Porsche effectively invented this arrangement in speed-record-setting racing cars in the early 20th century, for example in the Lohner-Porsche Mixed Hybrid. There is an ideal distributed platform to utilize various energy sources pointed out by Wu and Wang [8] that allows the use of renewable energy (e.g. proton exchange membrane fuel cell) and also advanced power machines (e.g. Linear Joule Engine Generator [9]). Products in this arrangement could be found in most international automotive companies, such as BMW i3, Audi A1e-tron, Chevrolet VOLT, etc.

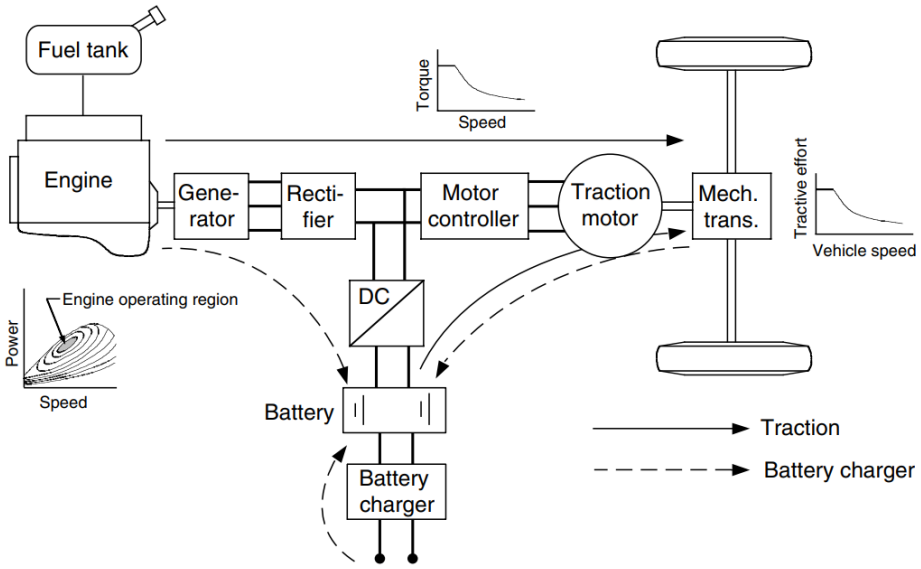

Fig. 1-2. Configuration of a series hybrid electric drivetrain [10]

Fig. 1-2 shows the powertrain of the layout of typical series HEVs, wherein the ICE is the central energy converter to transfer the primary energy in fuel to mechanical energy. Then the mechanical energy drives an electric generator to generate electricity. The motor machine drives the main reducer by using the electricity generated from the ICE or battery packages. As the ICE and the vehicle wheels are decoupled, there is no effect from the vehicle speed in controlling the rotation speed of ICEs. In fact, the series arrangement necessitates a heavier, more complicated battery and motor to meet its power demands. The supplement of a generator often makes them more costly than a parallel arrangement. Because the ICE is not mechanically coupled to the wheels, the series arrangement is not as economical as the parallel arrangement for high-speed driving. The plug-in hybrid is available in both series and parallel that enables electricity from the grid for pure electric operation and zero exhaust emissions on short distance trips. The plug-in element, however, also enhances the cost [11].

Parallel hybrid drivetrains – A parallel hybrid system is the most popular hybrid arrangement as of 2016 [12] that has both an ICE and an electric motor. It allows both to individually drive the vehicle or to be coupled up together to assist the driving. The parallel arrangement relies more on recovery of braking energy and the ICE can also act as a generator for supplementary recharging. They usually use a smaller battery pack than other hybrid arrangements, so this lets them be more efficient in city 'stop-and-go' circumstances. Honda's early Insight and Civic are examples of parallel hybrid productions. General Motors' parallel hybrid truck, BAS hybrids such as the Saturn VUE and Aura Greenline, and Chevrolet's Malibu hybrids also adopt a parallel hybrid architecture.

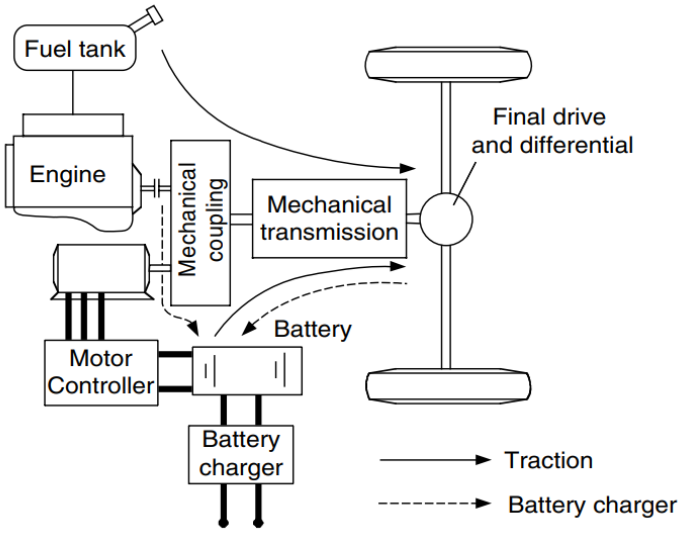

Fig. 1-3. Configuration of a parallel hybrid electric drivetrain [10]

A parallel hybrid arrangement is a drivetrain wherein the engine can mechanically provide power to the wheels like a traditional ICE-powered vehicle. It is supported by an electric motor mechanically coupled to a gearbox. The powers of the engine and electric motor are connected together by mechanical coupling, as shown in Fig. 1-3. The main drawback for a

parallel hybrid drivetrain is the engine and the driving wheels are mechanically coupled, so an automatic transmission is required, and the engine efficiency still cannot be fully exerted.

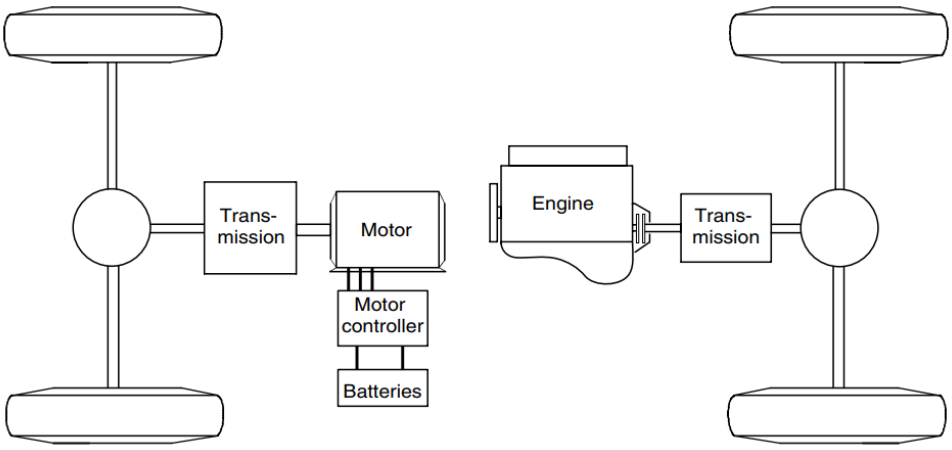

Fig. 1-4. The 'through the road type' of a parallel hybrid electric drivetrain [10]

An alternative parallel hybrid is the "through the road" type. [13] In this arrangement (as shown in Fig. 1-4) traditional drivetrain systems provide power for one axle, with an electric motor or motors driving another. The earliest "off-track" trolleybuses used this arrangement, in fact, it affords a complete backup powertrain. In modern electric motors, the battery is able to be charged by regenerative braking or loading electric drive wheels during cruising. This layout also has the benefit of supplying four-wheel drive in some cases. A practical instance of this principle is an electric bicycle equipped with a front-wheel hub motor that can assist the cyclist with pedal power on the rear wheels. Relevant commercial products include the Audi 100 Duo II and Subaru VIZIV concept cars, the PSA Group vehicles Peugeot 3008, Peugeot 508, 508 RXH, Citroen DS5 all using the HYbrid4 system, the Volvo V60 plug-in hybrid, the BMW 2 Series Active Tourer, BMW i8, and the second generation, Honda NSX.

Power-split hybrid drivetrains - A power-split hybrid is a parallel hybrid that combines power-split devices to allow power flow from an ICE to the wheels, in either a mechanical or electrical way. The main principle is to separate the power given by the primary source from the power demanded by the driver. Electric motors deliver full torque at a standstill, which is very suitable for making up for the problem of insufficient ICE torque at low RPM. In such a power-split arrangement, a smaller, less flexible, and more efficient engine is suggested. Inspired by the drivetrain layout of the well-known Toyota Prius, interesting variations can be found in the following vehicle models and their variants: Lexus CT 200h, Lexus RX400h, Lexus GS450h, Mercedes ML 450 hybrid, BMW X6 Active Hybrid, Chevrolet Tahoe Hybrid, BYD F3DM.

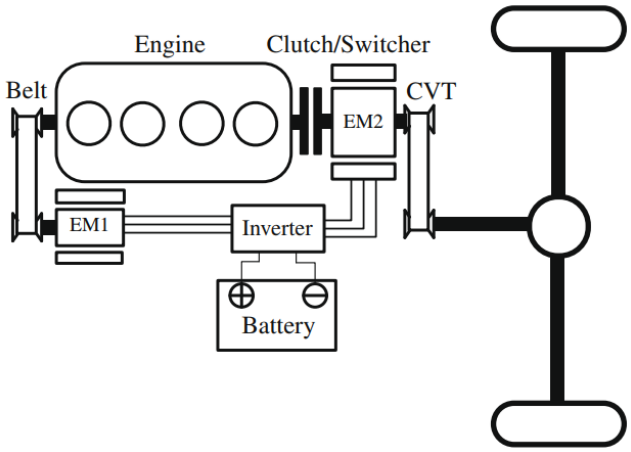

Fig. 1-5. Nissan-Tino series-parallel drivetrain [14]

In Fig. 1-5, a continuously variable transmission is introduced after the electric motors to transfer the energy from both the electric motors and the ICE to the wheels. A motor is used to generate power and start the ICE. An electromagnetic clutch is employed to shift the operation mode via locking and unlocking. [15] Such a system is more appropriate for light-duty cars because the transmission is expensive and unviable for a heavy-duty vehicle.

1.1.2. MODERN ENERGY MANAGEMENT AND DRIVING BEHAVIOUR

Modern energy management is needed for connected automatic vehicles and intelligent transportation systems that require a superior understanding of human driving behaviour. This is not only necessary to guarantee a safe and satisfactory performance, but also to acclimatise to the drivers' desires, and ultimately meet the drivers' preferences in a safe environment [16]. Consequently, it is critical to develop recognition of driving behaviour and driver intention inference.

Significance of driving behaviour in modern energy management - Fuel efficiency is mainly affected by (but not limited to) the following factors: vehicle dynamics, road features, traffic conditions and driving style. [17, 18] Although it is well known that driving behaviour seriously influences fuel efficiency, knowledge of the direct relationship is still limited. [19] Moreover, fuel consumption can be applied to simplify the relationship between driving behaviour and vehicle efficiency, [20] and to assist in portraying drivers' behaviour. [21] In a rare publication efforts in this direction by Bolovinou et al. [22] developed an algorithm capable of calculating the remaining range in a battery electric vehicle. Recent publications emphasized a potential margin of 20-40% for fuel consumption, [23] which is consistent with the margin of 5-40% claimed by the work of Manzoni et al. in a simulated environment. Nevertheless, this benefit is closely related to the road features. [24] Mudgal et al. reduced fuel consumption by 33% through correcting offensive driving on highways, but only by 5% on city roads. [25] Vagg et al. developed an embedded driver advisory tool that demonstrated real-world fuel savings of

7.6%, through changing driver behaviour by audible feedback. [26] Thus, modern energy management urgently needs to take into account the diversity of driving behaviours.

Driving behaviour classification and recognition - The signal selection for driving behaviour is closely related to the classification criteria and recognition algorithm used. There are two main approaches for categorizing driving behaviour via unique labelling. Usually, to categorize driving behaviours into classes the distribution information of the selected driving parameters and extracted features is used. [23] Before the classification algorithm design, these classes need to be carefully defined for all influencing parameters in a multi-factor cognition task. The trade-off between classification fineness and complexity should be considered to ensure the robustness of the algorithm, and interpretability for the end-user. [27] Another way to classify driving behaviour is through continuous indexing. The final classification into a large number of clusters includes consideration of a continuous index, which can eventually be used in a threshold-based algorithm to convert it into finite classes. [28, 29]

Once the classification method and the signals used are selected, driving behaviour recognition algorithms are expected to be developed. Driving behaviour recognition algorithms are generally realized through rule inference, models or using machine learning. A rule-based, also known as a threshold-based algorithm, is the most intuitive way to recognize driving behaviour. Inference rules are characterized using predetermined thresholds of monitoring variables that categorize driving behaviour into classes. Model-based algorithms include a set of equations with predefined features to describe driving style. The threshold

definition in the rule-based algorithm limits the robustness of the results and requires a lot of statistical analysis. Data-driven algorithms (using machine learning) are suitable for processing large amounts of data, consistently derive thresholds, and even completely develop other improved algorithms. Besides, they have adaptive functions that can serve for drivers whose data is not pre-trained. Such beneficial features have facilitated study on data-driven methods and regulate upcoming trends in driving behaviour recognition.

1.1.3. GOVERNMENT THRUST

Motivated by rising prosperity in the developing world, the demand for energy has increased significantly. As the BP Energy Outlook: 2019 edition reported, [30] the shifting to a low-carbon energy system continues, and the importance of renewable energy and natural gas relative to oil and coal is increasing. The report points out that with the increase in vehicle efficiency, the growth of the transportation demand has dropped sharply compared to the past. By 2040, the proportion of passenger vehicle kilometres driven by electric vehicles will increase to about 25%, thanks to the increasing significance of fully autonomous vehicles and shared travel services. Fig. 1-6 indicates that oil consumption has risen (0.3% p.a.) for the first half of the period considered in the BP Energy Outlook, [30] although much slower than in the past, before plateauing in the 2030s.

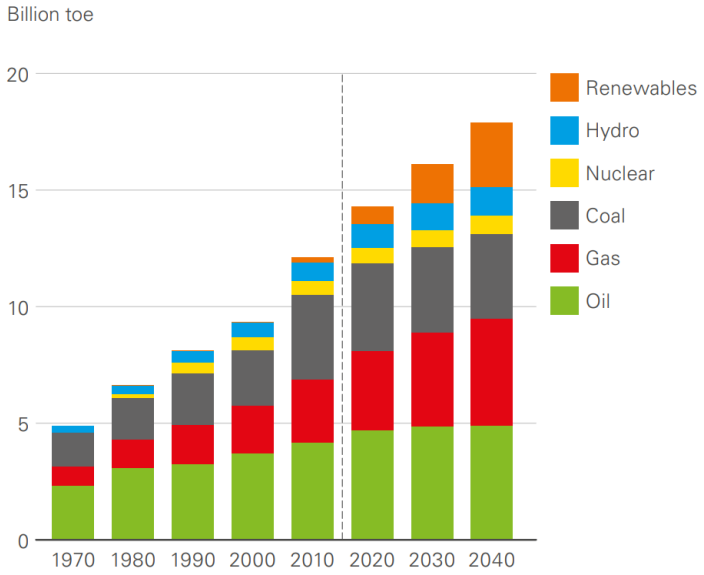

Fig. 1-6. Primary energy consumption by fuel [30]

Meanwhile, in 2017, the International Council on Clean Transportation updated the 'Light-duty vehicle greenhouse gas and fuel economy standards'. [31] Fig. 1-7 shows the EU CO_2 passenger car standards relative to similar global regulations. The graph converts all regulatory plans to the NEDC to make them comparable. Under the new regulation, the EU becomes the only market in the world that has set mandatory CO_2 emissions' targets for new vehicles by 2030. By 2025, the EU's CO_2 emissions' target is about 81 g/km, while the US and Canada have similar targets (99 g/km).

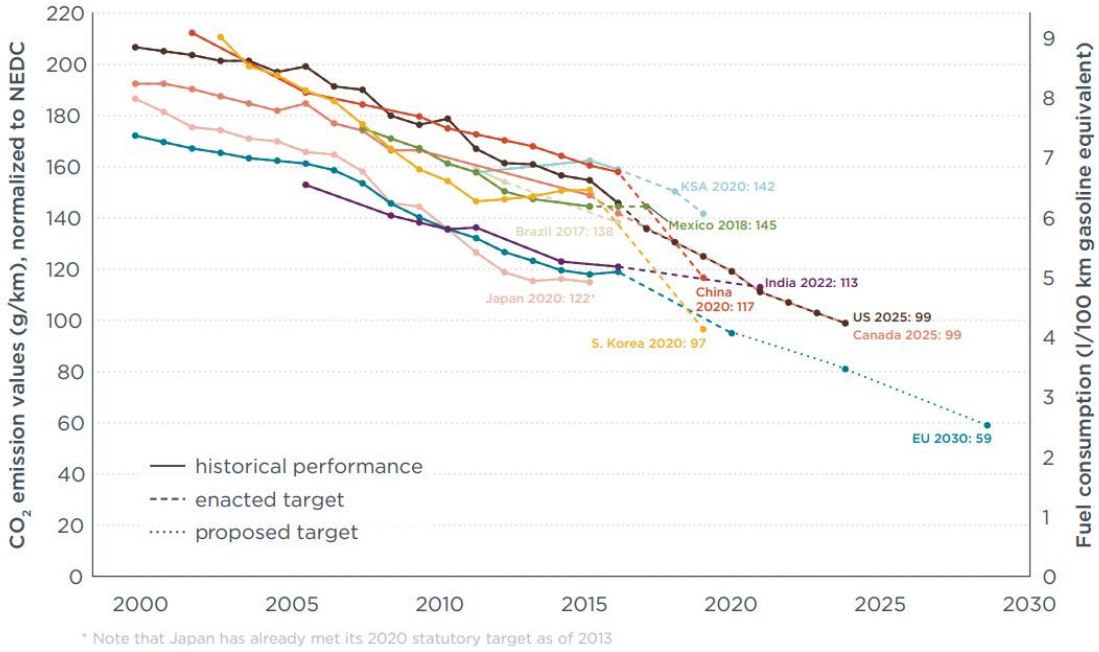

Fig. 1-7. Comparison of global CO_2 regulations for brand-new passenger cars [31]

Overall, governments are increasingly willing to implement and reinforce vehicle greenhouse gas emissions and fuel economy standards; which mirrors their growing recognition that decreasing greenhouse gas emissions and fuel consumption will improve environmental health (including fulfilling global climate change commitments), to ensure energy security, shield consumers from oil price fluctuations and promote technological revolution.

In October 2009, the European Council established applicable emission reduction targets for Europe and other advanced economies. By 2050, the emissions will be 80-95% lower than the 1990 level. To support this goal, the European Climate Foundation (ECF) launched a survey to establish the factual foundation behind the goal and discover its impact on European industry, especially the power industry.

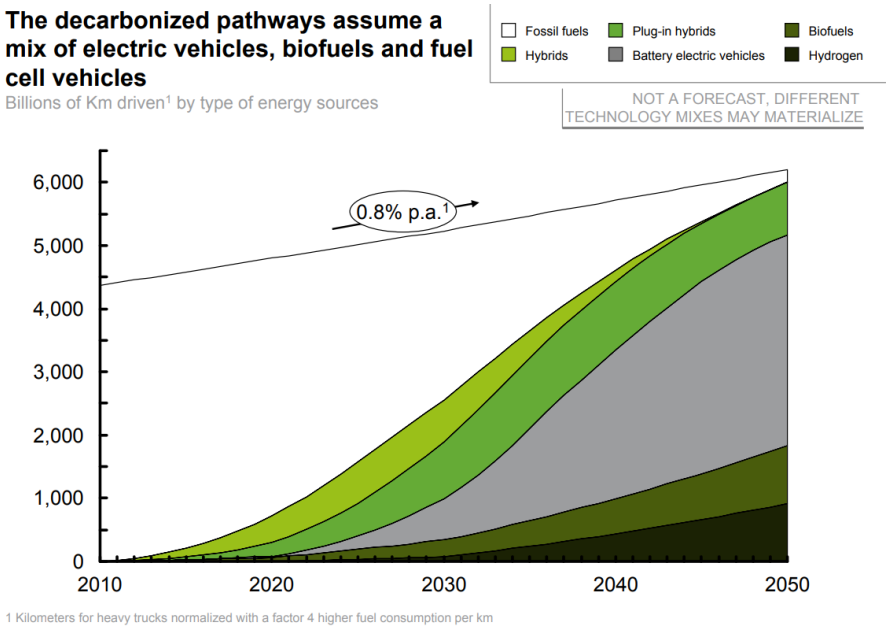

Fig. 1-8. The decarbonized pathways assume a mix of electric vehicles, biofuels and fuel cell vehicles [32]

As illustrated in Fig. 1-8, the electrification began with hybrid and plug-in hybrid powertrain systems for urban vehicles (approximately 20% penetration by 2020). Up to 2020, the penetration of full electric vehicles is still very small. As the pioneers of electrification, plug-in and HEVs take the lead in replacing fossil fuel vehicles. To ensure the smooth entry of battery electric and other renewable vehicles into the market, hybrid and plug-in hybrid play an irreplaceable role in prior technical reserve and market expansion. In addition, human drivers (or their behaviour) as primary decision makers greatly affect energy consumption and driving safety. To build a safe and energy-saving intelligent transportation system, driver's information fusion gradually becomes a research focus that promotes the development of future connected and autonomous vehicles with all types.

In the ‘Europe on the Move’, a road transport strategy for Europe, the Commission proposed in May 2017 to reward the most environmentally friendly vehicles with reduced road charges.

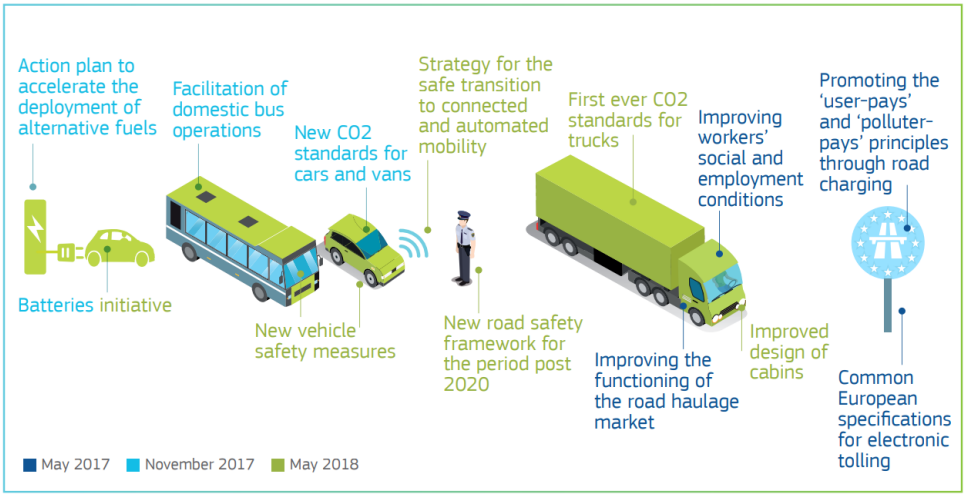

Fig. 1-9. Key actions proposed since May 2017 [33]

Fig. 1-9 displays some key actions taken by the European Commission. To enable this, the Commission put forward new CO_2 standards for light vehicles in November 2017, followed in May 2018 by the first-ever CO_2 standards for trucks. In parallel, the Commission took actions to strengthen the internal road freight market and to better protect drivers. Put together, all these initiatives will offer safe, clean, and competitive mobility to Europeans by 2025.

1.2. SCOPE AND OBJECTIVES

This work builds on previous study in a centre for Connected and Autonomous Systems for Electrified Vehicles (CASE-V) that has involved developing a modular HEV architecture [34]. The architecture has been demonstrated by an industrial partner, Douglas Motors Ltd, and can be engaged in testing and analysing the existing control strategies from the state of the art, as well as for designing a series of new control strategies. The richness of this version is

not only expected to obtain more reliable results, but will also reveal dynamic characteristics of each component that result in new control requirements. In addition, because this version belongs to a series architecture, it is possible to conduct fundamental research on series HEVs and extend it to parallel or power split architectures.

The research performed as challenging work in the centre for CASE-V has implicated a wide range of interdisciplinary topics being investigated. A substantial portion of my research activity is instigated in engineering, but enlarges to include human and computational intelligence, which extends to methodology development of driver-oriented supervisory control strategies. However, studying HEVs, with a driver-oriented architecture, the research topic faces a very different control problem e.g. extra degrees of freedom in vehicle design and new uncertainties from human drivers. The vehicle used for the research based on the developed HEV architecture is a hybridized medium passenger car with series-parallel drivetrain, where its underlying component models are partially simplified. The system-level suitability has been established and proved by BYD Auto Co. Ltd. As such, it was considered best to limit the scope of the thesis to my work only on supervisory control systems of the series-parallel drivetrain for energy management personalization.

For the work on HEVs, an additional four projects have been pursued together with final year undergraduate and postgraduate students. These consist of one project on an adaptive controlling series hybrid aircraft trailer; one project on modelling and analysing fuel consumptions and emissions; one project on equivalent consumption minimization strategy;

and one project on Markov-chain-based model predictive control. Over the past four years, the work on each research path has been greatly developed, mainly by the students themselves, but under my indispensable guidance. These additional projects could have been formed as a chapter, but there is still much room for improving them. This work needs to be perfected and consolidated at a later stage.

The PhD research aims to develop driver-oriented intelligent control methodology for energy management personalization of series-parallel hybrid electric vehicles, by using computational intelligence techniques. The key objectives of the thesis are as follows:

a) To develop a system-level series-parallel HEV model that is suitable to test control strategies
b) To study and learn from existing work on control strategies and driving behaviour
c) To establish a driver-oriented supervisory control framework with accessible communication between human drivers and intelligent hybrid vehicles
d) To design personalized non-stationary inference for robustness enhancement of the vehicle system
e) To propose the method of spectrum-guided fuzzy feature extraction for global optimum enhancement of the vehicle system
f) To create a back-to-back competitive learning mechanism for synergy enhancement of the vehicle system
g) To propose dual-loop online intelligent programming for predictability enhancement of the vehicle system

h) To expose and understand the characteristics of each proposed control strategy

i) To analyse and evaluate the vehicle system's performance in each phase

These objectives can in a loose order be associated with each of the chapters from Chapter 2 to Chapter 8.

1.3. THESIS OUTLINE

This thesis will begin with a comprehensive literature study. Thereafter, the research methodology and experimental facilities will be described; wherein the vehicle model will be presented, and it will be used throughout the rest of the thesis. This will be followed by delivering the driver-oriented intelligent control methodology and the design of a family of power-split control strategies to maximize powertrain efficiency. In addition, each control strategy will be designed with a specific targeted goal. The remarkable performance of these goal-oriented strategies will lead to a discussion about the nature of a synthesized optimal solution for HEVs and their reliability. Each chapter is briefly described below.

CHAPTER 2 The literature review exhaustively elaborates three sections, which are offline optimization approaches, online optimization approaches, and driver-oriented optimization approaches. Overall, the narrative sequence follows the complexity of implementation and the degree of information fusion.

CHAPTER 3 This chapter, for the first time, introduces interaction topology in HEV energy management; where a system composed of human drivers and a hybrid vehicle, along with the corresponding research technical route are illustrated. Then, modelling of the powertrain components is explained collectively with their interconnection. This focuses on core operating behaviours related to component efficiency and performance. Finally, experimental facilities, including the driving simulation platform and hardware-in-the-loop (HiL) test bench are presented for experimental validation.

CHAPTER 4 Heuristic supervisory control systems have been favoured by industry due to easy implementation and strong robustness. However, their limitations remain obvious due to (i) computational burden (ii) the poor adaptability of its control system to various driving styles. To systematically address the identified technical challenges, this paper aims to establish an online driver-oriented energy management methodology which incorporates the factor of driving styles into vehicle controller optimization. The difference of the current system to the previous ones in the literature is that it introduces real-time monitoring driving behaviour to increase robustness of HEV energy management systems. In this chapter establishment of a connected driver-oriented control framework will be carried out; wherein a novel approach of using personalized non-stationary inference is proposed. The outcome of this chapter has been submitted with *IEEE Transactions on SMC: Systems*.

CHAPTER 5 Most of the existing research on the division of driver behaviour is using continuous indexing. Such treatment, however, results in the consequence that the control

policy optimized for a single style may lose the global optimal advantage during mode switching. This chapter introduces the concept of the driver-identified supervisory control system, which forms a novel architecture of adaptive energy management for HEVs. As a man–machine system, the proposed system can accurately identify the human driver from natural operating signals and provides driver-identified globally optimal control policies as opposed to mere control actions. The outcome of this chapter has been published with *IEEE Transactions on Fuzzy Systems*. [35]

CHAPTER 6 Online energy management intends to real-time evaluate the HEV system effectiveness to acclimate to stochastic driving conditions over real-world driving. Due to computational burden, however, robustness and efficiency of HEV systems are hard to guarantee simultaneously during real-time optimization. For synergistic promotion of robustness and efficiency of HEV systems, this chapter introduces a novel back-to-back competitive learning mechanism. This mechanism allows continuous competition between two fuzzy logic controllers during real-world driving. The leading controller will have the regulatory function of the supervisory control system. Its technology core has been published with *IEEE Transactions on Industrial Electronics*. [36]

CHAPTER 7 The accuracy of the predictor is a prerequisite condition for implementing online predictive energy management of HEVs. This chapter introduces dual-loop online intelligent programming to ensure the effectiveness of an optimal control sequence for HEV systems. By re-considering the change of driving behaviours at each look-ahead step, the new

methodology with higher precision of predicted velocity trajectories involves two online iteration loops to simultaneously update the predictive model and optimize the control sequence. The outcome of the chapter has been published with *Applied Energy*. [37]

CHAPTER 8 Conclusions and highlights are presented in this chapter for the whole thesis and then the innovations and impacts are summarized. This is followed by an outline of future directions for the PhD research.

REFERENCES

[1] F. Zhang, X. Hu, R. Langari, and D. Cao, "Energy management strategies of connected HEVs and PHEVs : Recent progress and outlook," *Progress in Energy and Combustion Science*, vol. 73, pp. 235–256, 2019.

[2] W. Su, H. Eichi, W. Zeng, and M. Chow, "A Survey on the Electrification of Transportation in a Smart Grid Environment," *IEEE Transactions on Industrial Informatics*, vol. 8, no. 1, pp. 1–10, 2012.

[3] J. P. F. Trovão, V. D. N. Santos, C. H. Antunes, P. G. Pereirinha, and H. M. Jorge, "A Real-Time Energy Management Architecture for Multisource Electric Vehicles," *IEEE Transactions on Industrial Electronics*, vol. 62, no. 5, pp. 3223–3233, 2015.

[4] X. Hu, J. Jiang, and S. Member, "Advanced Power-Source Integration in Hybrid Electric Vehicles : Multicriteria Optimization Approach," *IEEE Transactions on Industrial Electronics*, vol. 62, no. 12, pp. 7847–7858, 2015.

[5] T. Stillwater, K. S. Kurani, and P. L. Mokhtarian, "The combined effects of driver attitudes and

in-vehicle feedback on fuel economy," *Transportation Research Part D*, vol. 52, pp. 277–288, 2017.

[6] T. Eckenfels, F. Kolb, S. Lehmann, W. Neugebauer, and M. Calero, "48 V Hybridization-A Smart Upgrade for the Powertrain," *Mobility for Tomorrow*, 2018. [Online]. Available: http://schaeffler-events.com/symposium/lecture/h3/index.html.

[7] R. Matthé and U. Eberle, *The Voltec System-Energy Storage and Electric Propulsion*. Elsevier, 2014.

[8] D. W. Wu and R. Z. Wang, "Combined cooling, heating and power: A review," *Progress in Energy and Combustion Science*, vol. 32, no. 5–6, pp. 459–495, 2006.

[9] B. Jia, D. Wu, A. Smallbone, C. Lawrence, and A. P. Roskilly, "Design, modelling and validation of a linear Joule Engine generator designed for renewable energy sources," *Energy Conversion and Management*, vol. 165, no. December 2017, pp. 25–34, 2018.

[10] M. Ehsani, Y. Gao, S. Longo, and K. Ebrahimi, *Modern electric, hybrid electric, and fuel cell vehicles*. CRC press, 2018.

[11] "Plug-in Hybrids," *U.S. Department of Energy Office of Transportation and Air Quality*. [Online]. Available: https://www.fueleconomy.gov/feg/phevtech.shtml.

[12] S. Alegre, J. V. Míguez, and J. Carpio, "Modelling of electric and parallel-hybrid electric vehicle using Matlab/Simulink environment and planning of charging stations through a geographic information system and genetic algorithms," *Renewable and Sustainable Energy Reviews*, vol. 74, no. March, pp. 1020–1027, 2017.

[13] N. F. A. T. T. R. Center, "Trans Forum," *Argonne National Laboratory*, vol. 14, no. 1, 2010.

[14] W. Xiong, Y. Zhang, and C. Yin, "Optimal energy management for a series-parallel hybrid electric bus," *Energy Conversion and Management*, vol. 50, no. 7, pp. 1730–1738, 2009.

[15] I. Matsuo, S. Nakazawa, H. Maeda, and E. Inada, “Development of a high-performance hybrid propulsion system incorporating a CVT,” *SAE Technical Papers*, no. 724, 2000.

[16] C. M. Martinez, M. Heucke, F. Wang, B. Gao, and D. Cao, “Driving Style Recognition for Intelligent Vehicle Control and Advanced Driver Assistance : A Survey,” *IEEE Transactions on Intelligent Transportation Systems*, vol. 19, no. 3, pp. 666–676, 2018.

[17] E. Ericsson, “Variability in urban driving patterns,” *Transportation Research Part D: Transport and Environment*, vol. 5, no. 5, pp. 337–354, 2000.

[18] E. Ericsson, “Independent driving pattern factors and their influence on fuel-use and exhaust emission factors,” *Transportation Research Part D: Transport and Environment*, vol. 6, no. 5, pp. 325–345, 2001.

[19] T. Lee and J. Son, “Relationships between driving style and fuel consumption in highway driving,” *SAE Technical Papers*, 2011.

[20] J. Neubauer and E. Wood, “Thru-life impacts of driver aggression, climate, cabin thermal management, and battery thermal management on battery electric vehicle utility,” *Journal of Power Sources*, vol. 259, pp. 262–275, 2014.

[21] C. Miyajima et al., "Driver Modeling Based on Driving Behavior and Its Evaluation in Driver Identification," in Proceedings of the IEEE, vol. 95, no. 2, pp. 427-437. 2007.

[22] A. Bolovinou, I. Bakas, A. Amditis, F. Mastrandrea, and W. Vinciotti, “Online prediction of an electric vehicle remaining range based on regression analysis,” *2014 IEEE International Electric Vehicle Conference, IEVC 2014*, pp. 1–8, 2014.

[23] R. Wang, “Review of Driving Conditions Prediction and Driving Style Recognition Based Control Algorithms for Hybrid Electric Vehicles,” *2011 IEEE Vehicle Power and Propulsion Conference*, pp. 1–7, 2011.

[24] V. Manzoni, A. Corti, P. De Luca, and S. M. Savaresi, “Driving style estimation via inertial measurements,” *IEEE Conference on Intelligent Transportation Systems, Proceedings, ITSC*, pp. 777–782, 2010.

[25] A. Mudgal, S. Hallmark, A. Carriquiry, and K. Gkritza, “Driving behavior at a roundabout: A hierarchical Bayesian regression analysis,” *Transportation Research Part D: Transport and Environment*, vol. 26, pp. 20–26, 2014.

[26] C. Vagg, C. J. Brace, D. Hari, S. Akehurst, J. Poxon, and L. Ash, “Development and field trial of a driver assistance system to encourage eco-driving in light commercial vehicle fleets,” *IEEE Transactions on Intelligent Transportation Systems*, vol. 14, no. 2, pp. 796–805, 2013.

[27] A. Doshi and M. M. Trivedi, “Examining the impact of driving style on the predictability and responsiveness of the driver: Real-world and simulator analysis,” *IEEE Intelligent Vehicles Symposium, Proceedings*, pp. 232–237, 2010.

[28] Y. L. Murphey, R. Milton, and L. Kiliaris, “Driver’s style classification using jerk analysis,” *2009 IEEE Workshop on Computational Intelligence in Vehicles and Vehicular Systems, CIVVS 2009 - Proceedings*, pp. 23–28, 2009.

[29] A. Augustynowicz, “Preliminary classification of driving style with objective rank method,” *International Journal of Automotive Technology*, vol. 10, pp. 607–610, 2009.

[30] BP p.l.c., “BP Energy Outlook 2019 edition,” *BP Energy Outlook 2019*, 2019.

[31] A. B. ZIFEI YANG, “2017 Global update: Light-duty vehicle greenhouse gas and fuel economy standards,” *International Council of Clean Transpoartation*, p. 36, 2017.

[32] European Commission, “Roadmap 2050 - Technical & Economic Analysis - Full Report,” *Publications Office of the European Union*, pp. 1–100, 2016.

[33] European Commission, “Factsheet: Shaping the future of mobility,” *Publications Office of the*

European Union, no. September, 2018.

[34] Q. Zhou, W. Zhang, S. Cash, O. Olatunbosun, H. Xu, and G. Lu, "Intelligent sizing of a series hybrid electric power-train system based on Chaos-enhanced accelerated particle swarm optimization," *Applied Energy*, vol. 189, pp. 588–601, 2017.

[35] J. Li, Q. Zhou, Y. He, H. Williams, and H. Xu, "Driver-identified Supervisory Control System of Hybrid Electric Vehicles based on Spectrum-guided Fuzzy Feature Extraction," *IEEE Transactions on Fuzzy Systems*, vol. 6706, no. c, pp. 1–1, 2020.

[36] J. Li, Q. Zhou, H. Williams, and H. Xu, "Back-to-back Competitive Learning Mechanism for Fuzzy Logic based Supervisory Control System of Hybrid Electric Vehicles," *IEEE Transactions on Industrial Electronics*, vol. 2, no. c, pp. 1–1, 2019.

[37] J. Li *et al.*, "Dual-loop online intelligent programming for driver-oriented predict energy management of plug-in hybrid electric vehicles," *Applied Energy*, vol. 253, no. November, p. 113617, 2019.

CHAPTER 2

LITERATURE REVIEW

This chapter presents a wide-ranging literature review for energy management optimization approaches of hybrid electric vehicles (HEVs) concerning: 1) offline optimization approaches; 2) online optimization approaches; 3) driver-oriented optimization approaches and 4) a summary and some future trends. The section of the driver-oriented optimization approaches for HEV energy management also studies the online co-optimization approaches for energy management and driver dynamics. In addition, there will be a discussion on how to develop the system composed of a vehicle and drivers.

2.1. OFFLINE OPTIMIZATION APPROACHES FOR HEV ENERGY MANAGEMENT

The purpose of offline (route previewed) optimization is to exploit the static data (e.g. road gradient, speed limit) to obtain a longer field of view when inventing the energy management system, for a well-defined trip which enhances the energy efficiency of HEVs. Knowing the forthcoming terrain and traffic conditions helps to ensure a wiser use of the electricity by enlarging the planning scope. [1] In industry-level optimization of vehicle systems, the testing vehicle usually operates to track a given standard driving cycle (e.g. NEDC, WLTP) within restricted range errors. The optimization variables should be strictly calibrated or corrected for achieving the best performance of vehicle systems in that standard cycle. From the aspect of objects to be optimized, the author divides the literature concerning offline optimization

into two categories: 1) supervisory controller calibration; and 2) action decision optimization. Then a comprehensive elaboration will be carried out.

2.1.1. SUPERVISORY CONTROLLER CALIBRATION

A supervisory controller is used to schedule many separate controllers or control loops in the HEV system, such as the engine control unit, motor control unit, and battery control unit. It refers to a high level of comprehensive monitoring of single process controllers, which is not necessary for the operation of each controller, but provides the operator with a view of the entire plant process and allows operation integration between controllers. [2] Therefore, accurate calibration of supervisory controllers is critical to ensure safety and efficiency of their system operation. The existing calibration methods of supervisory controllers used in HEVs are normally categorized into heuristic strategy and data-driven optimization.

In heuristic strategies, expert experience dominates the rules of the controller, producing deterministic and non-deterministic rule-based strategies. The thermostat (on/off) strategy is simple, robust, and easy to implement. [3, 4] Because of the stationary rules, it lacks the ability to treat the uncertainty caused by inaccurate models. The power follower control strategy is widespread and has been widely used in commercial HEVs, e.g. the Honda Insight and Toyota Prius. [5] Phillips et al. and Wang et al. proposed the state machine-based approach for HEVs. [6, 7] This strategy allows the switch between operating modes, such as ENGINE, BOOST, CHARGING, etc., to be governed by a state machine. [8] However, these strategies are overly

dependent on expert experience and are not friendly to newcomers. Here, fuzzy logic provides a good solution for them to transfer human knowledge to non-deterministic rules. Tian et al. developed an adaptive fuzzy-logic-based control strategy to follow the trend of the SoC reference curve for a plug-in hybrid electric bus. [9] Martinez et al. tried to use interval type-2 fuzzy rule in an energy management system [10, 11]; wherein type-2 MFs impose extra constraints on fuzzy rules for minimizing the effects of uncertainties in such heuristic systems. From the result of case studies, a fuzzy energy management system is able to give decision support for both managing system uncertainty, and explicitly representing the inference processes of its decision [12]; however, this relies heavily on expert experience.

To avoid bias from human knowledge during controller calibration, data-driven optimization ensures global optimality of the control model by using real-world feedback. Its performance relies upon the quality of the dataset that can be collected from the development of the experiment. Therefore, controller performance using conventional calibration methods can be further improved by machine learning algorithms. Khayyam et al. developed an adaptive intelligent system for HEVs, applying a hierarchical neuro-fuzzy inference system through genetic algorithm optimization [13]; in which a genetic algorithm is employed to directly calibrate fuzzy rule base (RB) and scalar parameters of the membership functions. A similarity in the work of [14], employing an improved genetic algorithm, solves the constrained bi-objective optimization problem for the fuzzy energy management system (EMS). Kamal et al. addressed the fuzzy energy management problem with hybrid algorithm optimization that synergistically enhances the robustness and efficiency of HEV systems, especially for ensuring

a better battery life. [15] Actually, the structure of these rules may be an obstacle to increasing global optimality and also their adaptability to the new scenarios is debatable. Lv et al. proposed a joint design optimization scheme for a vehicle system and controller parameters, in which Gaussian mixture models are adopted to differentiate driving styles. [16] For computational reasons, if the dimension of the clustering problem is too large, it may not work in practice. Chen et al. developed an intelligent power-split controller that treats the optimal solutions as a training material of artificial neural networks, for improving the adaptability and fuel economy of a HEV system. [17] In the work of Kong et al., recurrent neural networks have been applied to discover the distribution of the optimal torque in rule-based energy management systems. [18] However, it is hard to determine the network structure for achieving the best vehicle performance.

2.1.2. ACTION DECISION OPTIMIZATION

Action decision optimization aims to minimize the cost function through the power-split, which reflects energy economy and/or exhaust emissions over a permanent and known drive cycle. [19] These approaches break through the constraints of the fixed rules on the optimization performance of the HEV system, increasing the possibility of finding a global optimum solution. A global optimization algorithm on the powertrain flows has been developed because of the Bellman optimality principle, and widely applied to HEVs. [20] Overall, they are practical and beneficial for benchmark design or comparison purposes, such as deterministic/stochastic dynamic programming (DP), game theory, and nature-inspired

optimization algorithms e.g., the Genetic Algorithm, Particle Swarm Optimization, and Bees Algorithm.

DP, an industry-recognized global optimization algorithm, can efficiently deal with the constraints and nonlinearities of a Markov decision process problem and find a global optimal solution. [21] In 2006, DP was first launched in HEV energy management by Perez et al. [22], wherein two different sources are simplified and formulated into a finite horizon dynamic optimization problem. After that, Ansarey et al. improved an HEV model with a dual-storage fuel-cell. [23] The model had more degrees of freedom to enable multi-dimensional DP. Peng et al. and Chen et al. employed it for detecting the optimal actions of the engine in plug-in HEVs; and then re-calibrated them into control rules [24] and a neural network [25] respectively. Although it is an intelligent solution to recompile an optimal control policy into a vehicle controller, degree of state discretization in DP problems would affect the performance of the vehicle controller. For the same problem, Vagg et al. found the main reason was in minimizing battery stress during HEV control design; [26] which is control bifurcations caused by using different interpolation methods in DP implementation. Considering the strict environment of the algorithm application, Johannesson et al. assessed the potential for reduced fuel consumption of HEVs by the use of powertrain predictive control [27]; wherein stochastic DP to combine DP and a Markov chain model has been adopted for achieving the minimal attainable energy consumption. Learning from his previous work [26], Vagg et al. deployed a controller using stochastic DP for HEVs, to enhance adaptability in the real world. [28] This approach yielded a 13% reduction in electrical

powertrain stress without sacrificing any fuel savings. Dextreit et al. implemented one energy management controller for HEVs based on the application of game theory. [29] They demonstrated a better performance with a slight effort of calibration than the present benchmark controller that is calibrated from the deterministic or stochastic DP solutions over the NEDC cycle.

Nature-inspired optimization algorithms are the so-called metaheuristic algorithms. In a book of Nature-inspired Optimization Algorithms, the author Yang points out here Meta means “beyond” or “higher level,” and these algorithms normally behave better than simple heuristics. [30] In 1995, Kennedy et al. developed an evolutionary computation technique, namely, the particle swarm optimization (PSO), which is derived from a simulation of a simplified social model. [31] Relying on a simple algorithm structure and good convergence, the PSO has been widely used in automotive industrial practice. Soares et al. presented a modified PSO to schedule energy resources considering vehicle-to-grid. This allows it to be used to solve large-scale problems in the real world (2000 gridable vehicles), and to provide system operators with sufficient decision assistance and effective resource planning. [32] Rahman et al. compared HEV performance when using a standard PSO and an accelerated (A)-PSO, and the simulation results suggested using APSO for improvements in optimal adaptability and computing time. [33] Offline optimization approaches continue to play an essential role in industrial practice for supporting the development of vehicle subsystem calibration and optimization. In fact, the outcomes of offline optimization are finding it difficult to meet the increasing driver acceptance and regulation constraints.

2.2. ONLINE OPTIMIZATION APPROACHES FOR HEV ENERGY MANAGEMENT

Recently, new opportunities brought by the development of computer science to the automotive industry emerged as promising methods for breaking the bottleneck caused by conventional energy management in HEVs. [34] Contrary to offline optimization, online optimization is dedicated to further improving the dynamic characteristics of the HEV system, to adapt to the unknown driving environment with real-time evaluation. [35] It requires an extra module of real-time evaluation, and a reliable structure of new applied algorithms. Generally, these approaches contain an equivalent consumption minimization strategy (ECMS), model and model-free predictive control.

2.2.1. EQUIVALENT CONSUMPTION MINIMIZATION STRATEGY

The concept of the ECMS was first proposed by Paganelli et al. This is a method to transform a global minimization problem into an instantaneous minimization problem that has been solved at each time step. [36] The idea behind it is that the total fuel consumption is the sum of the actual fuel consumption of the ICE and the equivalent fuel consumption of the motor. In their subsequent work, experimental and simulation results are presented, demonstrating that this approach provides an improvement of fuel efficiency (up to 6% from the baseline), along with robustness and ease of implementation. [37] Chasse and Sciarretta proved accessibility when the ECMS is used for an engine-in-the-loop test bench, and pointed out there is no adaptation to future driving circumstances. [38] Thereupon, Musardo et al.

presented an improved control strategy, namely adaptive ECMS (A-ECMS), where an on-the-fly algorithm is added to the ECMS framework to estimate an equivalence factor based on driving patterns. [39] Similarly, Amir Rezaei et al. proposed an A-ECMS that is designed with an estimated equivalent factor, to catch energy-saving opportunities without the need for predicting power demand. [40] To further assess the optimal value of the co-state for the A-ECMS, they found upper and lower boundaries of the equivalent factor could be restricted by HEV architecture and were independent of the driving cycle. [41] The simulation results displayed that the optimal equivalent factor is always inside or close to the edge of the proposed range. Sciarretta et al. comprehensively studied a control benchmark on the energy management of a plug-in HEV; wherein the ECMS implementation was analysed. [42] From a comparison among several applications of the ECMS, map-based ECMS takes less computing effort but has a higher memory use; whilst the opposite is true for vector-based ECMS. This adaptive-enhanced algorithm exploits an instantaneous ECMS-like minimization of the fuel consumption, where the equivalent cost is evaluated on the basis of past and predicted data of the driving conditions. [43]

2.2.2. MODEL-BASED AND MODEL-FREE PREDICTIVE CONTROL

Model-based predictive control (MPC) is an advanced method used to control a process while satisfying a set of constraints. [44] Kachroudi et al. designed a predictive decision support system to optimally manage energy flow between the instantaneous power demand requested by the driver. [45] This methodology utilizes an online PSO algorithm to search for a global optimum relative to specific objective functions, which consider driving comfort

indexes, battery autonomy, and travel time. In the work of Banvait et al., the frozen-time MPC implements the same amount of power demand as that of the current step in the entire forecast range, but its performance depends largely on the drive cycle and length of the prediction horizon. [46] Wang et al. first employed an MPC to address the energy management problem in a hybrid electric tracked bulldozer, which reached over 98% of the fuel optimality of DP in standard working conditions. [47] Santucci et al. dealt with the coupling of a battery and a super capacitor for reducing battery ageing when the system was working in harsh climate conditions. [48] Similar to the work of Zhang et al. [49] and Golchoubian et al. [50], this MPC assumes it accurately knows all the future information, so it is challenging to operate it in real-time due to this unrealistic assumption. Recently, a considerable amount of successful cases emerged, indicating a type of modern optimization method to integrate artificial intelligence (AI) into the MPC frame. Liu et al. proposed a velocity predictor with fuzzy encoding to improve its prediction accuracy. [51] Nevertheless, such learning-based prediction methods rely on historical driving data, wherein once it has finished the training, the structure and weight of the prediction model cannot be changed. Other types of AI-based predictive model contain Bayesian algorithms, [52] fuzzy cognitive maps, [53] and auto-regressive models [54, 55]: they have a strong ability in modelling, learning, and predicting.

Unlike the MPC, the model-free control method i.e. reinforcement learning with model-free prediction uses the following steps: 1) what to do; 2) how to map situations to actions; 3) so as to maximize a numerical reward signal, estimate the value function of an unknown Markov

decision process. The learner will not be told what actions to take, but must try to discover which actions will get the most reward. [56] In 2012, Hsu et al. introduced a Q-learning algorithm to assist the power management of hybrid bicycles. [57] They quantify safety and comfort goals as an improvement in riding quality and battery energy utilization. Simulation results show that the quality-of-riding and energy-related objectives can be improved by 24% and 50%, respectively. Furthermore, Yue et al. proposed a temporal difference TD(λ)-learning-based online strategy to optimally control the energy flow in the ultracapacitor and battery of HEVs [58]. In the work of Fang et al., a TD(λ) learning algorithm is applied for training and learning the optimal Q-function using collected historical driving data. [59] The reinforcement learning based control implemented on hybrid electric buses aims to improve fuel economy and reduce emissions. Similarly, Lin et al. constructed a power management system in an advanced vehicle simulator (ADVISOR). [60] The deduced strategy is compared with the rule-based policy over various driving cycles and achieves up to 60.8% fuel reduction. However, how to achieve a series of operations that senses the states from the environment, taking particular actions, and acquiring goal-directed rewards, those are huge challenges. [56]

2.3. Driver-oriented Optimization Approaches For HEV Energy Management

Today, benefiting from informatics' expansion, plenty of optimization methods via information fusion for hybrid vehicles are appearing. As the primary decision-maker of modern vehicles, the human driver plays an important role in driving safety as well as in eco-driving. Therefore, a vehicle control strategy that seeks a highly optimized performance which

requires optimizing the system composed of the vehicle and the driver, needs to explicitly consider driver behaviour. [61] The main challenge is how to exploit driver-related data to precisely describe driving behaviour and establish a relationship with the vehicle's system. Therefore, a relevant literature survey is carried out from two categories: 1) driving behaviour modelling and 2) driver-oriented energy management. The summary and future trends will be listed at the end.

2.3.1. DRIVING BEHAVIOUR MODELLING

Driving behaviours differ among drivers. They differ in the way they press the gas and brake pedals; the way they turn the steering wheel; and how far away they keep when following a vehicle. [62] Consequently, energy management is anticipated to be tailored for each driver according to individual driving behaviours. To realise this goal, one way is to assist each driver by controlling a vehicle based on a driver model representing the typical driving patterns of the target driver. [63] Driver models for individual drivers or a subset of drivers classified based on their driving behaviours can be trained in offline or online mode. A vehicle controller needs to choose an appropriate driver model for supporting the target driver, by distinguishing the driver or assigning the model that fits his/her driving behaviours.

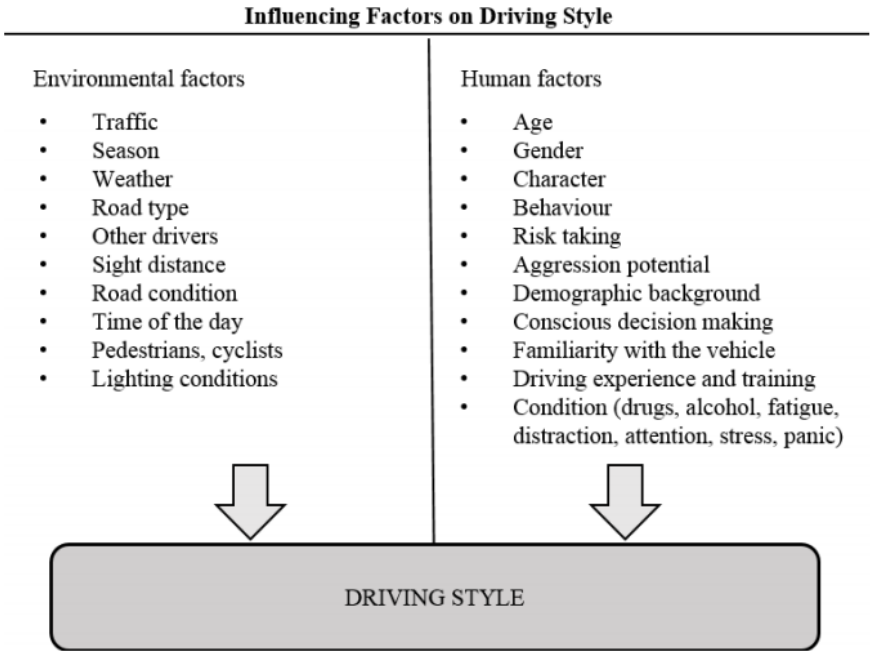

Fig. 2-1. Influencing factors on driving style [61]

Various definitions of a driver's driving style are caused by many influencing factors and possible explanations for the driver's reaction. Martinez et al. summarized some of these variables listed in Fig. 2-1. Given the large numbers and most factors that are difficult to measure, it is unreasonable to expect control over all factors. A simplified method of actual diving style identification focuses on its effect on a single number, for example: fuel consumption, [64, 65] average speed or range. However, these indicators may be oversimplified to assess different levels of traffic congestion and cannot represent a complete driving situation.

In contrast to previously, Augustynowicz classified driving behaviour in a range within (−1, 1); with −1, 0 and 1 being mild, normal and aggressive respectively. [66] This criterion is usually formulated based on the relative fuel consumption or overall efficiency rather than the

driver's level of aggressiveness. Manzoni et al. [67] used an estimated value of the fuel consumed during the trip and compared it with a benchmarked value, to calculate the percentage of excessive consumption, indicating additional costs. Neubauer and Wood [68] used fuel consumption to obtain vehicle efficiency as an indicator of driving behaviour. Similarly, Corti et al. [69] used an energy-oriented cost function to evaluate the driver's driving style, which estimated the excessive consumption of power. However, such classification methods based on whether discrete classes or continuous indexing are suitable for HEV energy management need to be further investigated.

In terms of driving style recognition algorithms, Murphey et al. [70] presented a similar approach based on counting aggressive manoeuvres. The final score is based on a percentage, where 'stays calm' is in the range below 50%, and 'stays aggressive' is in the range above 100%, otherwise between 50% and 100% the score is classed as normal. [70] Alternatively, for the classification of driving events, driving style can be grouped according to the fuel already contained or the total energy consumption. [67, 69] The use of the RB algorithm unifies simplicity, is easy to explain and implement, but limits the number of parameters that can be managed. Larger sets of variables generate unnecessarily complex rules that can be substituted by fuzzy logic (FL) maps. Syed et al. proposed an FL algorithm to evaluate optimal operation of the pedals in HEVs. [71] The algorithm can monitor the operation of the gas pedal and brake pedal, and then can calculate the appropriate correction value and produce tactile feedback to the driver. The author claims that fuel consumption can be reduced by at least 3.5% with the mildest driving in the simulated environment without compromising vehicle

performance. [71] Although the RB and FL algorithms unify the acceptable results by achieving simplicity, the quality of the classification is closely related to the choice of threshold.

The threshold definition in the RB algorithm decides the robustness of the results and requires a lot of data analysis. Unsupervised algorithms do not need to understand the underlying process. In the work of Miyajima et al., a Gaussian mixture model was implemented based on the analysis of car-following behaviour and pedal operation spectrum. [63] The car-following identifiability of the model is 69%, and the classification rate of the pedal spectrum analysis in the simulated environment is 89.6%, and in the field test is 76.8%. [63] Mudgal et al. implemented a multi-layer Bayesian regression model to characterize driving style at a roundabout. [72] The unsupervised algorithm has proved its applicability to driving style identification. However, the output needs to be guided based on the number of interpretations and clusters. In addition, the classification performance may be worse than the supervised algorithm. Supervised algorithms represent understanding the driving style of the data used for training. Augustynowicz applied an Elman neural network (NN) to identify driving behaviour by speed and accelerator pedal position. [66] The Markov model has also successfully achieved driving style recognition. Guardiola et al. defended the advantages of combining the Markov model with the Monte Carlo application, [73] thereby generating random patterns based on previous data in the driving style representation. Pentland and Liu defended the adaptability of the dynamic Markov model to driving style, which was supported by the fact that it is best to capture human movements through a series of control steps. [74]

2.3.2. DRIVER-ORIENTED ENERGY MANAGEMENT

Driver information is not easily exploited by classical control strategies, but a new framework for a driver-machine system appears to be appropriate for this purpose. Most of the literature assumes that the optimal velocity at a higher level can be accurately followed and then determines the corresponding power split. In fact, the driver may not follow the optimal velocity precisely, since the uncertainty of driver behaviour (e.g. lane changing, disposition) may affect the velocity tracking performance and further contribute to fuel consumption.

In the work of Zhang et al., a novel method for driving blocks' classification is proposed to classify the driving pattern into different groups, as opposed to using the existing unbroken driving cycles. [75] One concern is that as the driving cycle grows, more driving blocks need to be classified. Langari et al. designed a driving condition recognition component which uses long-term and short-term numerical characteristics of the driving cycle, to evaluate the driving conditions, the driving style of the driver and the operation mode of HEVs. [76] Another alternative method involves a self-reporting driving behaviour questionnaire designed by Zhang et al. for offline cluster analysis. [77] Martinelli et al. proposed a machine-learning-based method to continuously characterize the driver by data analysis for built-in vehicle sensors. They found with the features such as cold start-up, cruising down the motorway and idling in heavy traffic they were able to discriminate the car owner by an impostor. [78] Adaptability can be also added into the ECMS in another form, which is the driving style recognition employed by Yang et al. [79] and Tian et al. [80] Differing from the work of Yang, the nearest neighbour method needs labelled learning materials for training purposes, as

opposed to statistical classification. An interesting piece of work by Gu et al. proposed a pedestrian-aware engine management strategy that considers the environmental effects of the vehicles on pedestrians outside of the vehicles. [81] The strategy helps EMSs switch to EV mode when a cloud server informs them that the density of pedestrians has become higher. As applied in [82], an accelerator pedal opening and its change rate are considered as inputs of a driving style recognizer, to define a driving style factor for optimal control of plug-in HEVs. Driver models using fuzzy sets can be well integrated with energy management. However, how to establish the mapped relationship between driving style and control actions is still a big challenge.

A highly dynamic driver model is not only dependent on historical driving data, but also must consider the current driving data. It utilizes up-to-date driving segments of the driver to model, thus ensuring an accurate judgment of prediction trends. Through real-time or regularly updating driver models, their reliability can be relatively guaranteed. The Markov decision process, also called stochastic DP is mainly used to model and solve dynamic decision-making problems. [83] In the work of Liu et al. [84, 85] an on-board learning algorithm for Markov chain models is engaged to produce transition probability matrices of power requirements. Differing from the work of [85] fuzzy encoding technology is applied for Markov chain models to add in ports of continuous intervals in reinforcement-learning-based energy management. [84] Cairano et al. [86] developed a self-learning stochastic MPC for driver-oriented predictive control of an HEV; where using quadratic programming, larger state dimension models than in stochastic DP can be reconfigured in real-time to adapt to changes in driving behaviours.

Bichi et al. used a linear filtering algorithm to estimate a transformation possibility matrix. [87] The driver model is learned in real-time, hence permitting the control algorithm to adapt to various drivers and drivers' behaviours. Gomozov et al. introduced the non-uniform sampling time concept in MPC strategies that accepts a mixture of both conditions: fast dynamics control and the long-term prediction of power demand. [88] From the results, the proposed MPC strategy is able to more effectively balance the power and energy of the dual energy storage system and lessen the pressure on the battery. Obviously, the price of the improvement is mainly to sacrifice computing resources in exchange for high-precision state information. As indicated by Moore's Law, it is anticipated this relation can be gradually improved and perform on the actual on-board controller of HEVs for real-time energy saving in the near future.

2.4. SUMMARY

According to this exhaustive analysis, great efforts have been made in the field of EMS optimization for HEVs, following the three aspects of: 1) offline optimization approaches; 2) online optimization approaches; and 3) driver-oriented optimization approaches. To further improve mobility, fuel economy, driving performance, and safety, the author summarises a series of future directions based on the state of the art. Thus, future trends and challenges are recommended from the following four perspectives to encourage more innovative ideas.

1) The MPC fashion combining a velocity trajectory predictor and an energy-flow splitter has great potential for HEV energy management. However, its performance is mainly restricted by the accuracy of the predictive models, the length of the predictive horizon,

and the optimization ability of control algorithms. It still takes a lot of effort to promote them.

2) The human factor has long been ignored in the development of control strategies. At present, it has become one of the core issues hindering the performance of hybrid vehicles. A driver-oriented supervisory control framework with a driver-machine accessible communication channel is worth exploring. There is an opportunity to reveal the interaction process between human drivers and hybrid powertrains and then to create a personalized energy-saving control strategy.

3) Computational intelligence (CI), i.e. fuzzy systems, neural networks, and evolutionary computation is a promising technology for driver-machine systems. Since the driver can feedback into the learning loop of the vehicle controller, this technology can help further improve the robustness and global optimality. Although recent advances in CI in the computer industry are giving momentum to human-in-the-loop, academia awareness of such a new direction is still limited, and its application is even more limited.

REFERENCES

[1] C. Zhang, A. Vahidi, P. Pisu, X. Li, and K. Tennant, "Role of terrain preview in energy management of hybrid electric vehicles," *IEEE Trans. Veh. Technol.*, vol. 59, no. 3, pp. 1139–1147, 2010, doi: 10.1109/TVT.2009.2038707.

[2] T. B. Sheridan, *Telerobotics , Automation and Human Supervisory Control*. MIT Press, 1992.

[3] F. R. Salmasi, "Control strategies for hybrid electric vehicles: Evolution, classification, comparison, and future trends," *IEEE Trans. Veh. Technol.*, vol. 56, no. 5 I, pp. 2393–2404, 2007, doi: 10.1109/TVT.2007.899933.

[4] S. Il Jeon, S. T. Jo, Y. Il Park, and J. M. Lee, "Multi-mode driving control of a parallel hybrid electric vehicle using driving pattern recognition," *J. Dyn. Syst. Meas. Control. Trans. ASME*, vol. 124, no. 1, pp. 141–149, 2002, doi: 10.1115/1.1434264.

[5] K. T. Chau and Y. S. Wong, “Overview of power management in hybrid electric vehicles,” *Energy Convers. Manag.*, vol. 43, no. 15, pp. 1953–1968, Jan. 2002, doi: 10.1016/S0196-8904(01)00148-0.

[6] A. M. Phillips, M. Jankovic, and K. E. Bailey, “Vehicle system controller design for a hybrid electric vehicle,” *IEEE Conf. Control Appl. - Proc.*, vol. 1, pp. 297–302, 2000, doi: 10.1109/cca.2000.897440.

[7] Y. Wang, Z. Sun, and Z. Chen, “Energy management strategy for battery/supercapacitor/fuel cell hybrid source vehicles based on finite state machine,” *Appl. Energy*, vol. 254, no. December 2018, p. 113707, 2019, doi: 10.1016/j.apenergy.2019.113707.

[8] K. Çağatay Bayindir, M. A. Gözüküçük, and A. Teke, “A comprehensive overview of hybrid electric vehicle: Powertrain configurations, powertrain control techniques and electronic control units,” *Energy Convers. Manag.*, vol. 52, no. 2, pp. 1305–1313, 2011, doi: 10.1016/j.enconman.2010.09.028.

[9] H. Tian, X. Wang, Z. Lu, Y. Huang, and G. Tian, “Adaptive Fuzzy Logic Energy Management Strategy Based on Reasonable SOC Reference Curve for Online Control of Plug-in Hybrid Electric City Bus,” *IEEE Trans. Intell. Transp. Syst.*, vol. 19, no. 5, pp. 1607–1617, 2018, doi: 10.1109/TITS.2017.2729621.

[10] J. Solano, R. I. John, D. Hissel, and M. Péra, “A survey-based type-2 fuzzy logic system for energy management in hybrid electrical vehicles,” *Inf. Sci. (Ny).*, vol. 190, pp. 192–207, 2012, doi: 10.1016/j.ins.2011.12.013.

[11] J. Solano Martínez *et al.*, “Experimental validation of a type-2 fuzzy logic controller for energy management in hybrid electrical vehicles,” *Eng. Appl. Artif. Intell.*, vol. 26, no. 7, pp. 1772–1779, 2013, doi: 10.1016/j.engappai.2012.12.008.

[12] J. M. Garibaldi and S. Member, “The Need for Fuzzy AI,” *IEEE/CAA J. Autom. Sin.*, vol. 6, no. 3, pp. 610–622, 2019, doi: 10.1109/JAS.2019.1911465.

[13] H. Khayyam and A. Bab-hadiashar, “Adaptive intelligent energy management system of plug-in hybrid electric vehicle,” *Energy*, vol. 69, pp. 319–335, 2014, doi: 10.1016/j.energy.2014.03.020.

[14] R. Zhang and J. Tao, “GA-Based Fuzzy Energy Management System for FC / SC-Powered HEV Considering H2 Consumption and Load Variation,” *IEEE Trans. Fuzzy Syst.*, vol. 26, no. 4, pp. 1833–1843, 2018, doi: 10.1109/TFUZZ.2017.2779424.

[15] E. Kamal, “Hierarchical Energy Optimization Strategy and Its Integrated Reliable Battery Fault Management for Hybrid Hydraulic-Electric Vehicle,” *IEEE Trans. Veh. Technol.*, vol. 67, no. 5, pp. 3740–3754, 2018, doi: 10.1109/TVT.2018.2805353.

[16] C. Lv, X. Hu, A. Sangiovanni-, Y. Li, C. M. Martinez, and D. Cao, “Driving-Style-Based Co-Design Optimization of an Automated Electric Vehicle : A Cyber- Physical System Approach,” *IEEE Trans. Ind. Electron.*, vol. PP, no. c, p. 1, 2018, doi: 10.1109/TIE.2018.2850031.

[17] Z. Chen, C. C. Mi, J. Xu, X. Gong, and C. You, “Energy management for a power-split plug-in hybrid electric vehicle based on dynamic programming and neural networks,” *IEEE Trans. Veh. Technol.*, vol. 63, no. 4, pp. 1567–1580, 2014, doi: 10.1109/TVT.2013.2287102.

[18] L. Feldkamp, M. A. Nasr, and I. V. Kolmanovsky, “Recurrent neural network training for energy management of a mild hybrid electric vehicle with an ultra-capacitor,” *2009 IEEE Work. Comput. Intell. Veh. Veh. Syst. CIVVS 2009 - Proc.*, pp. 29–36, 2009, doi: 10.1109/CIVVS.2009.4938720.

[19] H. Wang, Y. Huang, H. He, C. Lv, W. Liu, and A. Khajepour, “Energy Management of Hybrid Electric Vehicles,” in *Modeling, Dynamics, and Control of Electrified Vehicles*, Elsevier Inc., 2018, pp. 159–206.

[20] R. Bellman, “on the theory of dynamics programming,” *Proc. Natl. Acad. Sci. U. S. A.*, vol. 38, no. 8, pp. 716–719, 1952.

[21] R. Bellman, “Dynamic Programming,” *Science (80-.).*, vol. 153, no. 3731, pp. 34–37, 1966.

[22] L. V. Pérez, G. R. Bossio, D. Moitre, and G. O. García, “Optimization of power management in an hybrid electric vehicle using dynamic programming,” *Math. Comput. Simul.*, vol. 73, no. 1-4 SPEC. ISS., pp. 244–254, 2006, doi: 10.1016/j.matcom.2006.06.016.

[23] M. Ansarey, M. Shariat Panahi, H. Ziarati, and M. Mahjoob, “Optimal energy management in a dual-storage fuel-cell hybrid vehicle using multi-dimensional dynamic programming,” *J. Power Sources*, vol. 250, pp. 359–371, 2014, doi: 10.1016/j.jpowsour.2013.10.145.

[24] J. Peng, H. He, and R. Xiong, “Rule based energy management strategy for a series – parallel plug-in hybrid electric bus optimized by dynamic programming,” *Appl. Energy*, vol. 185, pp. 1633–1643, 2017, doi: 10.1016/j.apenergy.2015.12.031.

[25] Z. Chen, C. C. Mi, J. Xu, and S. Member, “Energy Management for a Power-Split Plug-in Hybrid Electric Vehicle Based on Dynamic Programming and Neural Networks,” *IEEE Trans. Veh. Technol.*, vol. 63, no. 4, pp. 1567–1580, 2014.

[26] C. Vagg, C. J. Brace, S. Akehurst, and L. Ash, “Minimizing battery stress during hybrid electric vehicle control design: Real world considerations for model-based control development,” *2013 9th IEEE Veh. Power Propuls. Conf. IEEE VPPC 2013*, pp. 329–334, 2013, doi: 10.1109/VPPC.2013.6671713.

[27] L. Johannesson, M. Åsbogård, and B. Egardt, “Assessing the Potential of Predictive Control for Hybrid Vehicle Powertrains Using Stochastic Dynamic Programming,” *IEEE Trans. Intell. Transp. Syst.*, vol. 8, no. 1, pp. 71–83, 2007.

[28] C. Vagg, S. Akehurst, C. J. Brace, and L. Ash, “Stochastic Dynamic Programming in the Real-World Control of Hybrid Electric Vehicles,” *IEEE Trans. Control Syst. Technol.*, vol. 24, no. 3, pp. 853–866, 2016, doi: 10.1109/TCST.2015.2498141.

[29] I. V Kolmanovsky, “Game Theory Controller for Hybrid Electric Vehicles,” vol. 22, no. 2, pp. 652–663, 2014, doi: 10.1109/TCST.2013.2254597.

[30] X.-S. Yang, “Introduction to Algorithms,” in *Nature-Inspired Optimization Algorithms*, Elsevier, 2014, pp. 1–21.

[31] Kennedy, James, and Russell Eberhart. "Particle swarm optimization." Proceedings of ICNN'95-International Conference on Neural Networks. Vol. 4. IEEE, 1995.

[32] J. Soares, T. Sousa, H. Morais, Z. Vale, B. Canizes, and A. Silva, “Application-Specific Modified Particle Swarm Optimization for energy resource scheduling considering vehicle-to-grid,” *Appl. Soft Comput. J.*, vol. 13, no. 11, pp. 4264–4280, 2013, doi: 10.1016/j.asoc.2013.07.003.

[33] I. Rahman, P. M. Vasant, B. S. M. Singh, and M. Abdullah-Al-Wadud, “On the performance of accelerated particle swarm optimization for charging plug-in hybrid electric vehicles,” *Alexandria Eng. J.*, vol. 55, no. 1, pp. 419–426, 2016, doi: 10.1016/j.aej.2015.11.002.

[34] K. Kim and P. R. Kumar, “Cyber – Physical Systems : A Perspective at the Centennial,” *Proc. IEEE*,

vol. 100, pp. 1287–1308, 2012, doi: 10.1109/JPROC.2012.2189792.

[35] P. P. J. Van Den Bosch and D. B. Kok, “Online Energy Management for Hybrid Electric Vehicles,” *IEEE Trans. Veh. Technol.*, vol. 57, no. 6, pp. 3428–3440, 2008.

[36] G. Paganelli, T. M. Guerra, S. Delprat, J. J. Santin, M. Delhom, and E. Combes, “Simulation and assessment of power control strategies for a parallel hybrid car,” *Proc. Inst. Mech. Eng. Part D J. Automob. Eng.*, vol. 214, no. 7, pp. 705–717, 2000, doi: 10.1243/0954407001527583.

[37] P. Rodatz, G. Paganelli, A. Sciarretta, and L. Guzzella, “Optimal power management of an experimental fuel cell/supercapacitor- powered hybrid vehicle,” *Control Eng. Pract.*, vol. 13, no. 1, pp. 41–53, 2005, doi: 10.1016/j.conengprac.2003.12.016.

[38] A. Chasse and A. Sciarretta, “Supervisory control of hybrid powertrains: An experimental benchmark of offline optimization and online energy management,” *Control Eng. Pract.*, vol. 19, no. 11, pp. 1253–1265, 2011, doi: 10.1016/j.conengprac.2011.04.008.

[39] C. Musardo, G. Rizzoni, Y. Guezennec, and B. Staccia, “A-ECMS: An adaptive algorithm for hybrid electric vehicle energy management,” *Eur. J. Control*, vol. 11, no. 4–5, pp. 509–524, 2005, doi: 10.3166/ejc.11.509-524.

[40] A. Rezaei, J. B. Burl, B. Zhou, and M. Rezaei, “A New Real-Time Optimal Energy Management Strategy for Parallel Hybrid Electric Vehicles,” *IEEE Trans. Control Syst. Technol.*, vol. 27, no. 2, pp. 830–837, 2019, doi: 10.1109/TCST.2017.2775184.

[41] A. Rezaei, J. B. Burl, and B. Zhou, “Estimation of the ECMS Equivalent Factor Bounds for Hybrid Electric Vehicles,” *IEEE Trans. Control Syst. Technol.*, vol. 26, no. 6, pp. 2198–2205, 2018, doi: 10.1109/TCST.2017.2740836.

[42] A. Sciarretta *et al.*, “A control benchmark on the energy management of a plug-in hybrid electric vehicle,” *Control Eng. Pract.*, vol. 29, pp. 287–298, 2014, doi: 10.1016/j.conengprac.2013.11.020.

[43] C. Sun, F. Sun, and H. He, “Investigating adaptive-ECMS with velocity forecast ability for hybrid electric vehicles,” *Appl. Energy*, vol. 185, pp. 1644–1653, 2017, doi: 10.1016/j.apenergy.2016.02.026.

[44] S. J. Qin and T. A. Badgwell, “A survey of industrial model predictive control technology,” *Control Eng. Pract.*, vol. 11, pp. 733–764, 2003, doi: 10.1016/S0967-0661(02)00186-7.

[45] S. Kachroudi, M. Grossard, and N. Abroug, “Predictive driving guidance of full electric vehicles using particle swarm optimization,” *IEEE Trans. Veh. Technol.*, vol. 61, no. 9, pp. 3909–3919, 2012, doi: 10.1109/TVT.2012.2212735.

[46] H. Banvait, S. Member, and J. Hu, “Energy Management Control of Plug-in Hybrid Electric Vehicle using Hybrid Dynamical Systems,” *IEEE Trans. Intell. Transp. Syst.*, pp. 1–13, 2013.

[47] H. Wang, Y. Huang, A. Khajepour, and Q. Song, “Model predictive control-based energy management strategy for a series hybrid electric tracked vehicle,” *Appl. Energy*, vol. 182, pp. 105–114, 2016, doi: 10.1016/j.apenergy.2016.08.085.

[48] A. Santucci, A. Sorniotti, and C. Lekakou, “Power split strategies for hybrid energy storage systems for vehicular applications,” *J. Power Sources*, vol. 258, pp. 395–407, 2014, doi: 10.1016/j.jpowsour.2014.01.118.

[49] S. Zhang, R. Xiong, and F. Sun, “Model predictive control for power management in a plug-in

hybrid electric vehicle with a hybrid energy storage system q," *Appl. Energy*, vol. 185, pp. 1654–1662, 2017, doi: 10.1016/j.apenergy.2015.12.035.

[50] P. Golchoubian and N. L. Azad, "Real-Time Nonlinear Model Predictive Control of a Battery-Supercapacitor Hybrid Energy Storage System in Electric Vehicles," *IEEE Trans. Veh. Technol.*, vol. 66, no. 11, pp. 9678–9688, 2017, doi: 10.1109/TVT.2017.2725307.

[51] T. Liu, X. Hu, S. E. Li, and D. Cao, "Reinforcement Learning Optimized Look-Ahead Energy Management of a Parallel Hybrid Electric Vehicle," *IEEE/ASME Trans. MECHATRONICS*, vol. 22, no. 4, pp. 1497–1507, 2017.

[52] J. Unger, M. Kozek, and S. Jakubek, "Nonlinear model predictive energy management controller with load and cycle prediction for non-road HEV," *Control Eng. Pract.*, vol. 36, pp. 120–132, 2015, doi: 10.1016/j.conengprac.2014.12.001.

[53] W. Stach, L. A. Kurgan, and W. Pedrycz, "Numerical and Linguistic Prediction of Time Series With the Use of Fuzzy Cognitive Maps," *IEEE Trans. Fuzzy Syst.*, vol. 16, no. 1, pp. 61–72, 2008.

[54] J. Jing, D. Filev, A. Kurt, E. Özatay, J. Michelini, and Ü. Özgüner, "Vehicle Speed Prediction using a Cooperative Method of Fuzzy Markov Model and Auto-regressive Model," in *Intelligent Vehicles Symposium (IV), 2017 IEEE*, 2017, no. Iv, pp. 881–886.

[55] K. Vatanparvar, S. Faezi, I. Burago, M. Levorato, M. Abdullah, and A. Faruque, "Extended Range Electric Vehicle with Driving Behavior Estimation in Energy Management," *IEEE Trans. SMART GRID*, vol. 14, no. 8, pp. 1–10, 2018, doi: 10.1109/TSG.2018.2815689.

[56] R. S. Sutton and A. G. Barto, *Reinforcement Learning: An Introduction*. The MIT Press, 2017.

[57] R. C. Hsu, C. Liu, and D. Chan, "A Reinforcement-Learning-Based Assisted Power Management With QoR Provisioning for Human – Electric Hybrid Bicycle," *EEE Trans. Ind. Electron.*, vol. 59, no. 8, pp. 3350–3359, 2012.

[58] S. Yue, Y. Wang, Q. Xie, D. Zhu, and M. Pedram, "Model-Free Learning-Based Online Management of Hybrid Electrical Energy Storage Systems in Electric Vehicles," *IECON 2014 - 40th Annu. Conf. IEEE Ind. Electron. Soc.*, pp. 3142–3148, doi: 10.1109/IECON.2014.7048959.

[59] Y. Fang, C. Song, B. Xia, and Q. Song, "An Energy Management Strategy for Hybrid Electric Bus Based on Reinforcement Learning," *27th Chinese Control Decis. Conf. (2015 CCDC)*, pp. 4973–4977, 2015, doi: 10.1109/CCDC.2015.7162814.

[60] X. Lin, Y. Wang, P. Bogdan, N. Chang, and M. Pedram, "Reinforcement Learning Based Power Management for Hybrid Electric Vehicles Categories and Subject Descriptors," *2014 IEEE/ACM Int. Conf. Comput. Des.*, pp. 33–38, 2014, doi: 10.1109/ICCAD.2014.7001326.

[61] C. M. Martinez, M. Heucke, F. Wang, B. Gao, and D. Cao, "Driving Style Recognition for Intelligent Vehicle Control and Advanced Driver Assistance : A Survey," *IEEE Trans. Intell. Transp. Syst.*, vol. 19, no. 3, pp. 666–676, 2018, doi: 10.1109/TITS.2017.2706978.

[62] Fancher, Paul, et al. Intelligent cruise control field operational test. No. UMTRI-97-11. United States. National Highway Traffic Administration, 1998.

[63] B. C. Miyajima *et al.*, "Driver Modeling Based on Driving Behavior and Its Evaluation in Driver Identification," 2007.

[64] B. V. Padma Rajan, A. McGordon, and P. A. Jennings, "An investigation on the effect of driver style and driving events on energy demand of a PHEV," *World Electr. Veh. J.*, vol. 5, no. 1, pp.

173–181, 2012, doi: 10.3390/wevj5010173.

[65] J. Neubauer and E. Wood, “Thru-life impacts of driver aggression, climate, cabin thermal management, and battery thermal management on battery electric vehicle utility,” *J. Power Sources*, vol. 259, pp. 262–275, 2014, doi: 10.1016/j.jpowsour.2014.02.083.

[66] A. Augustynowicz, “Preliminary classification of driving style with objective rank method,” *Int. J. Automot. Technol.*, vol. 10, pp. 607–610, 2009, doi: https://doi.org/10.1007/s12239-009-0071-8.

[67] V. Manzoni, A. Corti, P. De Luca, and S. M. Savaresi, “Driving style estimation via inertial measurements,” *IEEE Conf. Intell. Transp. Syst. Proceedings, ITSC*, pp. 777–782, 2010, doi: 10.1109/ITSC.2010.5625113.

[68] J. S. Neubauer and E. Wood, “Accounting for the variation of driver aggression in the simulation of conventional and advanced vehicles,” *SAE Tech. Pap.*, vol. 2, 2013, doi: 10.4271/2013-01-1453.

[69] A. Corti, C. Ongini, M. Tanelli, and S. M. Savaresi, “Quantitative driving style estimation for energy-oriented applications in road vehicles,” *Proc. - 2013 IEEE Int. Conf. Syst. Man, Cybern. SMC 2013*, pp. 3710–3715, 2013, doi: 10.1109/SMC.2013.632.

[70] Y. L. Murphey, R. Milton, and L. Kiliaris, “Driver’s style classification using jerk analysis,” *2009 IEEE Work. Comput. Intell. Veh. Veh. Syst. CIVVS 2009 - Proc.*, pp. 23–28, 2009, doi: 10.1109/CIVVS.2009.4938719.

[71] F. U. Syed, D. Filev, and H. Ying, “Fuzzy rule-based driver advisory system for fuel economy improvement in a hybrid electric vehicle,” *Annu. Conf. North Am. Fuzzy Inf. Process. Soc. - NAFIPS*, pp. 178–183, 2007, doi: 10.1109/NAFIPS.2007.383833.

[72] A. Mudgal, S. Hallmark, A. Carriquiry, and K. Gkritza, “Driving behavior at a roundabout: A hierarchical Bayesian regression analysis,” *Transp. Res. Part D Transp. Environ.*, vol. 26, pp. 20–26, 2014, doi: 10.1016/j.trd.2013.10.003.

[73] C. Guardiola, B. Pla, D. Blanco-Rodríguez, and A. Reig, “Modelling driving behaviour and its impact on the energy management problem in hybrid electric vehicles,” *Int. J. Comput. Math.*, vol. 91, no. 1, pp. 147–156, 2014, doi: 10.1080/00207160.2013.829567.

[74] A. Pentland and L. Andrew, “Modeling and prediction of human behavior,” *Neural Comput.*, vol. 11, no. 1, pp. 229–242, 1999, doi: 10.1162/089976699300016890.

[75] S. Zhang and R. Xiong, “Adaptive energy management of a plug-in hybrid electric vehicle based on driving pattern recognition and dynamic programming,” *Appl. Energy*, vol. 155, pp. 68–78, 2015, doi: 10.1016/j.apenergy.2015.06.003.

[76] R. Langari, S. Member, and J. Won, “Intelligent Energy Management Agent for a Parallel Hybrid Vehicle — Part I : System Architecture and Design of the Driving Situation Identification Process,” *IEEE Trans. Veh. Technol.*, vol. 54, no. 3, pp. 925–934, 2005.

[77] Y. Zhang *et al.*, “Optimal energy management strategy for parallel plug-in hybrid electric vehicle based on driving behavior analysis and real time traffic information prediction,” *Mechatronics*, vol. 46, pp. 177–192, 2017, doi: 10.1016/j.mechatronics.2017.08.008.

[78] F. Martinelli, F. Mercaldo, A. Orlando, V. Nardone, A. Santone, and A. K. Sangaiah, “Human behavior characterization for driving style recognition in vehicle system,” *Comput. Electr. Eng.*,

vol. 0, pp. 1–16, 2018, doi: 10.1016/j.compeleceng.2017.12.050.

[79] S. Yang, W. Wang, F. Zhang, Y. Hu, and J. Xi, “Driving-style-oriented adaptive equivalent consumption minimization strategies for HEVs,” *IEEE Trans. Veh. Technol.*, vol. 67, no. 10, pp. 9249–9261, 2018, doi: 10.1109/TVT.2018.2855146.

[80] X. Tian, Y. Cai, X. Sun, Z. Zhu, and Y. Xu, “An adaptive ECMS with driving style recognition for energy optimization of parallel hybrid electric buses,” *Energy*, vol. 189, p. 116151, 2019, doi: 10.1016/j.energy.2019.116151.

[81] Y. Gu, M. Liu, J. Naoum-sawaya, E. Crisostomi, G. Russo, and R. Shorten, “Pedestrian-Aware Engine Management Strategies for Plug-In Hybrid Electric Vehicles,” vol. 19, no. 1, pp. 92–101, 2018.

[82] Q. Guo, Z. Zhao, P. Shen, X. Zhan, and J. Li, “Adaptive optimal control based on driving style recognition for plug-in hybrid electric vehicle,” *Energy*, vol. 186, p. 115824, 2019, doi: 10.1016/j.energy.2019.07.154.

[83] R. Bellman, “A Markovian decision process,” *J. Math. Mech.*, pp. 679–684, 1957.

[84] T. Liu and X. Hu, “A Bi-Level Control for Energy Efficiency Improvement of a Hybrid Tracked Vehicle,” *IEEE Trans. Ind. Informatics*, vol. 14, no. 4, pp. 1616–1625, 2018, doi: 10.1109/TII.2018.2797322.

[85] T. Liu, B. Wang, and C. Yang, “Online Markov Chain-based energy management for a hybrid tracked vehicle with speedy Q-learning,” *Energy*, vol. 160, pp. 544–555, 2018, doi: 10.1016/j.energy.2018.07.022.

[86] S. Di Cairano, D. Bernardini, A. Bemporad, and I. V Kolmanovsky, “Stochastic MPC With Learning for Driver-Predictive Vehicle Control and its Application to HEV Energy Management,” vol. 22, no. 3, pp. 1018–1031, 2014.

[87] M. Bichi, G. Ripaccioli, S. Di Cairano, D. Bernardini, A. Bemporad, and I. V. Kolmanovsky, “Stochastic model predictive control with driver behavior learning for improved powertrain control,” *Proc. IEEE Conf. Decis. Control*, pp. 6077–6082, 2010, doi: 10.1109/CDC.2010.5717791.

[88] O. Gomozov, J. P. F. Trovao, X. Kestelyn, and M. R. Dubois, “Adaptive Energy Management System Based on a Real-Time Model Predictive Control with Nonuniform Sampling Time for Multiple Energy Storage Electric Vehicle,” *IEEE Trans. Veh. Technol.*, vol. 66, no. 7, pp. 5520–5530, 2017, doi: 10.1109/TVT.2016.2638912.

CHAPTER 3

RESEARCH METHODOLOGY AND EXPERIMENTAL FACILITIES

This PhD thesis focuses on the development of driver-oriented intelligent control methodology for a medium passenger vehicle with a series-parallel hybrid drivetrain. The methodology attempts to incorporate driver dynamics into the supervisory control system; which offers an additional possibility for further improving mobility, fuel economy, driving performance, and safety. This chapter starts with introducing interaction topology in energy management of hybrid electric vehicles (HEVs). This is followed by the research technical route, indicating research modules and the development process in the PhD research. Then, a system-level control-oriented model of the target vehicle including vehicle dynamics and powertrain components is analysed. Finally, experimental facilities for driving simulation and hardware-in-the-loop tests are presented.

3.1. RESEARCH METHODOLOGY

The research methodology for this PhD study is determined from investigating interaction topology in HEV energy management. Here, conventional and driver-oriented interaction forms will be described, followed by their characteristics and drawbacks. According to these drawbacks, a series of goals are formulated, resulting in a technical route intending to lead to their achievement.

3.1.1. INTERACTION TOPOLOGY IN HEV ENERGY MANAGEMENT

Due to the shortage of computing power in the past, the ECU can only provide a limited development platform for vehicles, resulting in energy management systems (EMSs) with simple control logic. Fig. 3-1 shows an interactive process of conventional EMSs, in which state information is environment condition and driver's response to the environment that will be mixed and sent to a conventional EMS for operating energy management. However, conventional EMSs do not have the ability to extract valuable references from a large amount of unknown information. Due to having no reliable information to support, predictivity and adaptability of the system will be seriously restricted. This could be one reason why vehicles with conventional EMSs pass the laboratory test but still give a poor performance during real-world driving.

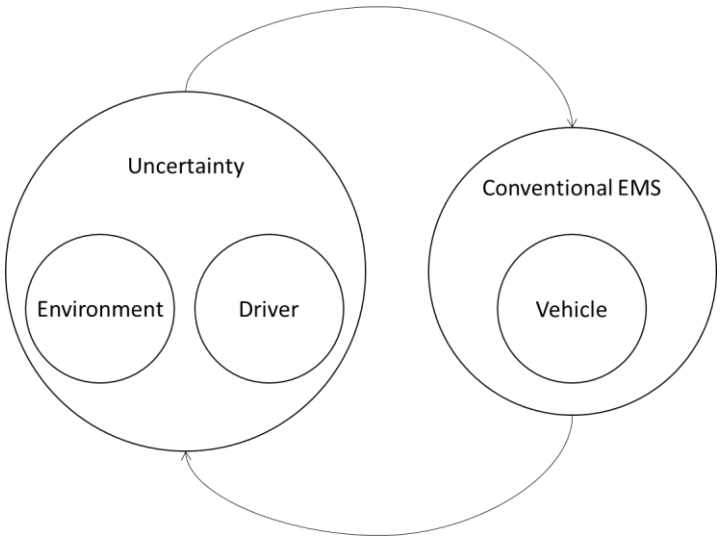

Fig. 3-1. Interactive process of conventional EMSs

In the past decade, their interactive processes have started to change. The industry realized that at this stage uncertainties about the environment and the driver have been the main reason hindering the overall performance of vehicles. For clean and safe driving, these

external uncertainties need to be defined and quantified. However, HEVs designed with extra degrees of freedom could increase the difficulty of quantifying external uncertainties and then magnify the effect on energy consumption. In this case, there is an urgent need for modern energy management schemes for HEVs that can effectively deal with uncertainty. In this work the author has investigated if there is a feasible way to improve energy management efficiency by considering the impact of human drivers on state-of-the-art EMSs.

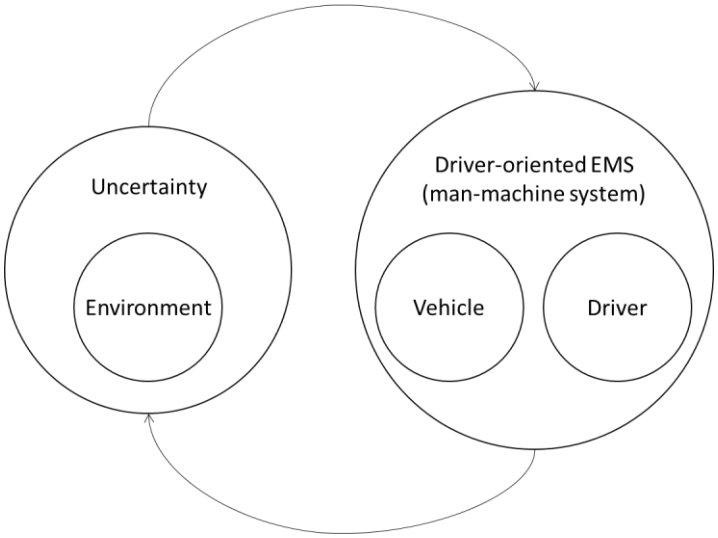

Fig. 3-2. Interactive process of driver-oriented EMSs

Differing from the conventional EMSs, the uncertainty of drivers is considered in the design of these EMSs. As independent sub-models, they work in parallel with the vehicle powertrain. As shown in Fig. 3-2, a driver model has been moved from a conventional EMS to make a new driver-oriented EMS i.e. a man-machine system. Uncertainty about drivers can be quantified in the new system and state information becomes more abundant. Thus, this form of interaction makes it possible to reduce external uncertainties. Although the transfer of a driver model may bring new design problems into the EMS, its significance is to break the structural framework of the conventional system and disclose driving behaviour

characteristics' effects on HEV energy management; finally working towards a new level of human-machine fusion.

3.1.2. RESEARCH TECHNICAL ROUTES

To guide the development of the driver-oriented supervisory control methodology, research technical routes are designed to clarify work contents and the development process. As illustrated in Fig. 3-3, the driver-oriented EMS with additional driver dynamics delivers new opportunities to improve the performance of four critical elements of the vehicle system. They are adaptability (ability to adapt to unknown driving conditions), global optimality (ability to find the global optimal solution), synergy (synergistic promotion for multiple evaluation indexes), and predictability (accuracy and length of prediction). For the new driver-oriented EMS, the author plans to break them off from the following four phases individually.

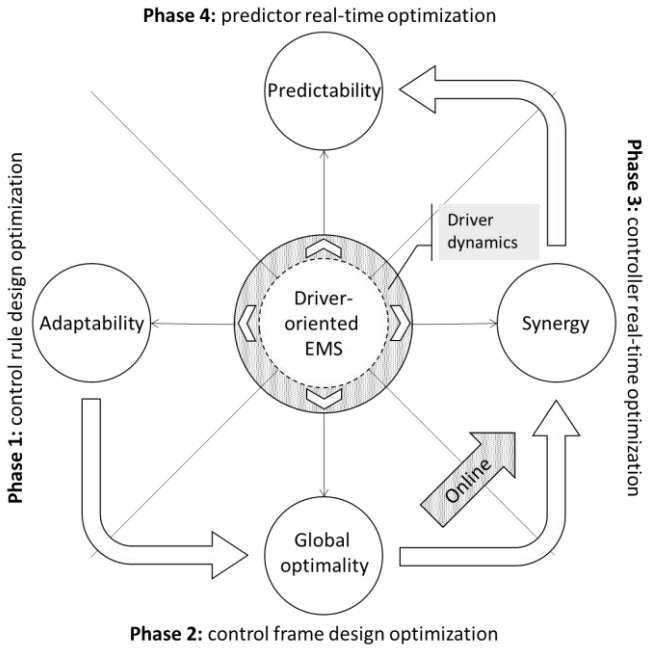

Fig. 3-3. Roadmap for enhancing driver-oriented EMS performance in four elements

In Phase 1: control rule design optimization, a new approach of using personalized non-stationary inference is proposed to increase robustness of the rule-based control system. The difference of the current system to the previous ones in the literature is that it introduces real-time driving behaviour monitoring to increase the robustness of HEV energy management systems. In Phase 2: control frame design optimization, the concept of the driver-identified supervisory control system is introduced, which forms a novel architecture of adaptive energy management for HEVs. As a man-machine system, the proposed system can accurately identify the human driver from natural operating signals and provides driver-identified globally optimal control policies as opposed to mere control actions. Starting from the work in Phase 3, all work is upgraded to an online level, which means the process of optimization and control will be simultaneously carried out during real-world driving. In Phase 3: controller real-time optimization, a novel back-to-back competitive learning mechanism is proposed. This mechanism allows continuous competition between two fuzzy logic controllers during real-world driving. In Phase 4: predictor real-time optimization, an online predictive control strategy is investigated; resulting in a novel online optimization methodology named the dual-loop online intelligent programming, that is proposed for velocity prediction and energy-flow control.

3.2. TARGET VEHICLE

The target vehicle, a medium passenger car, is a virtual computing model based on MATLAB/Simulink. Its series-parallel hybrid drivetrain supervised by the vehicle controller includes one gasoline engine, one integrated starter-generator (ISG), one trans-motor and two

energy sources of fuel and electricity as shown in Fig. 3-4. In this case, the powers from the ICE after the transmission and the trans-motor are combined by coupling their speeds; where the speeds of the two power plants are decoupled to be chosen freely as described in [1]. The peak power of the trans-motor is $P_{mot^*} = 75\ \mathrm{kW}$ (kilowatt) with $270\ \mathrm{N\ m}$ (newton - metre) peak torque. The peak power of the gasoline engine is $P_{ICE^*} = 63\ \mathrm{kW}$ with $140\ \mathrm{N\ m}$ peak torque. The peak power of the ISG is $P_{ISG^*} = 32\ \mathrm{kW}$. The data for all the components is provided by ADVISOR software and their suitability has been proved by BYD Auto Co Ltd. The main parameters of the HEV model are shown in Table 3-1.

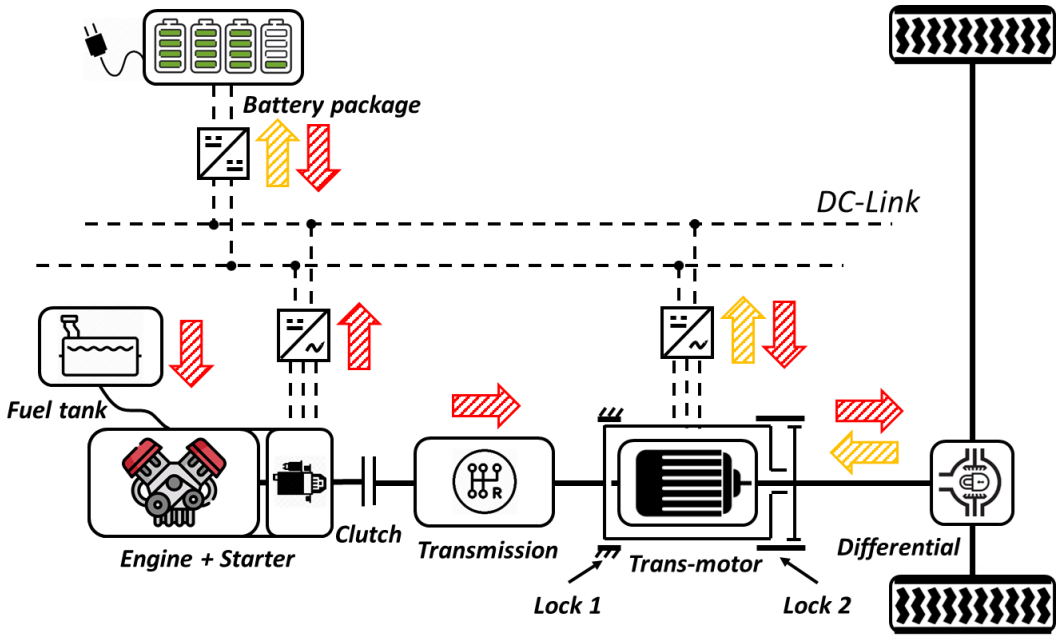

Fig. 3-4. Overall structure of the series-parallel plug-in HEV model

Table 3-1. Main parameters of the vehicle model

Symbol	Parameters	Value
M	Gross mass	$1{,}500\ kg$
A_f	Windward area	$2\ m^2$
R_{wh}	Tyre rolling radius	$0.3\ m$
C_d	Air drag coefficient	0.3
i_0	Differential ratio	3.75
i_g	Transmission ratio	$3.55/1.96/1.30/0.89/0.71$
η_{i_0}	Efficiency of speed reducer	0.98
η_{trans}	Transmission efficiency	0.98
η_{inv}	Inverter efficiency	0.95
η_{dc-dc}	DC-DC converter efficiency	0.95

In normal driving the chosen plug-in HEV architecture has three modes of operation: EV mode, in which the clutch is open, Lock 1 is closed, and Lock 2 is open; hybrid mode, in which the clutch is closed and the locks are both open; and ICE mode, in which the clutch is closed, Lock 1 is open and Lock 2 is closed. All other combinations are either prohibited or used as “park” settings. In the current research, attention is restricted to the EV mode, which incorporates regenerative braking and the hybrid mode. This allows ICE power to be used to simultaneously fully drive the vehicle and charge the battery packages, or to partially drive the vehicle supplemented by the trans-motor depleting the charge of the battery packages, depending on the sign of the trans-motor speed, n_{mot} (negative charges, positive depletes).

3.2.1. VEHICLE DYNAMICS

The modelled vehicle illustrates the longitudinal vehicle dynamics and employs a mechanical multibody system model. In the vehicle dynamics model, the traction force F_t needs to overcome various resistances for keeping the force balance in the vehicle. The traction force F_t and resistances can be sequentially expressed as:

$$F_t = F_f + F_w + F_i + F_j$$

$$\begin{cases} F_f = Mgf\cos\theta \\ F_w = \dfrac{C_d A_f}{21.15}u_a^2 \\ F_i = Mg\sin\theta \\ F_j = \delta Ma \end{cases} \quad (3-1)$$

where, F_f, F_w, F_i, F_j are rolling, aerodynamic, grade and accelerative resistance forces respectively; f is the rolling resistance coefficient; θ is the road slope; u_a is the vehicle speed in km/h; δ is the vehicle rotating quality conversion coefficient; a is the vehicle acceleration; and u is the vehicle velocity. Derived from Eq. (3-1), the demand power P_d of the vehicle can be calculated as given by:

$$P_d = P_f + P_w + P_i + P_j = \left(Mgf\cos\theta + \frac{C_d A_f}{21.15}u_a^2 + Mg\sin\theta + \delta Ma\right)u \quad (3-2)$$

In which the demand torque T_d after a reducer is calculated as given by:

$$T_d = \left(Mgf\cos\theta + \frac{C_d A_f}{21.15}u_a^2 + Mg\sin\theta + \delta Ma\right)\frac{R_{wh}}{i_0 \cdot \eta_{i_0}} \quad (3-3)$$

where, R_{wh} is tire rolling radius; i_0 is a reducer ratio; and $\eta_{i_0} = 0.95$ is the efficiency of the bevel-gear speed reducer.

3.2.2. MAIN POWERTRAIN COMPONENTS

Traction motor – In this speed-coupling parallel hybrid electric drive train, an interesting device used in speed coupling is an electric motor i.e. a trans-motor as called by Ehsani et al. [1] As shown in Fig. 3-5, the stator which is usually fixed on the frame is released as a power input port. The other two ports are the rotor and the air gap, through which electrical energy is converted into mechanical energy. Commonly, the motor speed is the relative speed of the rotor to the stator. Due to the action and reaction forces, the torque action on the stator and rotor is always the same, and the constants are $k_1 = 1$ and $k_2 = 1$.

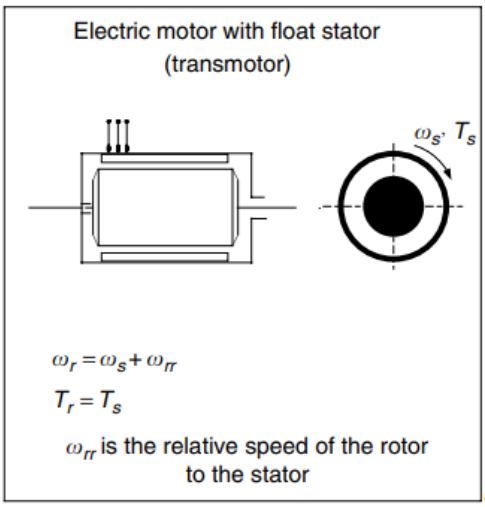

Fig. 3-5. speed-coupling devices by trans-motors [1]

The model uses a Westinghouse 75 kW (continuous) AC induction motor with 0.92 peak efficiency, which means that its construction is quite simple in nature, robust and mechanically strong. Compared to permanent magnet motors, it offers a higher starting torque, reliable speed regulation and acceptable overload capacity. [1] Due to having no brushes, the maintenance required is quite low. Considering the torque and power limitation of the motor under certain motor speeds, n_{mot}, it can be described as:

$$T_{mot} = \begin{cases} \min\left(T_d, T_{max\_dis}(n_{mot})\right), & T_d \geq 0 \\ \max\left(T_d, , T_{max\_chrg}(n_{mot})\right), & T_d < 0 \end{cases} \quad (3-4)$$

$$P_{mot} = \begin{cases} \dfrac{T_{mot} \cdot n_{mot}}{9550 \cdot \eta_{mot}}, & T_{mot} \geq 0 \\ \dfrac{T_{mot} \cdot n_{mot} \cdot \eta_{mot}}{9550}, & T_{mot} < 0 \end{cases} \quad (3-5)$$

where, T_d is the torque demand; T_{max_dis} is the maximum output torque at the current speed when it is discharging; T_{max_chrg} is the maximum regenerative torque; $\eta_{mot} = f(T_{mot}, n_{mot})$ is the efficiency of the motor which is determined from the motor efficiency map as shown in Fig. 3-6.

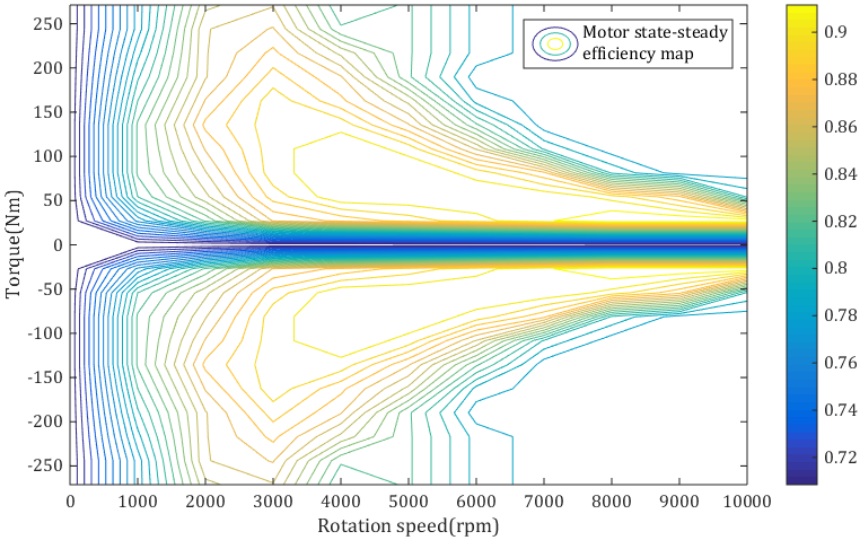

Fig. 3-6. State-steady efficiency map of the AC motor for variations in load torque

Internal combustion engine - The ICE converts the chemical energy of the fuel into mechanical energy to power the propulsion of the vehicle. It is the primary energy source of an HEV, and the only source of a conventional vehicle. The ICE model in the work represents a Saturn 1.9 L

spark ignition engine with a single overhead camshaft. The brake specific fuel consumption (BSFC) of the ICE is defined as:

$$BSFC_{ICE} = \frac{\dot{m}_{fuel}}{P_{ICE}} \qquad (3-6)$$

where $\dot{m}_{fuel}$ is the mass rate of fuel consumption and P_{ICE} is the output power of the ICE that is defined as:

$$P_{ICE} = T_{ICE}\omega_{ICE} \qquad (3-7)$$

where ω_{ICE} is the engine speed (in rad/s) and T_{ICE} is the output torque of the ICE. To define the BSFC at various operating points, the ICE model is simulated for $P_{ICE} \in [0, P_{ICE^*}]$ kW in 0.1 kW steps and $\omega_{ICE} \in [700, 5500]$ rpm in 100 rpm steps. The ICE efficiency map can be calculated based on the resulting BSFC map, which is presented in Fig. 3-7. It can be seen that the maximum efficiency is found in the island around ω_{ICE} = 1500 rpm and P_{ICE} = 18.136 kW. The envelope of the efficiency map depends on the feasibility of the ICE. The omitted data points at very low power requirements are not operationally feasible, or the model is not verified within this range.

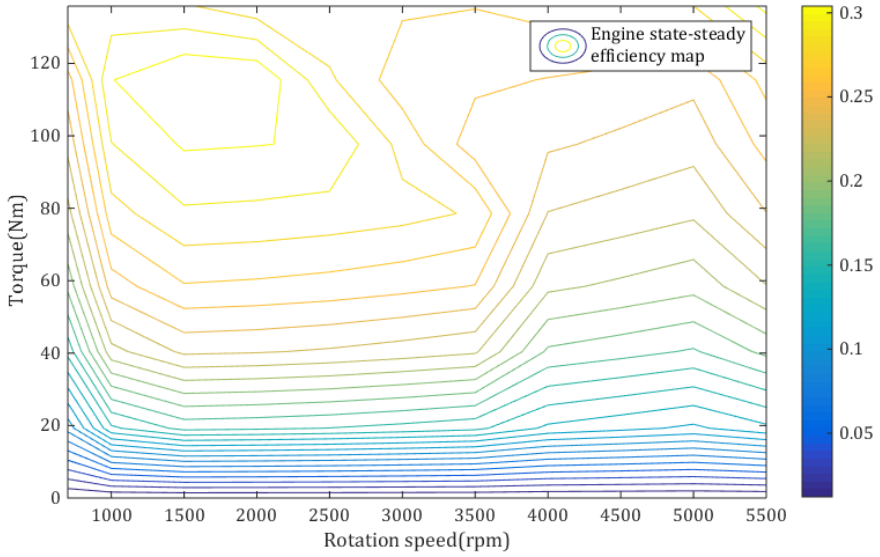

Fig. 3-7. State-steady efficiency map of the ICE for variations in load torque

Integrated-starter-generator - The ICE is connected to a DC-brushless motor, which works as an ISG. It replaces both the conventional starter and generator of an automobile in a single electric device. The model uses the Unique Mobility 32 kW permanent magnet motor; however, it is only operated with a negative torque. Therefore, the energy flow is reversed, and the machine converts mechanical energy into electrical energy (similar to the case of regenerative braking). The efficiency map of the ISG is shown in Fig. 3-8. Note that due to the above negative torque convention, the output power is expressed as a negative value.

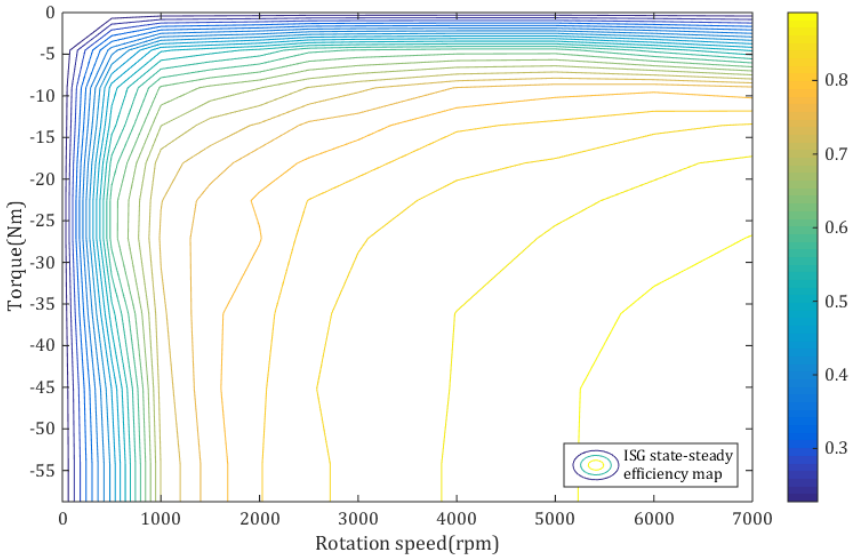

Fig. 3-8. State-steady efficiency map of the ISG for variations in load torque

Automatic transmission – The model uses a standard five-speed automatic gearbox to connect to the back end of the AC motor; it provides the ICE with a proper gear ratio to achieve efficient operation. In general, three rules need to be considered when tuning shifting points [2]: 1) shift up below the maximum RPM of the ICE; 2) shift down above the idle RPM of the ICE; and 3) the distance between the up and downshift points must be far enough so that the new RPM after shifting up is not lower than the downshift point (and vice versa). The first two rules are obvious. The third rule is needed to avoid the case where a vehicle shifts up, the RPM is reduced in the new gear, then the vehicle shifts back down, starting an infinite up and downshifting situation. On this basis, the shifting strategy adds supplementary constraints to the vehicle speed and acceleration, which ensure that a higher ratio always has priority when the gear ratio has more choices. Therefore, a gear ratio can be given:

$$i_g = \max\left(s_a(a_t), s_v(v_t)\right) \qquad (3-8)$$

where i_g indicates output of the gear ratio; s_a and s_v are look-up tables used to find the corresponding gear ratios; and a_t and v_t are vehicle speed and acceleration. The shifting maps are drawn as:

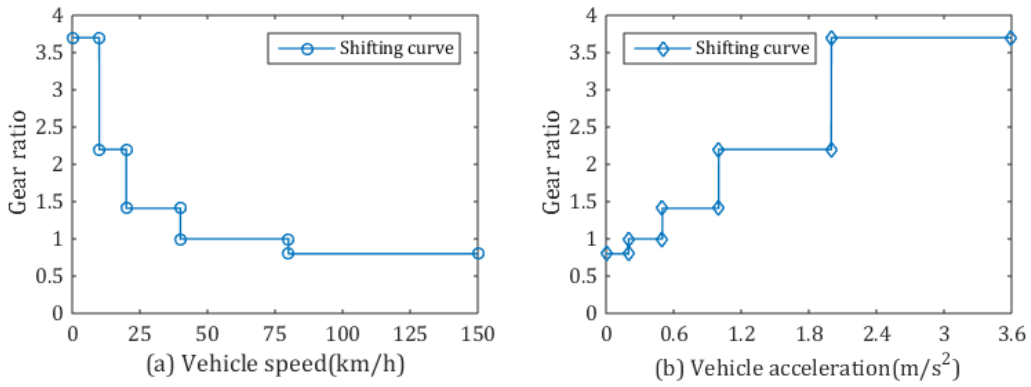

Fig. 3-9. Shifting maps used in the research

Battery package - The studied battery pack consist of the battery cell type NCR-18650 series supplied by Panasonic Automotive & Industrial System Ltd. The inputs to a battery package model are the number of battery cells n_{bc} and the required power P_{bp} from the DC link. The output of the battery package model is the battery state of charge (SoC) for the hybrid electric system. In this model, battery cell current and voltage are applied in iterative calculations to simulate the battery cell dynamics. Starting from each iteration, the battery cell current I_{bc} needs to be calculated firstly by the following formula:

$$I_{bc} = \frac{P_{bp}}{n_{bc} \cdot V_{bc}} \qquad (3-9)$$

where, V_{bc} is the open circuit voltage of the battery cell. Here, a standard two R-C equivalent battery model is employed to expose the current-voltage dynamics of a lithium-ion battery cell as displayed in Fig. 3-10.

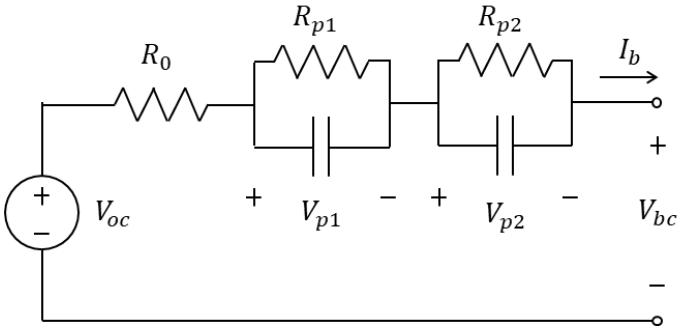

Fig. 3-10. Electric model of battery cell

The battery's voltage dynamics must obey:

$$\begin{cases} V_{bc} = V_{oc}(SoC) - V_{p1} - V_{p2} - R_0(SoC)I_b \\ C_{p1}(SoC) \cdot \dfrac{dV_{p1}}{dt} = I_b - \dfrac{V_{b1}}{R_{p1}(SoC)} \\ C_{p2}(SoC) \cdot \dfrac{dV_{p2}}{dt} = I_b - \dfrac{V_{b2}}{R_{p2}(SoC)} \end{cases} \quad (3-10)$$

where, R_0, R_{p1}, and R_{p2} indicate the effective series resistance, the short transient resistance and long transient resistance respectively; and each of them are a function of the battery cell's SoC; C_{p1} and C_{p2} indicate the short transient capacity and long transient capacity respectively, which are functions of the SoC as well. The SoC of the battery cell is calculated by:

$$SoC = SoC_0 - \int_0^t \frac{I_b}{Q_b} dt \quad (3-11)$$

where SoC_0 is the initial BP's SoC. The battery cell data and calibrated model parameters are organized in Table 3-2.

Table 3-2. Battery cell parameters [3]

Parameter	Description	Value
V_{bc_max}	Rated battery cell voltage	3.60 V
I_{bc_cmax}	Rated battery cell charge current (A)	2.25 A
I_{bc_dmax}	Rated battery cell discharge current (A)	11.25 A
Q_{bc_max}	Rated battery cell capacity (mAh)	2900 mAh
V_{oc}	$1.031 \cdot e^{-35 \cdot SoC} + 3.685 + 0.2156 \cdot SoC - 0.1178 \cdot SoC^2 + 0.3201 \cdot SoC^3$	
R_0	$0.1562 \cdot e^{-24.37 \cdot SoC} + 0.07446$	
R_{p1}	$0.3208 \cdot e^{-29.14 \cdot SoC} + 0.04669$	
R_{p2}	$6.603 \cdot e^{-155.2 \cdot SoC} + 0.04984$	
C_{p1}	$-752.9 \cdot e^{-13.51 \cdot SoC} + 703.6$	
C_{p2}	$-6056 \cdot e^{-27.12 \cdot SoC} + 4475$	

3.2.3. SUPERVISORY CONTROL SYSTEM

This section describes the integration of all powertrain elements; a driver module with feedback control; as well as the overall control by the baseline series-parallel control strategy. As shown in Fig. 3-11, each of the described components and the additional driver module are connected and governed by a local energy management power-split device. All energy-related indicators are aggregated into a module of monitors for later analysis.

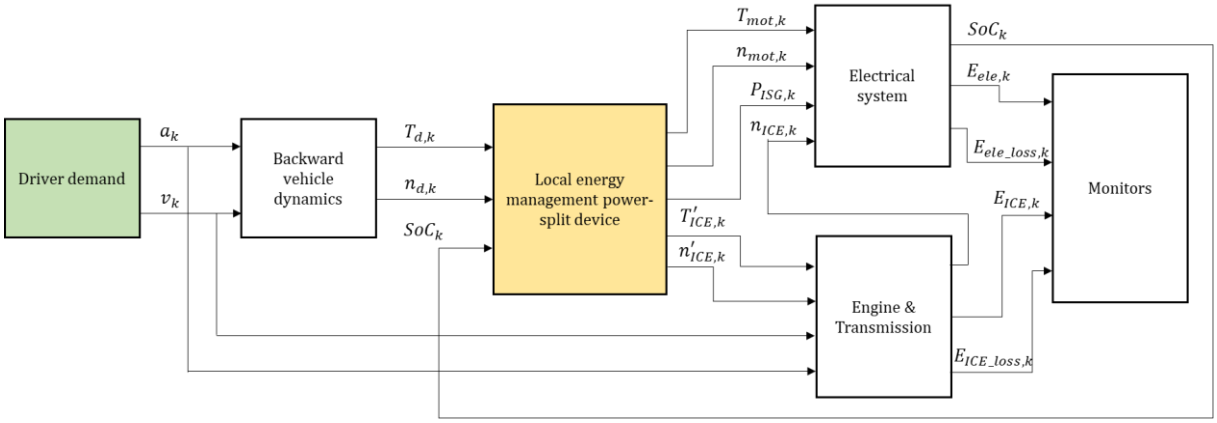

Fig. 3-11. Systemic diagram of a series parallel HEV control system

Driver dynamics - The commonly used approach of processing the accelerator pedal's angle of depression is adopted for driving style classification. Zhang et al. [4] provide a simplified sub-model to describe different types of driving styles by adjusting a style factor λ and it is used here. Through the model, driving cycles with different driving styles can be assigned to five grades: Very Gentle, Gentle, Normal, Aggressive, and Very Aggressive. The driver sub-model can be simplified as follows:

$$\begin{cases} \delta_{k+1} = f_{K_p,K_i,K_d}(e_k) \\ e_k = \lambda \cdot (v_k - v_{ref,k}) \end{cases} \quad (3-12)$$

where, δ is the degree of accelerator pedal depression; the style factor $\lambda \in [0,1]$ is an impact factor derived from the driving style type; the function f is a proportional–integral–derivative controller; K_p, K_i, K_d are coefficients of proportional, integral and derivative terms, respectively; and e_k is the error between the target speed, v_{ref}, and the vehicle speed,v_k.

Baseline series-parallel control strategy - To maximize the usage of electricity from grid, the baseline control policy is developed based on industry-recognized series-parallel charge depleting (CD) and charge sustaining (CS) strategies. [5] It will be treated as a benchmark for analysis of the later proposed control strategies. Here, a power-split vector $\boldsymbol{\xi}$ is constructed in Eq. (3-13) from the trans-motor torque, T_{mot}; the trans-motor speed, n_{mot}; the ICE torque, T_{ICE}; the ICE speed, n_{ICE}; the ISG power, P_{ISG}:

$$\boldsymbol{\xi} = [T_{mot} \quad n_{mot} \quad T_{ICE} \quad n_{ICE} \quad P_{ISG}] \quad (3-13)$$

In the electric traction mode, enough electricity can be supplied to satisfy the powertrain demand independently, so that both the ICE and the ISG do not need to work. The power distribution in this state is described as follows:

$$\boldsymbol{\xi} = [T_{d,k} \quad n_{d,k} \quad 0 \quad 0 \quad 0] \tag{3-14}$$

Series and parallel traction modes are governed by CD/CS control strategy. During this period, the switch condition of series and parallel hybrid traction modes is determined by value of the demand power to ensure the power and economy of the vehicle. A vehicle will, normally, favor electric traction, and then the battery will later be recharged by the power grid. When the trip is quite long and the battery SoC reaches a low level, the engine will be used to charge battery in a charge-sustaining manner. Therefore, the power distribution at each time step t is described as follows:

$$\left.\begin{aligned} \boldsymbol{\xi}_{series} &= [T_d \quad n_d \cdot (1-\chi_1) \quad T_d \quad n_d \cdot \chi_1 \quad 0] \\ \boldsymbol{\xi}_{parallel} &= [T_d \quad n_d \quad T'_{ICE}(P_{ISG}) \quad n'_{ICE}(P_{ISG}) \quad P_{ISG^*} \cdot \chi_2] \end{aligned}\right\} \tag{3-15}$$

where, χ_1 and χ_2 are the proportionality factors of the ICE and ISG, both determined according to the SoC. T'_{ICE} and n'_{ICE} are optimal torque and speed of the ICE converted based on demand power of the ISG P_{ISG}. Their definition uses the logistic function in a piecewise form, [6] given by the formula:

$$\chi_i(SoC) = \begin{cases} 1, & SoC \in [0,0.2] \\ \dfrac{1}{1+\exp\left(\dfrac{SoC_k}{SoC^*}\right)}, & SoC \in (0.2,0.5] \\ 0, & SoC \in (0.5,0.8] \end{cases} \tag{3-16}$$

where, SoC^* is a scaling coefficient of the BP's state of charge SoC_k.

3.3. EXPERIMENTAL FACILITIES

This research was carried out at the Vehicle Technology Research Centre at the University of Birmingham. Experimental facilities including a driving simulator platform and a hardware-in-the-loop testing bench were used for demonstration and testing validation in the PhD study. Their specification and function will be described as follows.

3.3.1. DRIVING SIMULATOR PLATFORM

A static experience platform driving simulator system is involved in this research, as shown in Fig. 3-12, which is the ideal tool for subjectively testing vehicle functions through direct experience. It makes the most of the advantages offered by the combination of a detailed and realistic human-machine interface simulation and a real-world driving experience, coupled with a state-of-the-art simulation tool for vehicle dynamics, the CarMaker open integration and test platform. [7]

Fig. 3-12. Driving simulator used in the research

Cockpit Package - There is one cockpit package supported by a Thrustmaster T500RS (as shown in Fig. 3-13) and one host PC with I5-6500 3.2GHz processor and 8GB RAM. Their communication relies on a 3.0 USB cable, in which the sampling frequency of the vehicle system and pedal data acquisition are both 10 Hz. The features and benefits of the system experience platform include [8]: 1) realistic haptics with real-time feedback; 2) real pedals and a real steering wheel to ensure a realistic driving experience; 3) optional coupling with virtual reality devices; and 4) the possibility of connecting to real control units.

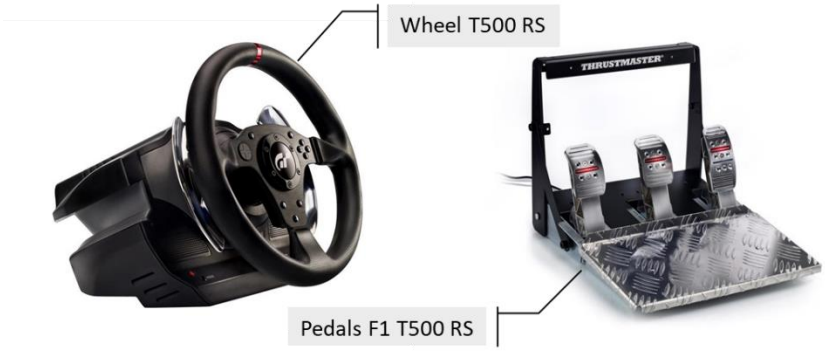

Fig. 3-13. Cockpit package supported by the Thrustmaster T500RS

Set-up for driving simulation - The driving simulator platform is used for generating real-world cycles. As Fig. 3-14 shows, data collection is conducted in the cockpit package (supported by a Thrustmaster T500RS) with the same scale HEV model with an automatic gearbox. This is to make sure the driving characteristics exhibited by drivers are under the same constraints and their results are comparable. With respect to real-world road conditions, the road map model used with reconstructed traffic simulates a cyclic undivided highway with uphill, downhill, curved and straight roads, and is provided by IPG CarMaker. It is developed specifically for testing passenger cars and light-duty vehicles. Users can accurately model real-world test

scenarios, including the entire surrounding environment, in the virtual world. To reduce the impact of differing traffic and road conditions on human drivers, they are restricted to the same cycling road conditions and required to follow the speed limits, stop signs, traffic lights, and other traffic regulations. It should be noted that the driver's pedal behaviour might be dependent on the vehicle, the pedal to torque map, and even the physical pedal resistance feedback.

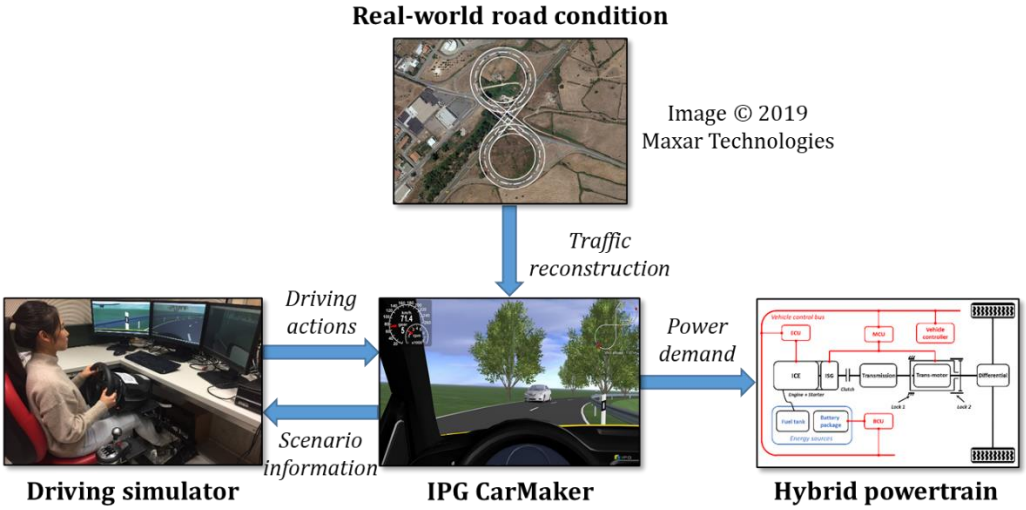

Fig. 3-14. Collection process of driving profiles

CarMaker supports the extension of its models with MATLAB Simulink to facilitate the development and testing of enhanced vehicle control algorithms. There is a pre-defined structure and it is represented in Simulink as a nested, multi-level model. The implementation of self-developed control algorithms is greatly restricted due to the subsystems not being completely open. This study deals with the power split for power machines and does not interfere with the drivetrain outputs out of consideration; verifying of the self-developed control algorithms can be conducted in the open-loop testing environment. In terms of data analyzation, IPG offers its own tool called IPGControl that was developed for viewing and

analysing purposes, and can also be used stand-alone. This study uses MATLAB for data analyzation.

3.3.2. HARDWARE-IN-THE-LOOP TESTING BENCH

Hardware-in-the-loop testing is a technology that is widely used in industry for development and testing of complex embedded systems. Real-time computing and signal emulating technologies are applied to implement functional testing of control systems. The ETAS group is one of the world's leading suppliers for HiL test equipment. For this PhD study the hardware supplied by ETAS was chosen to build a HiL test system as shown in Fig. 3-15, comprising a prototype controller (ES910) and a real-time computer (LABCAR). The ES910 is used to package an energy management strategy to control the LABCAR for functional verification. The LABCAR emulates the signals as in real vehicles using real-time models and communicates with the ES910 via a CAN bus. The ETAS software which contains ITECRIO, INCA, IP and EE is employed for the real-time implementation of control algorithms and HEV models.

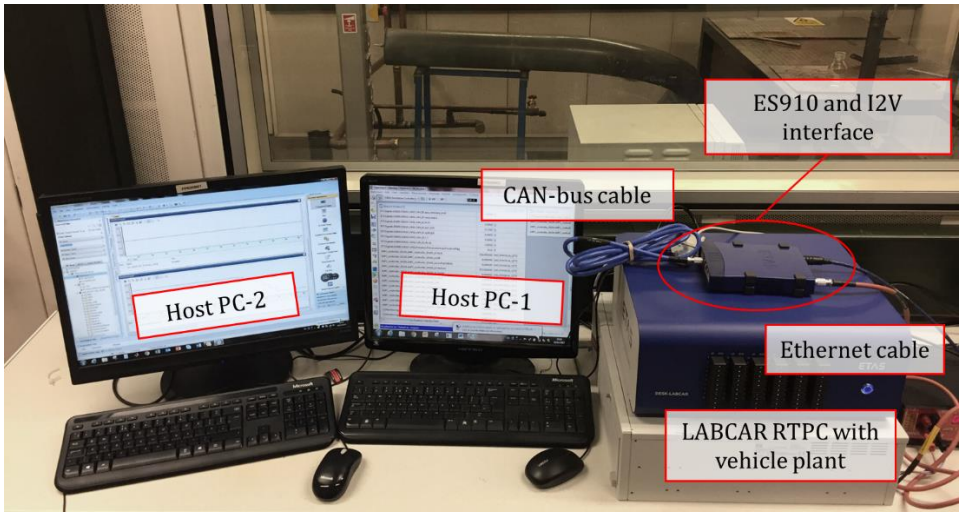

Fig. 3-15. Hardware-in-the-loop testing system

ETAS ES910 – The ES910 prototyping module with common ECU interfaces has high-performance computing in a compact and rugged housing. It is designed for testing in the development environment and in stand-alone operation.

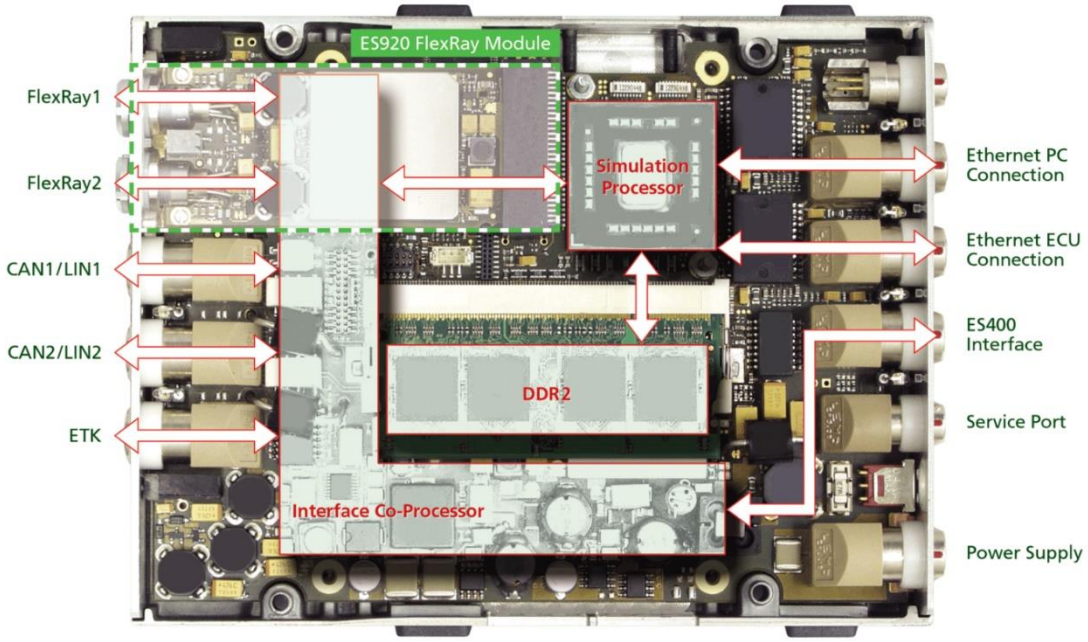

Fig. 3-16. Interfaces of ES910 – prototyping and interface module

The ETAS ES910 is a prototype controller, whose key elements consist of a 1.5 GHz microprocessor, 4Gb RAM, 1Gb/s Ethernet communication and communication interfaces. Communication interfaces incorporating CAN, LIN and ETK make it possible to control communication with downstream ECUs. Software and control functions can be realized in the ES910 and verified through the HiL test network, as displayed in Fig. 3-16. For my research, the ES910 acts as a supervisory HEV controller for functional validation of energy management strategies, in which CAN and LIN buses pass control signals to downstream controllers i.e. the LABCAR.

ETAS LABCAR - ES5100 - The ES5100.1 desktop housing is based on the ETAS RTPC (Real-Time PC) and the ETAS Multi-I/O Simulation Board ES5340.2. The ETAS RTPC offers multicore simulation functions in real time as the core of all LABCAR test systems. Alongside the ES5340.2, the housing of the ES5100.1 can accommodate two further PCI express boards. The ETAS Multi-I/O Simulation Board ES5340.2 can be adapted to suit all kinds of test scenarios. Fig. 3-17 shows (a) system diagram and (b) different views of the ES5100.1 desktop housing.

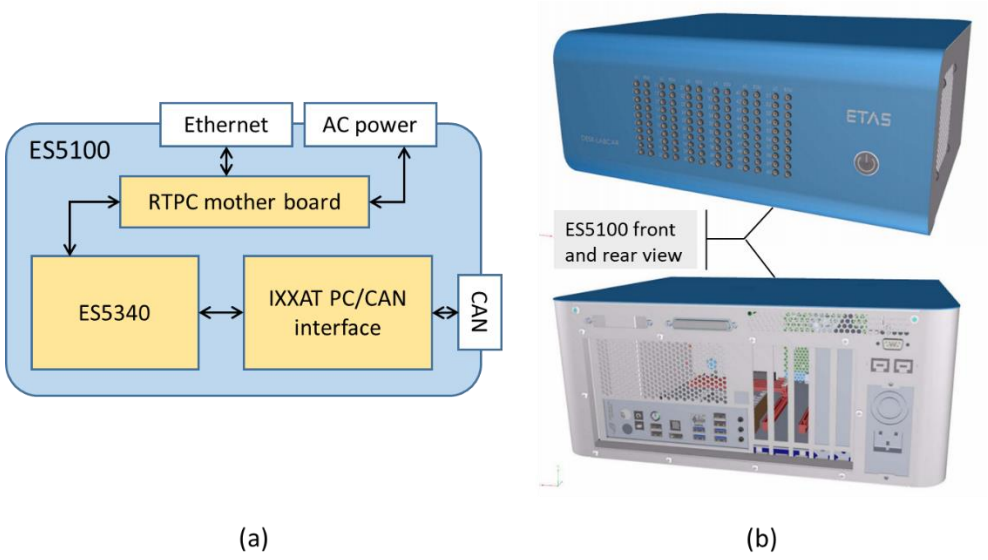

Fig. 3-17. Front (top) and rear view (bottom) of the ES5100.1 desktop housing

The ES5100 is a compact real-time computer for HiL testing as shown in Fig. 3-17. It has an embedded system with Linux pre-installed that allows real-time models can be downloaded from the host computer via Ethernet. The ES5100 is equipped with an Intel Core i7-4700 @3.1GHz processor, 8GB RAM and a 500-GB hard drive. Five external PCIe slots can be used for additional modules e.g. the ES 5400 HEV simulator and CAN card module. The ES5100 is equipped with a breakout-box (BoB) and located in the centre of the HiL system that enables signal bypass for controller testing via communicating with the host PC and external ECU.

ETAS LABCAR - ES5340 & IXXAT PCIe PC interface - The ES5340 hybrid vehicle simulation board is operated for signal-level ECU testing as shown in Fig. 3-18. It can emulate signal communications in the same way as in practice, wherein analogue signals, digital signals, and pulse-width modulation (PWM) inputs can be produced by the ES5340. Also, it accepts analogue signals, digital signals, and PWM inputs from other external controllers. In this work, the ES5340 is utilized for real-time simulation of the HEV plant model.

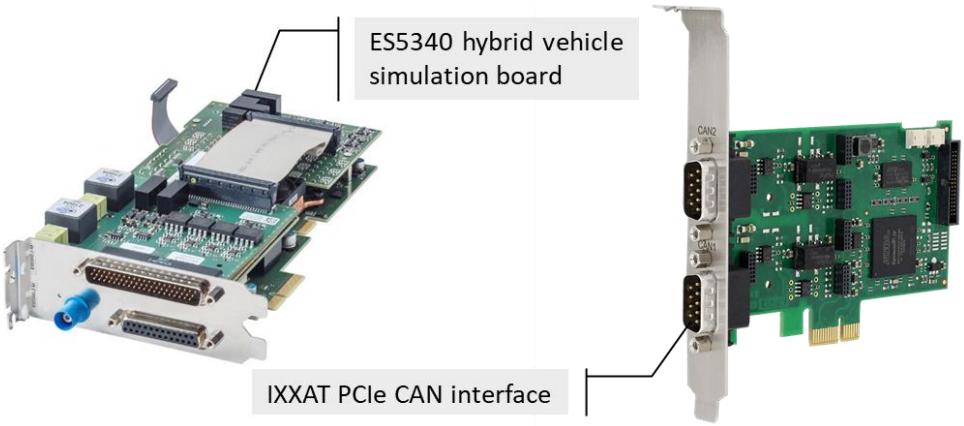

Fig. 3-18. ES5340 hybrid vehicle simulation board and IXXAT PCIe PC interface

The IXXAT iPC-I XC 16/PCIe PC-CAN interface is a powerful electronic component that can cause the interaction between the LABCAR and the external ECU via a CAN bus. It is mounted on the ES5100 with the PCIe interface. The PC-CAN interface is equipped with a 16-bit microprocessor, a 40-MHz clock, 512Kb RAM, 128Kb flash memory and two independent CAN lines. In this work, IXXAT PC/CAN interface is adopted to access the CAN bus communication between the LABCAR and the prototype controller.

Set-up for the HiL testing - HiL test software is mainly used for modelling, compilation, and implementation, as shown in Fig. 3-19. The software is installed in a host PC that

communicates with ETAS hardware via Ethernet. The real-time models of hybrid vehicles and energy management controllers are developed by MATLAB/Simulink. The real-time model is connected to a hardware interface (such as a CAN) and compiled into C-code to perform real-time calculations during the compilation process. ETAS EE and INTECRIO are model compilation software for LABCAR and ES910, respectively. Through the ETAS Experimental Environment (EE) and INCA, compatible models of vehicles and controllers are respectively implemented in the LABCAR and ES910. The model's performance in the LABCAR and ES910 can be observed in the host PC via EE and INCA.

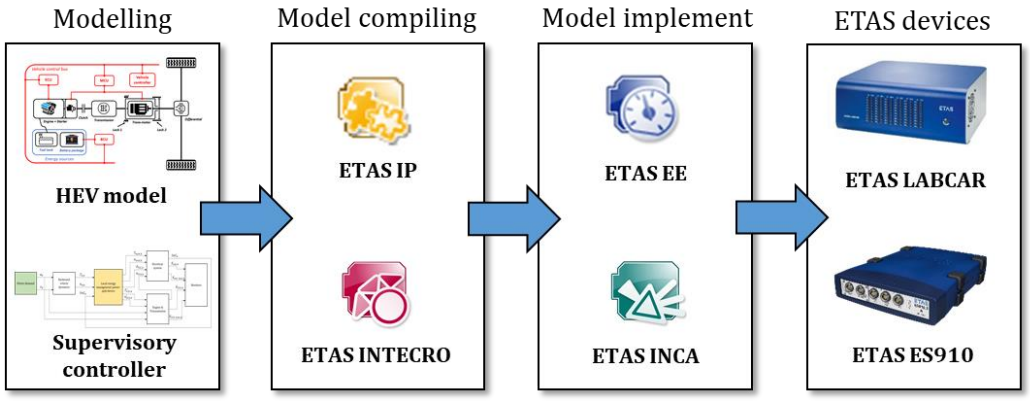

Fig. 3-19. Software used for HiL testing

3.4. SUMMARY

This chapter describes the research methodology and the involved experimental facilities. The main contributions relevant to this chapter are concluded as follows:

1) The interaction topology in HEVs' energy management has been developed and analysed. Its challenges inspire the design of the technical route for the overall research. The overall research objective is specified in four independent tasks:

adaptability, global optimality, synergy, and predictability. Each task will be carried out in turn in subsequent chapters.

2) The target vehicle is a virtual computing model based on MATLAB/Simulink that has been developed and analysed from three layers: 1) vehicle longitudinal dynamics; 2) real-time modelling of main powertrain components; and 3) developing the supervisory control system.

3) This chapter illustrated the work of the driving simulator platform and the HiL testing bench. Specifications and features of the main facilities used for the research are explained.

REFERENCES

[1] M. Ehsani, Y. Gao, S. Longo, and K. Ebrahimi, *Modern electric, hybrid electric, and fuel cell vehicles*. CRC press, 2018.

[2] CM Labs, "Automatic Transmission Shift Point Tuning." [Online]. Available: https://www.cm-labs.com/vortexstudiodocumentation/Vortex_User_Documentation/Content/Editor/editor_automatic_transmission_shift_point_tuning.html.

[3] Q. Zhou, "Design Optimisation and Real-Time Energy Management Control of an Electrified Off-highway Vehicle with Artificial Intelligence," University of Birmingham, 2019.

[4] Y. Zhang *et al.*, "Optimal energy management strategy for parallel plug-in hybrid electric vehicle based on driving behavior analysis and real time traffic information prediction," *Mechatronics*, vol. 46, pp. 177–192, 2017.

[5] J. Peng, H. He, and R. Xiong, "Rule based energy management strategy for a series – parallel plug-in hybrid electric bus optimized by dynamic programming," *Applied Energy*, vol. 185, pp. 1633–1643, 2017.

[6] Z. Chen, R. Xiong, C. Wang, and J. Cao, "An on-line predictive energy management strategy for plug-in hybrid electric vehicles to counter the uncertain prediction of the driving cycle," *Applied Energy*, vol. 185, pp. 1663–1672, 2017.

[7] IPG Carmaker, "System Experience Platform," *IPG Automotive, Karlsruhe, Germany*, 2014. [Online]. Available: https://ipg-automotive.com/products-services/test-systems/driving-simulators/#system-experience-platform.

[8] I. Automotive, "Driving simulators: Visualizing vehicle development." [Online]. Available: https://ipg-automotive.com/products-services/test-systems/driving-simulators/?cv=1.

CHAPTER 4

DRIVER-ORIENTED SUPERVISORY CONTROL SYSTEM WITH PERSONALIZED NON-STATIONARY INFERENCE

The content presented in the Chapter 4 is based on the author's submitted articles, 'Online Driver-oriented Energy Management of Connected Hybrid Electric Vehicles with Personalized Non-stationary Inference' in IEEE Transactions on Systems, Man, and Cybernetics: Systems. This chapter investigates an online driver-oriented energy management (ODEM) methodology for connected plug-in hybrid electric vehicles. A novel approach that uses personalized non-stationary inference is proposed to increase the robustness of the rule-based vehicle control system through real-time driving behaviour monitoring for vehicle energy economy improvement. Based on personalized WLTP cycles, optimal control parameters of the charge-depleting and charge-sustaining (CD/CS) control strategy are firstly obtained by separate offline optimization. Then interval type-2 fuzzy sets are applied to develop a real-time driving style recognition function so that the change of driving behaviour is better identified. The developed functionalities are integrated and implemented in a distributed driving style recognizer to provide the control signal, which is subsequently downloaded via V2X network to an on-board energy-flow controller for adjusting the vehicle control parameters in real-time. The proposed approach is validated by hardware-in-the-loop testing, which proves that the improved system is robust and it saves energy the studied driving cycles by up to 5% over the equivalent consumption minimization strategy (ECMS), especially for gentle drivers. Even

under harsh communication conditions (with signal loss 80+%), it still performs better than the ECMS (by 1.11%) and the CD/CS control strategy (by 4.31%).

4.1 CONNECTED VEHICLE SYSTEM

Modern road traffic is a complex and interconnected system, which includes traffic information centres, monitoring infrastructures, and vehicles with different energy sources. The V2X network is the communication medium of intelligent transport systems, connecting vehicles, infrastructure, and information centres. V2X possesses powerful cloud computing facilities that can implement an advanced optimization scheme for connected vehicles. This system has great potential to save energy for each connected vehicle and even for the whole transport system by managing traffic and individual vehicle operation.

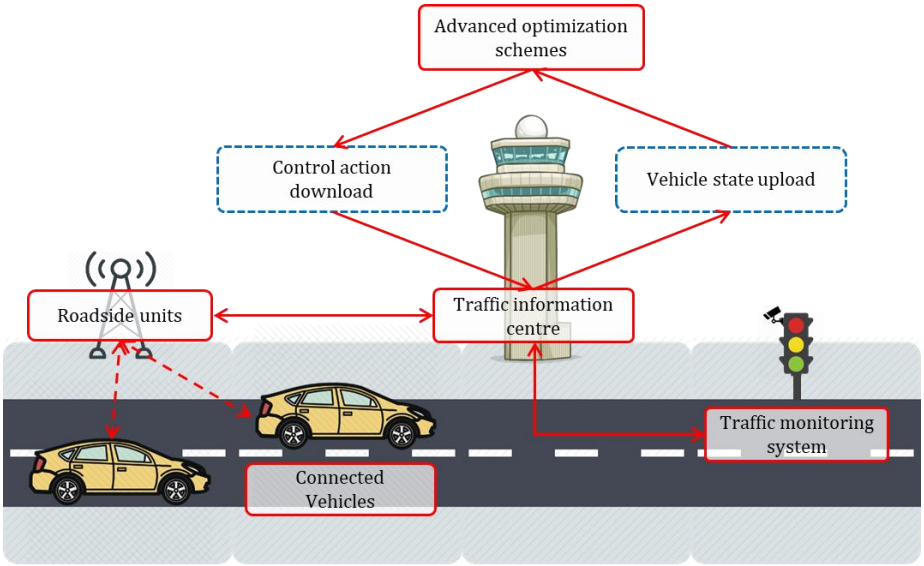

Fig. 4-1. The connected vehicle communication framework

Fig. 4-1 shows a connected HEV communication scenario studied in this chapter, and the workflow is explained as follows: i) roadside units receive the HEV real-time state signal

through the vehicle-to-infrastructure (V2I) network; ii) the information centre collects the HEV real-time state signal from the roadside units and operates an advanced optimization scheme to determine optimal control signals; iii) the information centre sends the command signal to the vehicle controller via the roadside units. This framework with cyber-physical technology can implement advanced intelligent algorithms to enable real-time driver-oriented energy management, which was previously limited by the performance of local vehicle controllers.

4.2 PROPOSED SOLUTION

To increase robustness of the rule-based vehicle control system, the ODEM methodology is established and presented in Fig. 4-2, is proposed. In the on-board control layer, the chaos-enhanced accelerated particle swarm optimization (CAPSO) algorithm is implemented to offline optimize control parameters (cut-in timing and conversion speed of the ICE and ISG) of CD/CS strategy based on classified driving styles. In the distributed control layer, a real-time driving style recognition function using interval type-2 fuzzy sets is developed to identify driving styles. The proposed methodology is expected to subvert the traditional reasoning process by activating its stationary inference. Via the V2X network, the distributed server receives uploaded feedback information, analysis driving behaviour, and computes real-time control signals. That signals will be downloaded to adjust the control parameters of the CD/CS strategy for minimizing the energy consumption and maintain the state of charge (SoC).

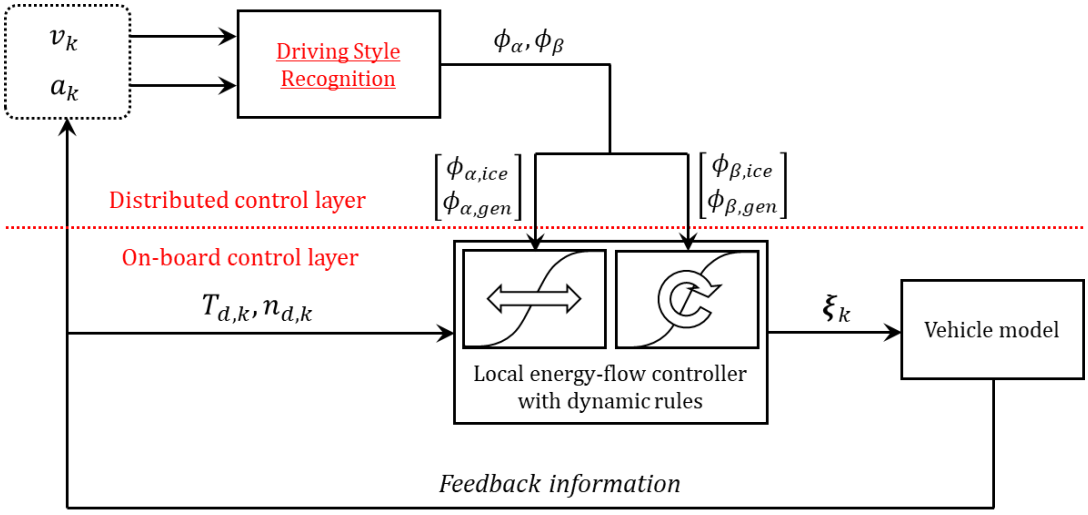

Fig. 4-2. The mechanism of online driver-oriented energy management

4.2.1. DRIVER-ORIENTED RULE OPTIMIZATION

In order to tailor personalized rules for various driving style, this section describes a driver-oriented problem formulation, and optimization process of the control parameters of the CD/CS strategy based on a range of driving styles.

A. Problem formulation

To adaptively adjust the boundary between CD and CS control modes, two control parameters ϕ_α and ϕ_β are introduced into Eq. (3-16) to enable optimization of cut-in timing and conversion speed of the ICE and ISG. So far, a total of four control parameters jointly define the position and slope of the curve in the logistic function. Here, the proportionality factors χ_i of the ICE and ISG with the control parameters are

$$\chi_i(SoC_k) = \frac{1}{1+\exp\left\{\left(\frac{SoC_k}{SoC^*}+\phi_\beta\right)\phi_\alpha\right\}}, \qquad SoC \in (0.2,0.5] \qquad (4-1)$$

where, for the given case study, the range of the control parameter ϕ_α is between $\varepsilon_\alpha^- = 0.01$ and $\varepsilon_\alpha^+ = 50$, its limits are the lowest requirement to ensure close to 0-90 degree slope search area (also depends on the length of sampling time); the control parameter ϕ_β is constrained between $\varepsilon_\beta^- = -6$ and $\varepsilon_\beta^+ = 6$, and limited by its horizontal search range.

In the multi-objective optimization problem formulation, there are two main targets: the final energy consumption from the fuel tank and the battery package (BP); and the BP's SoC. These optimization targets are given by

$$\left.\begin{aligned} J_1 &= \sum_{k=1}^{k_{end}} E_{fuel,k} \\ J_2 &= SoC_{k_{end}} \end{aligned}\right\} \qquad (4-2)$$

where, $E_{fuel,k}$ denotes the instantaneous fuel consumption at the kth time-step; and k_{end} is the final time of the driving cycle. Besides, delta SOC value is another form used in evaluation of HEV systems. Differing the value of SoC, the delta SOC value has a reference value of SoC which is more flexible in the problem formulation. Plug-in HEVs used in this thesis commit to maximize the usage of grid electricity, so there is no substantial difference of using these two formulations. Here, the weighted sum method [1] is utilized to convert the multi-objective optimization problem into a single objective optimization. Therefore, the optimal energy-flow control problem with constraints is described by

$$\min J = w\, J_1 \frac{1}{J_1^*} + (1-w)\frac{1}{J_2}\, J_2^* \qquad (4-3)$$

$$s.t.\begin{cases} SoC_k, & SoC_k \in [SoC^-, SoC^+] \\ n_{mot,k}, & n_{mot,k} \in [0, n_{mot^*}] \\ T_{mot,k}, & T_{mot,k} \in [-T_{mot^*}, T_{mot^*}] \\ P_{ice,k}, & P_{ice,k} \in [0, P_{ICE^*}] \\ P_{gen,k}, & P_{gen,k} \in [0, -P_{ISG^*}] \end{cases}$$

where, SoC^- and SoC^+ are the lower and upper limits of value of BPs' SoC. J_1^* and J_2^* are scaling coefficients of the optimization targets J_1, J_2. Here, the optimization target J_2 is formulated as a penalty function in the cost function.

B. CAPSO implementation

The standard accelerated particle swarm optimization (APSO) usually keeps the attraction parameters as a fixed value [2]: the solutions still change slightly, however, as the optima are approached. Inspired by chaotic mapping strategy, the CAPSO algorithm, with its higher convergence speed and probability of finding global optima, something that was first reported for energy management optimization by our team. [4, 5] This chapter uses this algorithm to optimize the control parameters for different driving behaviours in order to further improve the vehicle system adaptability. For the CAPSO, the particle's position updates with the following equation:

$$x^{(i+1,j)} = (1-\beta)\, x^{(i,j)} + \beta\, g^{(i,*)} + \alpha^{(i)}\, r^{(i,j)} \qquad (4-4)$$

In Eq. (4-4), $g^{(i,*)}$ is the best position in the ith iteration, β is the attraction parameter of CAPSO, α is the convergence parameters of CAPSO, and r is a $U[0,1]$ random variable. Here, α and β are updated in each iteration via:

$$\left.\begin{array}{c} \alpha^{(i)} = \alpha^{(0)}\, \gamma^i, \\ \beta^{(i+1)} = a\, \beta^{(i)}\, (1-\beta^{(i)}), \end{array}\right\} \qquad (4-5)$$

where, the settings, $\alpha^{(0)} = 0.9$ and $\gamma = 0.95$, were chosen; and the attraction parameter is mapped by the logistic map, in which the initial values $\beta^{(1)} = 0.6$ and $a = 4$ are used. When convergence has been achieved, the algorithm ends the main iteration and outputs the best position at the end iteration as the global optimal solution. In driver-oriented rule optimization, APSO modified by the chaotic mapping strategy is implemented with its higher search efficiency to optimize the control parameters ϕ_α, ϕ_β of the CD/CS control strategy. The weight value is set here to a fixed value of 0.7 to reflect an equal preference towards relatively lower total used energy and higher SoC.

4.2.2. DRIVING STYLE RECOGNITION

Driving style is a complex concept that affects driving safety and fuel economy during real-time driving. Driving style recognition is performed here by the nonlinear model (recognizer) to monitor driving behaviour, shown in Fig. 4-3, which includes an observation window, a type-2 FLC, and a final interpolation.

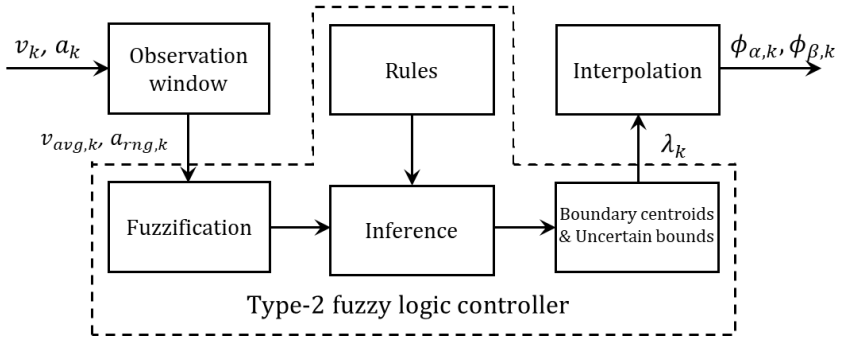

Fig. 4-3. Schematic diagram of driving style recognition

A. Observation window

This recognizer includes a short-term sliding window, a type-2 LFC and further signal processing. A short-term sliding window is introduced to restrict the sampling dimension and lengthen memory time of characteristic states. The dataset of driving operation signals is defined, in which each time step k of data is expressed as given by:

$$(\boldsymbol{v},\boldsymbol{a})^T = \begin{bmatrix} v_{k-h+1} & v_{k-h+2} & \cdots & v_k \\ a_{k-h+1} & a_{k-h+2} & \cdots & a_k \end{bmatrix} \tag{4-6}$$

where, $\boldsymbol{v}$ is a vector of vehicle speed $(\mathrm{m/s})$; $\boldsymbol{a}$ is a vector of vehicle acceleration $(\mathrm{m/s^2})$; and $h = 60\mathrm{s}$ is length of the short-term sliding window. As the core of the reasoning mechanism, a type-2 FLC is used to differentiate driving style during real-time driving, which can be expressed mathematically as follows

$$\lambda = G\left(v_{avg}, a_{rng}\right) \tag{4-7}$$

in which

$$\begin{cases} v_{avg} = \dfrac{\sum_{i=0}^{i=h}(\boldsymbol{v})^T}{h} \\ a_{rng} = \max(\boldsymbol{a})^T - \min(\boldsymbol{a})^T \end{cases} \tag{4-8}$$

where, ranges of vehicle acceleration are adopted to reflect operational proficiency of drivers. In general, drivers with higher operational proficiency have relatively low maximum range. Average values of vehicle speed are adopted as considered in [5] to reflect driving habits.

B. Interval type-2 fuzzy logic controller

Differing from type-1 fuzzy sets, type-2 fuzzy sets have the ability to handle higher-order uncertainty factors at lower computational cost and minimize the effects of uncertainties in rule-based fuzzy systems. In this case, type-2 fuzzy sets with linguistic terms are regulated by standard triangular membership functions (MFs), where the degree of membership is expressed as a function of normalized values in the interval, $[0,1]$. In the general structure of the interval type-2 (IT2) Takagi-Sugeno (T–S) FLC, the *l*th rule can be written as

$$R^{(l)}\text{: IF } z_1 \text{ is } \tilde{F}_1^l \text{ and } z_2 \text{ is } \tilde{F}_2^l\text{,…, and } z_v \text{ is } \tilde{F}_v^l\text{, THEN } x_{k+1} = A_l x_k + B_l u_k \qquad (4-9)$$

$$(l = 1,2,\dots,m)$$

where, $\tilde{F}_1^l$ is the interval type-2 fuzzy set, which corresponds to the membership function of rule l. The firing strength of the *l*th rule belongs to the following interval set

$$\omega_l(x) \in \left[\overline{\omega}_l(x), \underline{\omega}_l(x)\right], \qquad l = 1,2,\dots,m \qquad (4-10)$$

where

$$\begin{cases} \underline{\omega}_l(x) = \underline{\mu}_{\tilde{F}_1^l}(x)\, \underline{\mu}_{\tilde{F}_2^l}(x) \cdots \underline{\mu}_{\tilde{F}_m^l}(x) \\ \overline{\omega}_l(x) = \overline{\mu}_{\tilde{F}_1^l}(x)\, \overline{\mu}_{\tilde{F}_2^l}(x) \cdots \overline{\mu}_{\tilde{F}_m^l}(x) \end{cases} \qquad (4-11)$$

in which $\underline{\mu}_{\tilde{F}_i^l}(x)$ and $\overline{\mu}_{\tilde{F}_i^l}(x)$ denote the lower and upper membership grades, respectively. Then, the inferred IT2 T–S fuzzy model is defined by

$$x_{k+1} = \sum_{l=1}^{m} \left\{\alpha\, \underline{\omega}_l(x) + \beta\, \overline{\omega}_l(x)\right\}(A_l x + B_l u) = \sum_{l=1}^{m} \widetilde{\omega}_l(x)(A_l x + B_l u) \qquad (4-12)$$

where

$$\begin{cases} \widetilde{\omega}_l(x) = \alpha\ \underline{\omega}_l(x) + \beta\ \overline{\omega}_l(x) \in [0,1] \\ \sum_{l=1}^{m} \widetilde{\omega}_l(x) = 1 \end{cases} \qquad (4-13)$$

Here, the values of α and β are both set as 0.5, according to Ref. [6] To control a nonlinear plant based on the IT2 T–S fuzzy model described by Eq. (4-14), an IT2 T–S fuzzy controller is designed, and its fuzzy rules are given as follows:

$R^{(r)}$: IF z_1 is $\tilde{F}_1^r$ and z_2 is $\tilde{F}_2^r$,..., and z_v is $\tilde{F}_v^r$, THEN $u_k = \widetilde{K}_r x_k, \qquad (r \in L \coloneqq 1,2,\dots,m)$

where $\widetilde{K}_r$ stands for the *r*th local linear control gain. The output of this controller is defined to be

$$u(k) = \sum_{r=1}^{m} f\left(\omega_r^L(x), \omega_r^U(x)\right) \widetilde{K}_r\ x \qquad (4-14)$$

ω_r^L and ω_r^U satisfy the constraint,

$$\sum_{r=1}^{m} \omega_r^L(x) + \omega_r^U(x) = 1 \qquad (4-15)$$

and the value of $f\left(\omega_r^L(x), \omega_r^U(x)\right)$ depends on the TR methods and belongs to an interval. The TR method is employed in this section and based on minimax uncertainty bounds. [7] Assigning $\left(\omega_r^L(x), \omega_r^U(x)\right)/2$ to $\left(\omega_r^L(x), \omega_r^U(x)\right)$ and substituting it into Eq. (4-16); leads to

$$u_k \in \left[u_k^{(O)}, u_k^{(M)}\right] \qquad (4-16)$$

Then, the uncertainty bounds can be calculated to be

$$\begin{cases} \overline{u}_{c,k} = \min\left\{u_k^{(O)}, u_k^{(M)}\right\} \\ \underline{u}_{c,k} = \overline{u}_{c,k} - \left[\dfrac{\sum_{i=1}^{m}\overline{\omega}^i - \underline{\omega}^i}{\sum_{i=1}^{m}\overline{\omega}^i \sum_{i=1}^{m}\underline{\omega}^i} \times \dfrac{\sum_{i=1}^{m}\underline{\omega}^i(K_i - K_1)x \sum_{i=1}^{m}\overline{\omega}^i(K_m - K_i)x}{\sum_{i=1}^{m}\underline{\omega}^i(K_i - K_1)x + \sum_{i=1}^{m}\overline{\omega}^i(K_m - K_i)x}\right] \end{cases} \quad (4-17)$$

The lower bound $\underline{u}_{c,k}$ is assigned to be equal to the upper bound $\overline{u}_{c,k}$ if only one rule is fired (i.e., $m = 1$). The crisp output of the controller is

$$\begin{cases} u_k \approx \dfrac{1}{2}\left(\underline{u}_{c,k} + \overline{u}_{c,k}\right) \\ \lambda_k = u_k \end{cases} \quad (4-18)$$

So far, the optimized control parameters ϕ_α, ϕ_β were used to fit to the style factor λ using the linear interpolation,

$$\phi = \phi_i + (\phi_{i+1} - \phi_i)\frac{\lambda - \lambda_i}{\lambda_{i+1} - \lambda_i}, \qquad \lambda \in [\lambda_i, \lambda_{i+1}] \quad (4-19)$$

where, index i indicates the type of classified driving styles. Activated by Eq. (4-19), the proceed signal of driving style λ can be calculated and used to adjust the rules of CD/CS strategy based on mapping relations between the style factor λ and the control parameters ϕ_α, ϕ_β.

4.3 EXPERIMENTAL PLAN

4.3.1 DRIVING CYCLE PRODUCTION

In this case, driving cycles are considered based on the Worldwide Harmonised Light Vehicle Test Procedure (WLTP). These testing cycles are generated from the sub-driver model [8] by

adjusting the style factor λ, wherein five standard driving styles and one stochastically changing driving style are acquired, namely, V. Gentle, Gentle, Normal, Aggressive, V. Aggressive, Stochastic. It should be noted that the driving cycle with stochastic style changes is produced by adding a white noise signal to the style factor. Fig. 4-4 presents the probability density function of vehicle acceleration of all of the testing cycles.

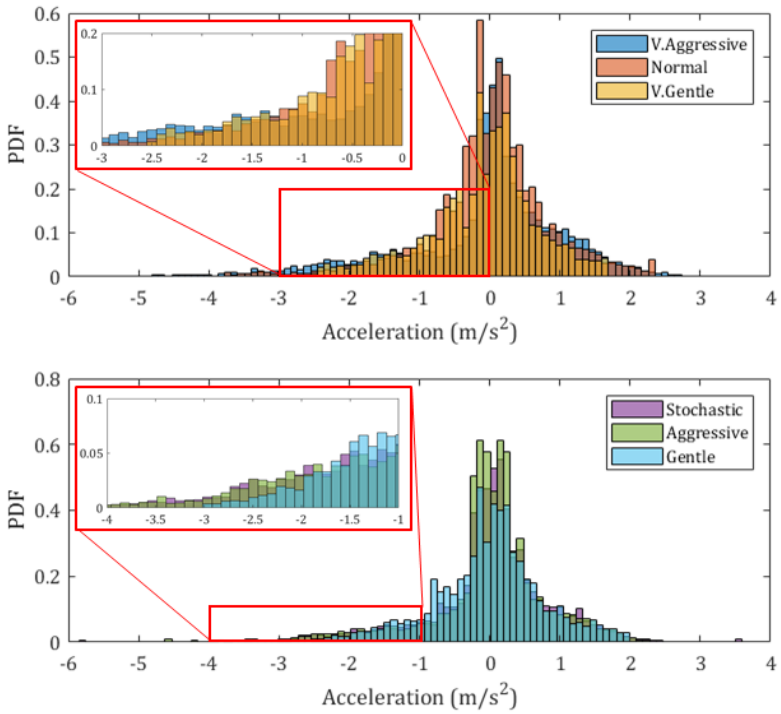

Fig. 4-4. Probability density of classified WLTP-based cycles

Fig. 4-4 shows that, for all the driving cycles, the acceleration distribution is unimodal with the mode being close to zero. It is also apparent that the dispersion of the acceleration distribution increases with driving aggressiveness. It is interesting to see that aggressive driving seems to come out in more deceleration events than acceleration events. The reason is that the maximum range of acceleration events is determined by the vehicle driving torque, and the maximum range of deceleration events depends on the braking force. Table 4-1 summarizes the specifications of the driving cycles through their style factors, maximum accelerations, and minimum decelerations.

Table 4-1. Driving cycle profiles under classified driving styles

Driving style type	Style factor	Max. acceleration (m/s^2)	Min. acceleration (m/s^2)
Very Gentle	λ_1	1.7	-2.5
Gentle	λ_2	2.0	-3.0
Normal	λ_3	2.3	-3.7
Aggressive	λ_4	2.8	-4.6
Very Aggressive	λ_5	3.6	-5.8
Stochastic	$[\lambda_1, \lambda_5]$	3.6	-5.8

4.3.2 HARDWARE-IN-THE-LOOP EXPERIMENT

Hardware in the loop testing is used for evaluating the cyber-physical system's real-time performance. This research uses the industry standard real-time testing facilities provided by the ETAS Group. The configuration of the HiL testing system is shown in Fig. 4-5. The distributed computing and V2I communication are performed by an ETAS ES910, whose core components are a 1.5GHz microprocessor with 4GB RAM and 1Gbps Ethernet communication. The control strategy and algorithm involved in the proposed ODEM methodology are programmed into host PC-1 and flashed to the ES910 by ETAS INTECRIO. The DESKLABCAR functions as the PHEV with a local controller and it communicates with the V2I interface (ES910) via a CAN bus. The vehicle and local controller are modelled and compiled in host PC-2 and downloaded to the DESK-LABCAR by the ETAS experimental environment via Ethernet protocol. In this study, the sampling time is 10 Hz and the vehicle performance is supervised by the ETAS experimental environment in host PC-2.

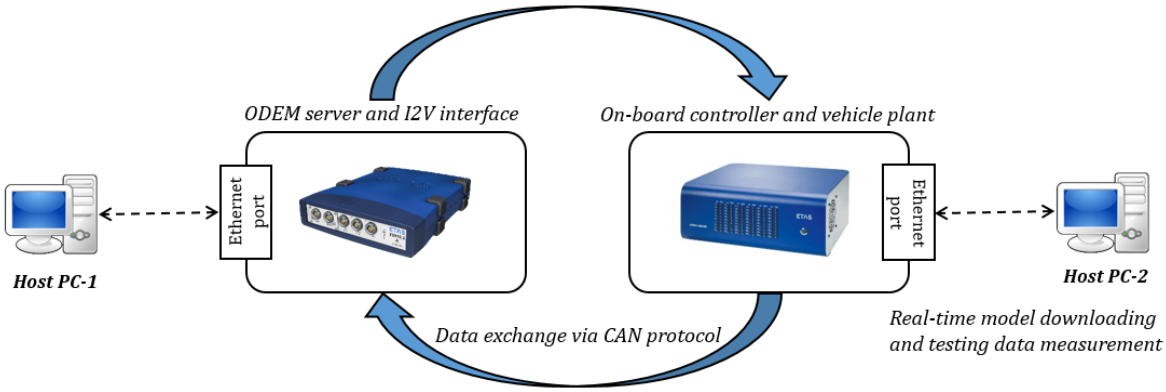

Fig. 4-5. Hardware-in-the-loop testing system

4.4 RESULT AND DISCUSSION

This section presents the experimental results of the study and provides an in-depth elaboration from the four aspects of energy-saving performance, vehicle system adaptability, and communication efficiency comparison.

4.4.1 ENERGY-SAVING PERFORMANCE

This section studies impact of different driving styles on energy-saving performance of the improved vehicle system. For comprehensive evaluation, the vehicle systems embedded with different control strategies are compared, including the ECMS and the CD/CS strategy of using stationary and personalized non-stationary inferences (the proposed ODEM). During the experiment, the PHEV's components work within their operational ranges in real-time for all involved strategies.

Fig. 4-6 illustrates the HiL result over the WLTP-based driving cycle with Normal driving style, in which the colour bar represents the corresponding thermal efficiency (%) of the ICE. The initial SoC value is set to 50% in order to focus on the conversion of multiple energy sources in CD/CS mode. It can be seen from the highlighted equivalent operating points (black dotted circle) that using the proposed ODEM methodology leads to more operating points of the engine in the high-efficiency area (marked in yellow) compared to the ECMS and CD/CS strategy.

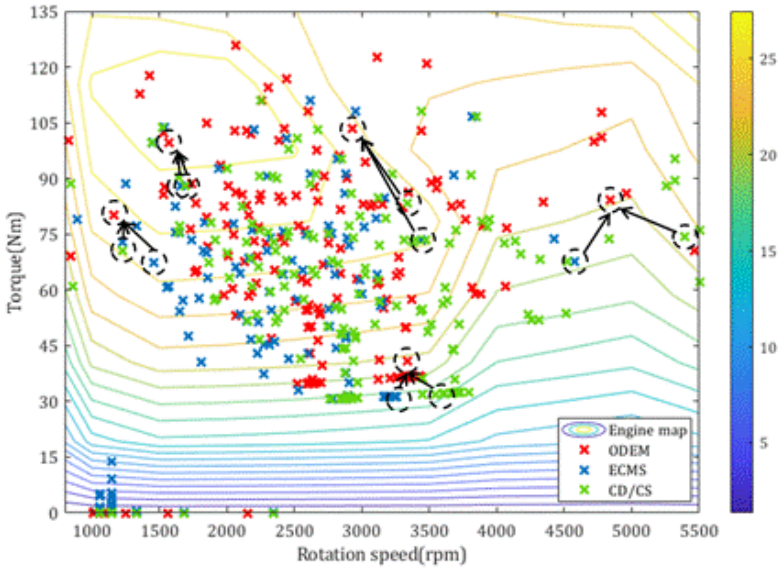

Fig. 4-6. Engine operation map during Normal in driving style

The performance comparison of the studied control strategies for each driving style is summarized in Table II. Evidently, the vehicle system using the proposed ODEM methodology outperforms the system using ECMS or CD/CS strategy for different driving styles in the WLTP cycle. There is a nonlinear relationship between the total energy and aggressiveness of driving style which rises first and then drops. It appears that too mild actions signify lower power demand so that the control strategy has greater latitude in optimizing between the different

traction modes. The results show the proposed ODEM system has a significant reduction in energy consumption of 9.16% from the conventional CD/CS control strategy in the Very Gentle driving style, compared to 4.33% reduction by using the ECMS.

Table 4-2. Performance comparison of using different control strategies

Driving style	Control strategy	Final SoC	Used fuel (g)	Total energy (J)	Savings (%)
Very Gentle	CD/CS	0.4141	2.1334e+03	9.8150e+07	-
	ECMS	0.2331	2.0309e+03	9.3896e+07	4.33%
	ODEM	0.3735	1.9380e+03	8.9162e+07	9.16%
Gentle	CD/CS	0.4038	2.1934e+03	1.0091e+08	-
	ECMS	0.2299	2.1439e+03	9.80943+07	2.78%
	ODEM	0.3797	2.1111e+03	9.6122e+07	4.76%
Normal	CD/CS	0.4021	2.2416e+03	1.0312e+08	-
	ECMS	0.2304	2.1942e+03	1.1014e+08	1.67%
	ODEM	0.3868	2.1649e+03	9.9598e+07	3.42%
Aggressive	CD/CS	0.4140	2.2976e+03	1.0570e+08	-
	ECMS	0.2350	2.2527e+03	1.0409e+08	1.52%
	ODEM	0.3998	2.2262e+03	1.0241e+08	3.12%
Very Aggressive	CD/CS	0.3987	2.2327e+03	1.0271e+08	-
	ECMS	0.2340	2.2075e+03	1.0201e+08	0.68%
	ODEM	0.3799	2.1956e+03	1.0031e+08	2.34%

4.4.2 VEHICLE SYSTEM ADAPTABILITY

Investigation of vehicle system adaptability when using the ODEM methodology is carried out over the driving cycle with stochastic changes in driving styles (produced in Section 4.3.1). For evaluation purposes, a type-1 fuzzy set is designed to compare the ODEM methodology with a type-2 fuzzy set. The type-1 and type-2 MFs of the inputs are shown in Fig. 4-7, wherein their

shapes are drawn following Ref. [6]. Type-2 MFs impose extra constraints on fuzzy rules for improving identifiability in fuzzy-logic-based driving style recognition. Here, 25 fuzzy rules are defined and used to infer an output of the style factor, as shown in Table 4-3.

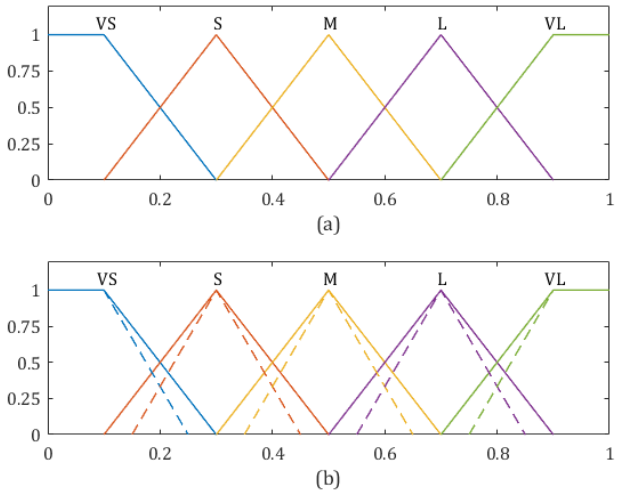

Fig. 4-7. MFs of the two input variables (i.e. v_{avg} and a_{rng}): (a) type-1 MFs; (b) type-2 MFs

Table 4-3. Rule base for 5×5 fuzzy logic inference

v_{avg}	a_{rng}				
	VS	S	M	L	VL
VS	VG	VG	G	G	N
S	VG	G	G	N	A
M	G	G	N	A	A
L	G	N	A	A	VA
VL	N	A	A	VA	VA

Fig. 4-8 shows the real-time performance of the PHEV system using the ODEM methodology, wherein type-1 and type-2 fuzzy sets are separately embedded, and their performance is investigated. From the result, both using two types of fuzzy sets has an ability to detect driving

behaviour (style factor). The trend of real-time performance from using these two types of fuzzy set is roughly the same and that their style factors vary in $[0,1]$. From the actions of the ICE in the intercepted period, the type-2 fuzzy set driven recognizer offers a relatively mild driving style. Under the conditions of the same MF distribution, using type-2 fuzzy set saves 2.35% total energy under the same final value of SoC compared to using type-1 fuzzy sets. In fact, there is a trade-off between the quantity of the parameters and the performance enhancement brought by introducing more parameters. Differing using discrete classes, using continuous indexing is no need to classify rare driving behaviours separately. The appropriate number of categories can reduce development cost and ensure the system robustness. Compared with the three discrete driving modes (i.e. eco, balanced, and sport modes) of mainstream luxury models, the adaptive sliding driving mode based on five categories is definitely a great improvement for the industry.

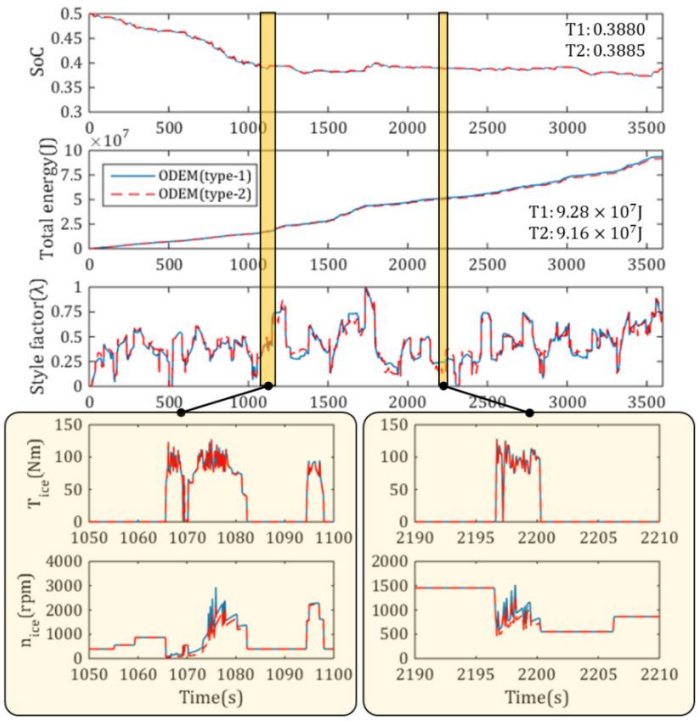

Fig. 4-8. Real-time performance of HEV system during stochastic changes in driving style

4.4.3 COMMUNICATION EFFICIENCY COMPARISON

This section compares communication efficiency for a connected vehicle system under different signal loss rates. A trigger square signal is designed to simulate communication quality of the V2X network between the vehicle and roadside unit. As shown in Fig. 4-9, six levels of signal loss rate are considered and used to expose the communication efficiency of the ODEM methodology. Each trigger segment is used to activate the function of driving style recognition and its duration is fixed at 30 s. Conversely, the non-trigger segment is used to deactivate the recognition function and its duration is based on the signal loss rate.

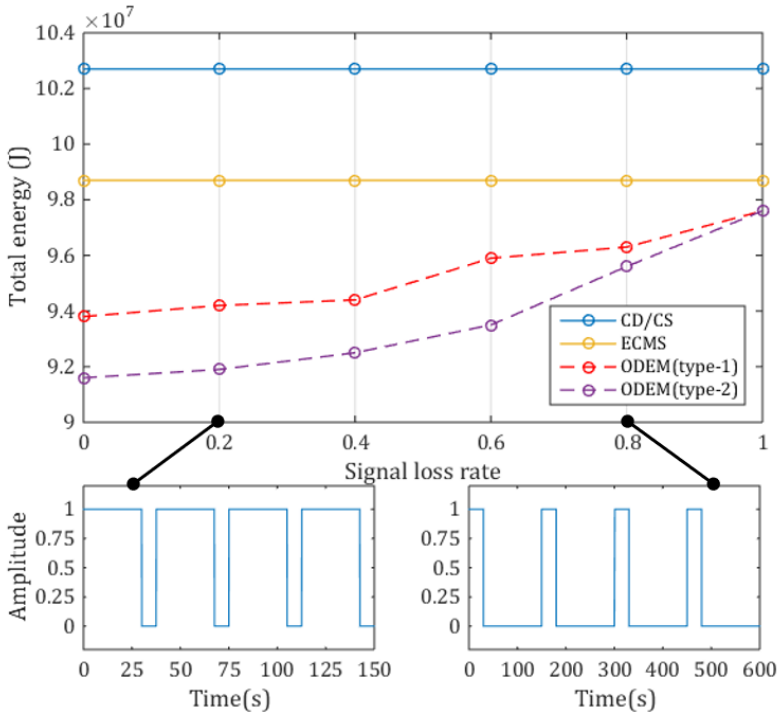

Fig. 4-9. Communication efficiency comparison under different signal loss rate

From the result, the ECMS and the conventional CD/CS strategy are not affected by signal loss because their control policies do not need to be updated during real-time driving. As signal loss rate increases, the energy consumption of the ODEM systems using type-1 and type-2

fuzzy sets both increase gradually. When the signal is completely lost, their performance is still higher than that obtained by using the ECMS (1.11%) and the conventional CD/CS strategy (4.31%). Therefore, the proposed ODEM methodology has an ability to help the connected PHEV system improve fuel economy even under harsh communication conditions, especially when using type-2 fuzzy sets.

4.5 SUMMARY

This chapter proposes and investigates a new personalized non-stationary inference approach for online driver-oriented energy management (ODEM) of connected plug-in hybrid electric vehicles. The vehicle system's performance with the proposed ODEM is evaluated in terms of the performance of energy saving, vehicle system adaptability and communication efficiency. The advantage of the vehicle system driven by the proposed ODEM methodology has been demonstrated through HiL testing. The conclusions drawn from the investigation are as follows:

1) The vehicle controller using the ODEM methodology adapts well to differing driving styles, including stochastic changes in driving style.
2) Compared to the CD/CS strategy with stationary inference, up to 9% total energy can be saved over the WLTP-based cycle by using personalized non-stationary inference, especially for very gentle drivers.
3) Compared to driven by type-1 fuzzy sets, driving style recognizer driven by type-2 fuzzy sets helps save a further 2.35% of total energy for stochastic changes in driving style.

4) When the control signal is completely lost, energy-saving performance of the improve vehicle system is still higher than that of the ECMS (1.11%) and the CD/CS strategy (4.31%).

The novelty of this chapter contributes to the field is that real-time monitoring of driving behaviour has been introduced to increase robustness of the HEV energy management system and that, via the V2X network, optimal control parameters for the rule-based control strategy, which is currently in wide use, can be determined in real-time to adapt to change of driving behaviour.

REFERENCES

[1] R. T. Marler and J. S. Arora, "The weighted sum method for multi-objective optimization : new insights," *Structural and multidisciplinary optimization*, vol. 41, no. 6, pp. 853–862, 2010.

[2] J. Kennedy, "Particle swarm optimization," in *Encyclopedia of machine learning*, Springer, pp. 760–766.

[3] Q. Zhou, Y. Zhang, Z. Li, J. Li, H. Xu, and O. Olatunbosun, "Cyber-Physical Energy-Saving Control for Hybrid Aircraft-Towing Tractor Based on Online," *IEEE TRANSACTIONS ON INDUSTRIAL INFORMATICS*, vol. 14, no. 9, pp. 4149–4158, 2018.

[4] Q. Zhou, W. Zhang, S. Cash, O. Olatunbosun, H. Xu, and G. Lu, "Intelligent sizing of a series hybrid electric power-train system based on Chaos-enhanced accelerated particle swarm optimization," *Applied Energy*, vol. 189, pp. 588–601, 2017.

[5] J. Li, Q. Zhou, Y. He, H. Williams, and H. Xu, "Driver-identified Supervisory Control System of Hybrid Electric Vehicles based on Spectrum-guided Fuzzy Feature Extraction," *IEEE Transactions on Fuzzy Systems*, vol. 6706, no. c, pp. 1–1, 2020.

[6] J. Cao, P. Li, and H. Liu, "An Interval Fuzzy Controller for Vehicle Active Suspension Systems," *IEEE Transactions on Intelligent Transportation Systems*, vol. 11, no. 4, pp. 885–895, 2010.

[7] J. M. Mendel, "Advances in type-2 fuzzy sets and systems," *Information Sciences*, vol. 177, no. 1, pp. 84–110, 2007.

[8] Y. Zhang *et al.*, "Optimal energy management strategy for parallel plug-in hybrid electric vehicle based on driving behavior analysis and real time traffic information prediction," *Mechatronics*, vol. 46, pp. 177–192, 2017.

CHAPTER 5

DRIVER-ORIENTED SUPERVISORY CONTROL SYSTEM BASED ON SPECTRUM-GUIDED FUZZY FEATURE EXTRACTION

The content presented in the Chapter 5 is based on the author's published article, 'Driver-identified Supervisory Control System of Hybrid Electric Vehicles using Spectrum-guided Fuzzy Feature Extraction' in IEEE Transactions on Fuzzy Systems. [1] Inspired by the personalized non-stationary inference approach proposed in Chapter 4, the author aimed to transfer driving style classification methods from continuous indexing towards discrete classes and expand the human-related factors from velocity and acceleration only towards velocity, gas pedal, brake pedal, and steering wheel angle. This chapter introduces the concept of the driver-identified supervisory control system, which forms a novel architecture of adaptive energy management for hybrid electric vehicles (HEVs). As a man-machine system, the proposed system can accurately identify the human driver from natural operating signals and provides driver-identified globally optimal control policies as opposed to mere control actions. To help improve the identifiability and efficiency of this control system, the method of spectrum-guided fuzzy feature extraction (SFFE) is developed. Firstly, the configuration of the HEV model and its control system are analysed. Secondly, design procedures of the SFFE algorithm are set out to extract 15 groups of features from primitive operating signals. Thirdly, long-term and short-term memory networks are developed as a driver recognizer and tested by the features. The driver identity maps to corresponding control policies optimized by dynamic programming. Finally, the comparative study includes involved extraction methods

and their identification system performance as well as their application to HEV systems. The results demonstrate that with help of the SFFE, the driver recognizer improves identifiability by at least 10% compared to that obtained using other involved extraction methods. The improved HEV system is a significant advance over the 5.53% reduction on fuel consumption obtained by the fuzzy-logic-based system.

5.1. PROBLEM STATEMENT

In order to rationally assign the demand power of the powertrain to different power sources, the demand power of the powertrain and the state of charge (SoC) value of the battery package (BP) are treated as two input variables and the two output variables are the rotational speed of traction motor and the required power of the ISG. Here, the supervisory control system comprises two modes of pure electric traction and optimization-based traction, which can be expressed as

$$\left(T_{mot}, n_{mot}, P_{ice}, P_{gen}\right) = \begin{cases} Mode_{EV}(P_d, SoC), 0.8 \geq SoC > 0.5 \\ Mode_{opt.}(P_d, SoC), 0.5 \geq SoC > 0.2 \end{cases} \qquad (5-1)$$

where, $Mode_{EV}$ indicates a pure electric traction mode; $Mode_{opt.}$ indicates an optimization-based control mode; T_{mot} is the torque of traction motor; n_{mot} is the rotational speed of traction motor; P_{ice} is the power of internal combustion engine; P_{gen} is the power of the integrated starter-generator; P_d is the demand power of the powertrain; and SoC is the BP's state of charge. To ensure the BP is performing under proper conditions and to protect the BP from over discharge, the battery's SoC should remain in the range, $0.2 < SoC \leq 0.8$ considered as Ref. [2].

In the electric traction mode, enough battery current can be supplied to satisfy the powertrain demand independently so that neither the ICE nor the ISG need to operate. The power distribution in this state is

$$\left.\begin{array}{c} T_{mot,k} = T_{d,k} \\ n_{mot,k} = \dfrac{P_{d,k}}{T_{mot,k}} \cdot 9550 \\ P_{gen,k} = 0 \\ P_{ICE,k} = 0 \end{array}\right\} . \qquad (5-2)$$

where 9550 is a conversion factor when units of torque, power and rotation speed are Newton, kilowatt and revolution per minutes separately. The optimization-based control mode allows ICE power to be used either to simultaneously drive the vehicle and charge the BP or to partially drive the vehicle supplemented by a BP-charge-depleting drive from the trans-motor, depending on the sign of the trans-motor speed, n_{mot} (negative charges, positive depletes). The power distribution in this state is therefore given by

$$\left.\begin{array}{c} T_{mot,k} = T_{d,k} \\ n_{mot,k} = n_{mot\_opt,k} \\ P_{gen,k} = P_{gen\_opt,k} \\ P_{ICE,k} = -P_{gen,k} + \left(P_{d,k} - \dfrac{T_{mot,k} \cdot n_{mot,k}}{9550}\right) \end{array}\right\} , \qquad (5-3)$$

where $n_{mot\_opt,k}$ is the optimal rotation speed of the traction motor; and $P_{gen\_opt,k}$ is the optimal demand power of the ISG. Based on Eq. (5-3), the state equation of the HEV model can be generally expressed in discrete-time format by the following equation

$$\left.\begin{array}{c} x_{k+1} = f(x_k, u_k) \\ x = SoC \\ u_k = [n_{mot\_opt,k} \quad P_{gen\_opt,k}] \end{array}\right\} , \qquad (5-4)$$

where, x is the state variable; k is the integer-valued discrete time variable; and u denotes the control variable expressed as a vector of the optimized rotational speed n_{mot_opt} of the traction motor and the optimized demand power P_{gen_opt} of the ISG.

The principal optimization target for HEV systems is to reduce fossil fuel consumption by obtaining energy from the electricity grid. The following cost function for minimizing fuel consumption will be adopted

$$\min J = \sum_{k=0}^{N-1} L(x_k, u_k) = \sum_{k=0}^{N-1} E_{fuel,k} \quad , \qquad (5-5)$$

where, N is the length of the driving cycle in discrete time-steps, L is the instantaneous cost, and E_{fuel} is the instantaneous fuel consumption at the kth time step. To ensure a smooth operation of engine, ISG, traction motor, and battery, the following constraints will be needed for the optimization.

$$s.t. \begin{cases} T_{mot,k}, & -T_{mot}^{*} \le T_{mot,k} \le T_{mot}^{*} \\ n_{mot\_opt,k}, & 0 \le n_{mot\_opt,k} \le n_{mot}^{*} \\ P_{ICE,k}, & 0 \le P_{ICE,k} \le P_{ICE}^{*} \\ P_{gen\_opt,k}, & -P_{ISG^{*}} \le P_{gen\_opt,k} \le 0 \\ SoC_k, & 0.2 < SoC_k \le 0.8 \end{cases} , \qquad (5-6)$$

where, T_{mot}^{*} and n_{mot}^{*} are the maximum torque and the maximum rotational speed of the traction motor; P_{ICE}^{*} and $P_{ISG^{*}}$ are the maximum power of the engine and of ISG.

5.2. PROPOSED SOLUTION

The proposed driver-identified supervisory control system includes one LSTM-based driver recognizer and one DP-based supervisory controller as shown in Fig. 5-1. During real-time driving, human drivers generate primitive operating signals which are collected by a driving simulator. Due to primitive operating signals with interference information redundancy, driving feature extraction is needed to improve the identifiability and the efficiency of this control system. Through feature extraction, these extracted signals will be used as inputs to the recognizer identifying drivers that each bridge to their own control policy in the supervisory controller. Finally, the driver-identified control signal will be sent to the HEV powertrain to manage energy utilization.

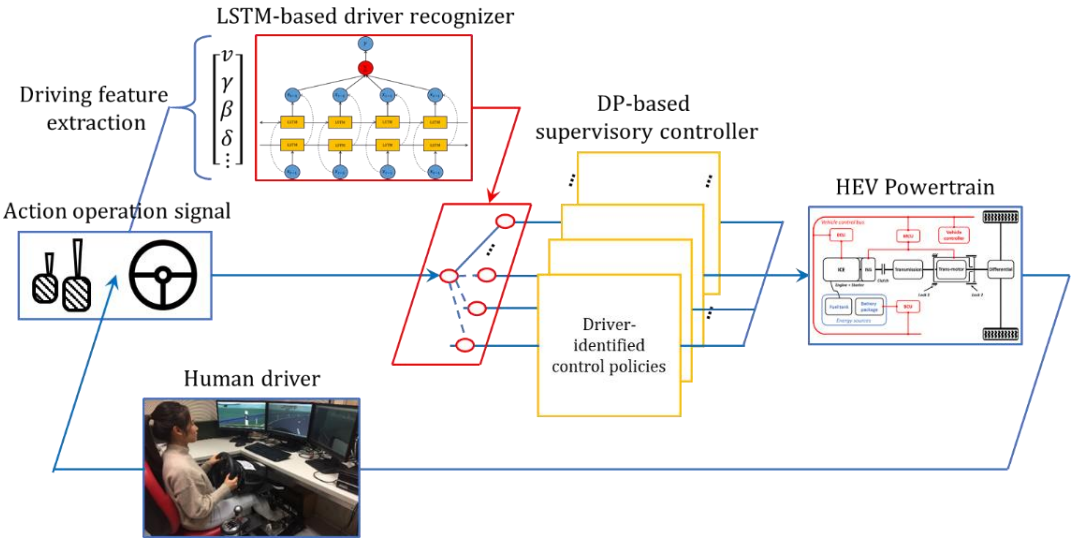

Fig. 5-1. Workflow of driver-identified supervisory control system

5.2.1. DRIVING FEATURE EXTRACTION

To improve identifiability of the driver-identified supervisory control system, characterization of the training material is needed for the extraction of hidden features from the time-series of the primitive operating signals. The driving operating signals studied in this chapter are vehicle speed, gas pedal deflection, brake pedal deflection, and steering angle. Compared to others need to be detected with additional sensors, they were shown to be a pragmatic choice for driving style recognition by Martinez et al. [3] This section starts with the primitive operation signals namely Feature 0 and follows by introducing the rest of 14 groups of features that are respectively extracted by time-domain, frequency-domain and the proposed SFFE methods.

Feature 0: The driving operating signals originally collected from a driving simulator are regarded as the baseline in this research and are combined into the row vector, $[v \quad \gamma \quad \beta \quad \delta]$, where v is vehicle speed (km/h); γ is gas pedal deflection (%); β is brake pedal force (%); and δ is the steering angle (rad). In the initial investigation on the human-related factors, the author has found that it is extremely hard to differentiate the drivers' identities under the similar driving conditions by only using velocity and acceleration for network training.

A. Time and frequency domain extractions

In the widely used time-domain extraction technique, a short-term sliding window is introduced to standardize the sampling dimension and lengthen the memory time of characteristic states. Here, the dataset of driving operating signals is defined, in which each time step k of data is expressed as given by:

$$(\boldsymbol{v},\boldsymbol{\gamma},\boldsymbol{\beta},\boldsymbol{\delta})^T = \begin{bmatrix} v_{k-h+1} & v_{k-h+2} & \cdots & v_k \\ \gamma_{k-h+1} & \gamma_{k-h+2} & \cdots & \gamma_k \\ \beta_{k-h+1} & \beta_{k-h+2} & \cdots & \beta_k \\ \delta_{k-h+1} & \delta_{k-h+2} & \cdots & \delta_k \end{bmatrix} \quad (5-7)$$

where, h is length of the short-term sliding window, which is taken to be the discrete time equivalent of 60 seconds.

Feature 1: The maximum values of the four elements in the time-domain are adopted to reflect the operating intensity of drivers. Based on Eq. (5-7), their values can be calculated by

$$(v_{max},\gamma_{max},\beta_{max},\delta_{max}) = \max(\boldsymbol{v},\boldsymbol{\gamma},\boldsymbol{\beta},\boldsymbol{\delta}_{abs})^T \quad , \quad (5-8)$$

where $\boldsymbol{\delta}_{abs}$ denotes the element wise absolute value of $\boldsymbol{\delta}$.

Feature 2: The maximum ranges of the four elements in the time-domain are adopted to reflect the operating proficiency of drivers. In general, drivers with higher operating proficiency have lower maximum range. Based on Eq. (5-7), their values can be calculated by

$$\left(v_{rng.},\gamma_{rng.},\beta_{rng.},\delta_{rng.}\right) = \max(\boldsymbol{v},\boldsymbol{\gamma},\boldsymbol{\beta},\boldsymbol{\delta}_{abs})^T - \min(\boldsymbol{v},\boldsymbol{\gamma},\boldsymbol{\beta},\boldsymbol{\delta}_{abs})^T \quad . (5-9)$$

Feature 3: The average values of the four elements in the time-domain are adopted to reflect driving habits. The authors hypothesize that this factor is related to the driving geography and the environment but a discussion of this hypothesis is beyond the scope of this chapter and will be left as a topic for future research. Based on Eq. (5-7), the average values of the four elements in the time-domain are

$$\left(v_{avg.},\gamma_{avg.},\beta_{avg.},\delta_{avg.}\right) = \frac{\sum_{i=0}^{i=h}(\boldsymbol{v},\boldsymbol{\gamma},\boldsymbol{\beta},\boldsymbol{\delta}_{abs})^T}{h} \quad . \quad (5-10)$$

Another mainstream extraction method to determine the extent of pre-processing human behaviours is frequency domain extraction. [4] Here, the discrete (fast) Fourier transform (DFT)

is used to calculate three principal features and they will be examined later when training the recognizer. Therefore, the DFT of matrix Eq. (5-11) can be written

$$\left(\boldsymbol{H}_v, \boldsymbol{H}_\gamma, \boldsymbol{H}_\beta, \boldsymbol{H}_\delta\right)^T = \begin{bmatrix} H_{v,1} & H_{v,2} & \cdots & H_{v,L} \\ H_{\gamma,1} & H_{\gamma,2} & \cdots & H_{\gamma,L} \\ H_{\beta,1} & H_{\beta,2} & \cdots & H_{\beta,L} \\ H_{\delta,1} & H_{\delta,2} & \cdots & H_{\delta,L} \end{bmatrix} \qquad (5-11)$$

where, $H_v, H_\gamma, H_\beta, H_\delta$ denote the single-sided amplitude spectra corresponding to vehicle speed, gas pedal deflection, brake pedal force, and steering angle, respectively; and $L = h/2$.

Feature 4: The maximum magnitudes of the four elements in the frequency domain are used to express the spectral intensity of driving operation via the equation,

$$\left(H_{v\_max,k}, H_{\gamma\_max,k}, H_{\beta\_max,k}, H_{\delta\_max,k}\right) = \max\left(\boldsymbol{H}_v, \boldsymbol{H}_\gamma, \boldsymbol{H}_\beta, \boldsymbol{H}_\delta\right)^T \quad , \qquad (5-12)$$

Feature 5: The frequencies corresponding to the maximum magnitudes (denoted by $\max freq$) of the four elements in the frequency domain are used to express the regularity of driving operation via the equation,

$$\left(f^*_{v\_max,k}, f^*_{\varrho\_max,k}, f^*_{\sigma\_max,k}, f^*_{\varsigma\_max,k}\right) = \max freq\left(\boldsymbol{H}_v, \boldsymbol{H}_\gamma, \boldsymbol{H}_\beta, \boldsymbol{H}_\delta\right)^T \quad . \quad (5-13)$$

Feature 6: As another feature to express the regularity of driving operation, the frequencies corresponding to the centroids of the four elements in the frequency domain are considered. They are defined as follows:

$$\left(H^*_{v\_cen,k}, H^*_{\varrho\_cen,k}, H^*_{\sigma\_cen,k}, H^*_{\varsigma\_cen,k}\right) = \frac{\sum_{i=1}^{i=L} f_i \times \left(H_{v,i}, H_{\gamma,i}, H_{\beta,i}, H_{\delta,i}\right)}{\sum_{i=1}^{i=L} f_i} \quad , (5-14)$$

in which

$$f_i = \frac{Fs}{h} i, \qquad i = 1,2, \dots, L, \tag{5-15}$$

where, $Fs = 1000$ Hz is the sampling frequency.

B. Spectrum-guided fuzzy feature extraction

It should be noted that instantaneous changes in driver behaviour might affect the characteristic expression of the time-series data during real-time driving. The SFFE activates the sampling window and uses frequency-domain characteristics as the basis for adaptively adjusting the window size. It is developed to ensure the classification accuracy while adaptively searching for a more appropriate minimum size of the sliding window. Ideally, it can enable the elimination of the effects of sudden driver behaviour changes on the characteristic expression of the time-series data through adaptively adjusting the size of the short-term sliding window. The consideration of spectral features easily captures essential attributes from the dynamic driving signals and they can be exploited as an important factor in adjusting window size. Inspired by fuzzy encoding technology, all spectral features are integrated to balance the contribution of each element to the window size, thereby guiding time-domain extraction. The design procedures of the SFFE are:

Feature 7-15: The fuzzy sets with linguistic terms are regulated with standard triangular membership functions (MFs), where the degree of membership is expressed as a function of normalized values in the interval, $[0,1]$. The values of the MFs in the FLC are set at three levels: Low, Medium, and High. These functions fuzzify the crisp inputs. Here, the inputs of the FLC need to be sensitively scaled to maintain the boundaries of their working area. They are formulated mathematically through the relationship,

$$(v^*, \gamma^*, \beta^*, \delta^*) = \left(\frac{v_f - v_f^-}{v_f^+ - v_f^-}, \frac{\gamma_f - \gamma_f^-}{\gamma_f^+ - \gamma_f^-}, \frac{\beta_f - \beta_f^-}{\beta_f^+ - \beta_f^-}, \frac{\delta_f - \delta_f^-}{\delta_f^+ - \delta_f^-}\right), \qquad (5-16)$$

where, $v_f, \gamma_f, \beta_f, \delta_f$ indicate spectral feature signals related to speed, gas, brake and steering angle; $\cdot^-$ and $\cdot^+$ indicate the corresponding minimum and maximum; and $\cdot^*$ indicates the corresponding scaled input, $[0,1]$. The rule base determines the control output O with the inputs states A, B, C, and D by applying a 'if A and B and C and D then O' policy. A mathematical expression of the 'if A and B and C and D then O' policy is

$$O = (A \times B \times C \times D) \circ R\,. \qquad (5-17)$$

where, 'A', 'B', 'C', 'D' denote the fuzzy sets of scaled spectral signals related to speed, gas, brake and steering angle; 'O' denotes the crisp of the reference of scalar coefficient $[0,1]$ for the size of sliding windows; and 'R' denotes the fuzzy relation matrix by cross-product of four fuzzy sets of inputs.

To simplify the expression of $3^4 = 81$ fuzzy logic inferences, we assign values to linguistic sets: 'Short' $= 1$; 'Medium' $= 2$; 'Long' $= 3$. Therefore, the reasoning process that is based on Eq. (17) with the Sugeno fuzzy set can then be described by the following if-then statements:

$$\left.\begin{array}{c}\text{if } A+B+C+D \in [4,6] \\ \text{if } A+B+C+D \in [7,9] \\ \text{if } A+B+C+D \in [10,12]\end{array}\right\} \text{ then O is} \begin{cases}\text{Long} \\ \text{Medium} \\ \text{Short}\end{cases} \qquad (5-18)$$

In this inference mechanism, the implied fuzzy sets are produced using the max–min composition. In defuzzification, these implied fuzzy sets are combined to provide a crisp value of the controller outputs. There are several approaches [5] to accomplish the defuzzification process, of which the centroid of area method has been chosen for this case. The final output

is then measured as the average of the individual centroids weighted by their membership values as follows:

$$\left.\begin{aligned} O &= \frac{\sum_{i=1}^{n} Out_i \cdot \varphi_i}{\sum_{i=1}^{n} \varphi_i} \\ h^* &= h - \frac{h}{2} O \end{aligned}\right\}, \qquad (5-19)$$

where, Out_i is the output of rule base i; φ_i is the centre of the output MF; and h^* is the size of the adaptive sliding window. In this chapter, these functions are taken as a triangular membership function as follows:

$$q_i = \max\left(\min\left(\frac{x-(0.5i-0.9)}{0.4}, \frac{(0.5i-0.1)-x}{0.4}\right), 0\right), \qquad i = 1,2,3. \ (5-20)$$

Through fuzzy encoding technology, the proposed method extracts 3×3 permutations between time and frequency domain. i.e. nine groups of extra features. Their mapping relation is expressed as shown in the following table:

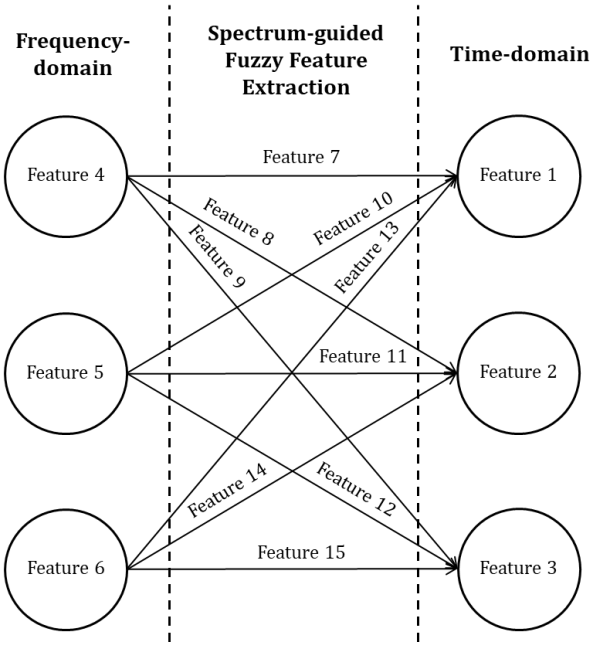

Fig. 5-2. Mapping relation in spectrum-guided fuzzy feature extraction

An upgrade version of time-domain extraction, the purpose is the elimination of the effects of sudden driver behaviour changes on the characteristic expression of the time-series data. So far, 15 groups of features extracted from the original operating signals are obtained and then used as training data for the driver recognizer. These will be discussed in the next section.

5.2.2. RECOGNIZER TRAINING AND CONTROLLER OPTIMIZATION

This section introduces two principal parts to develop the driver-identified supervisory control system: 1) the structure and training data of networks to be trained; 2) the driver-identified dynamic programming for controller optimization.

A. Bidirectional LSTMs and training data

To efficiently classify each time step of the extracted sequence data, a bidirectional recurrent neural network (RNN) is adopted as a model that can overcome various restrictions inherent in conventional RNNs. This model divides regular RNN neuron states into forward and backward. These two networks connect to the same output layer to generate output information. With this structure, both past and future situations of sequential inputs in a time frame are evaluated without delay. [6] After 20 times of repeatability test for 10, 20, 50, 100, 200 number of one-cell memory blocks, using 100 one-cell memory blocks achieves the highest value of average identifiability. Thus, a Bi-directional LSTM network, with two hidden LSTM layers, both containing 100 one-cell memory blocks of one cell each is used in this research.

To gain a better understanding of the contribution of each feature to driver identification, ablation studies are performed to divide the training data and the extracted features into two categories for each extraction method: one category is target features; the remaining category is non-target features. In each ablation, one feature is removed from all combinations of single types. E.g. in time-domain extraction methods, if Feature 1 is regarded as a target feature, Features 2 and 3 are the corresponding non-target features. If Feature 2 is regarded as the target feature, Features 1 and 3 are the corresponding non-target features. Similar arguments can be applied in other cases.

B. Driver-identified dynamic programming

According to the decision of the LSTM-based driver recognizer, the control policies in the DP-based control mode need to be adaptively switched for each driver. Therefore, the control variables must be redetermined and their definition is

$$u_k = \Phi_i(SoC_k), \tag{5-21}$$

in which

$$i = \mathbb{Z}_{lstm}(v_k, \gamma_k, \beta_k, \delta_k), i = [A, B, C, D, \dots], \tag{5-22}$$

where u is the control variable; Φ_i is the DP-based control policy for index i driver; and $\mathbb{Z}_{lstm}$ is the LSTM-based network to determine the driver behaviour.

In the optimization-based control mode, DP is employed to locate the optimized control actions at each stage by minimizing the fuel consumption cost function over a certain driving cycle. As an industry-recognized global optimization algorithm, DP can efficiently handle the

constraints and nonlinearity of a problem and find a global optimal solution. [7] Here, the DP problem is described as the recursive Eqs. (5-23) and (5-24), which can be solved through backward recursion. The sub-problem for the $(N_i - 1)$th step is

$$J^*_{N_i-1}(x_{N_i-1}) = \min_{u_{N_i-1}} \left[L(x_{N_i-1}, u_{N_i-1}) + G(x_{N_i}) \right] . \qquad (5-23)$$

For the kth $0 \leq k < N_i - 1$ step, the sub-problem is given by

$$J^*_k(x_k) = \min_{u_k} [L(x_k, u_k) + G(x_k)] \quad , \qquad (5-24)$$

where, $J^*_k(x_k)$ is the optimal cost-to-go function at state x_k from the k th step to the termination of the driving cycle, and x_{k+1} is the state in the $(k+1)$th step after the control variable u_k is applied to state x_k at the kth step according to Eq. (5-24). Eventually, the results will be used to calibrate the lookup tables of driver-identified control policies. For calculating each case, it takes about 4 hours.

5.3. EXPERIMENTAL PLAN

5.3.1. DATA COLLECTION IN DRIVER SIMULATOR

In this chapter, data collection is conducted on the cockpit package (supported by a Thrustmaster T500RS) with the same HEV model with an automatic gearbox as Fig. 5-3. This is to make sure the driving characteristics exhibited by them are under the same constraint and their results are comparable. With respect to real-world road conditions, the road map model used with reconstructed traffic simulates a cyclic undivided highway with uphill, downhill, curved and straight roads and is provided by IPG CarMaker. To reduce the impact of differing

traffic and road conditions on human drivers, they are restricted to the same cycling road conditions and required to follow the speed limits, stop signs, traffic lights, and other traffic regulations. It should be noted that the driver's pedal behaviour might be dependent on the vehicle, the pedal to its torque map, and even the physical pedal resistance feedback.

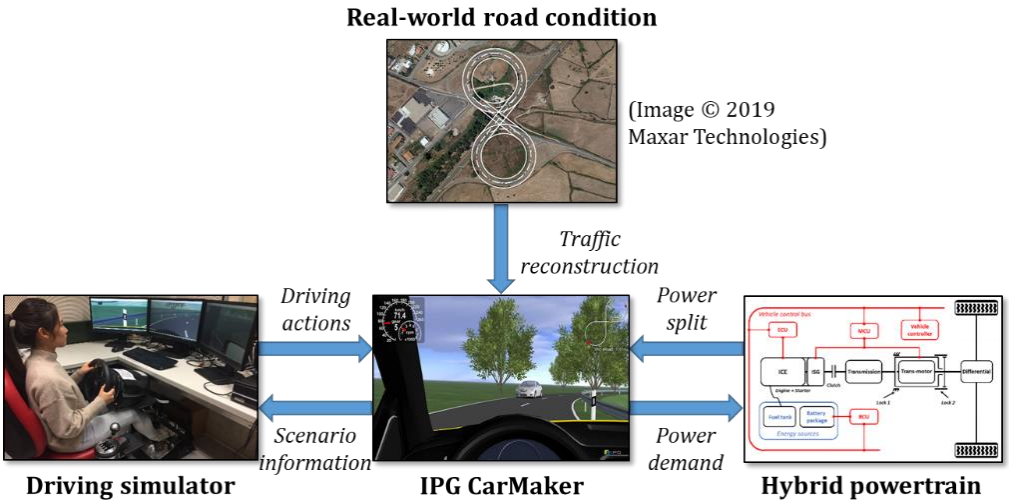

Fig. 5-3. Collection process of driving profiles

5.3.2. DRIVING OPERATION PATTERNS

Observable driving signals can be categorized into three groups [4]: 1) driving behaviour, e.g., gas and brake pedal pressures and steering angles; 2) vehicle status, e.g., velocity, acceleration, and engine speed; and 3) vehicle position, e.g., following distance, relative lane position, and yaw angle. Among these driving signals, we focus on driving behaviour with respect to the relationship between velocity, gas, brake pedal, and steering angle operating signals. Table 5-1 organizes driving-related information about six subjects.

Table 5-1. driving information of six subjects

Driver	Age	Time to hold a driving license (yrs.)	Annual mileage (mile)	Driving geography
A	27	10	2000	Urban
B	27	5	3000	Hybrid
C	24	7	2500	Hybrid
D	26	10	1500	Hybrid
E	26	4	6000	Motorway
F	30	1	1000	Urban

Fig. 5-4 shows driving operation pattern examples of 10-min driving signals collected in the simulator with a 10Hz sampling frequency, wherein (a) is used for training and (b) is used for testing and their data capacity ratio is 5:6. For one single driver, 6000×4 original signal data has been collected. Data from Driver F is only used as testing data to further validate the system robustness. It can be seen that primitive driving operation patterns are like a 'yarn ball' and their fragments are intertwined. It is difficult to distinguish their owners under the same road conditions.

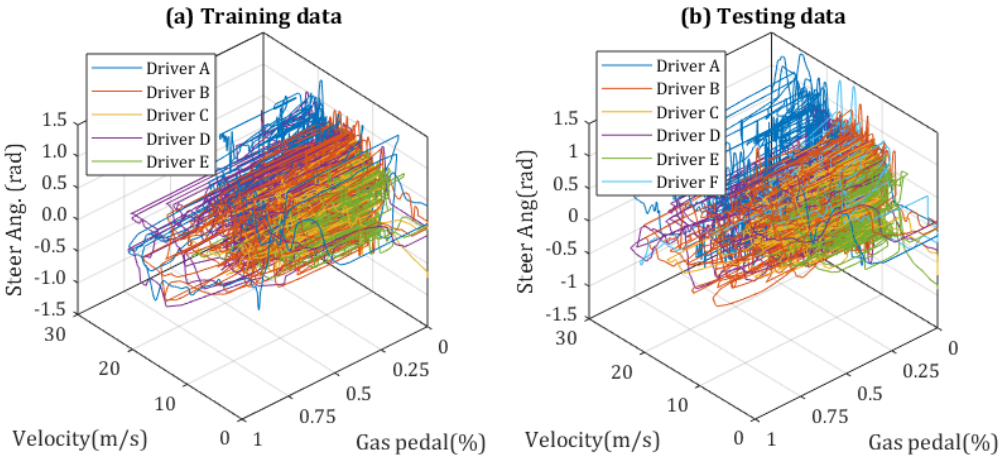

Fig. 5-4. Driving profiles during designed road condition

5.4. RESULT AND DISCUSSION

5.4.1. SIGNIFICANT DIFFERENCE ANALYSIS

In this section, the significant difference of extraction results is analysed and the Mann-Whiney U test is conducted to determine whether two independent driver samples were selected from populations having the same distribution without the assumption of normal distributions. Fig. 5-5 shows p-value results of assuming no significant difference between the two drivers of primitive operation data, in which p-values greater than 0.05 are marked in red. From the results, the primitive velocity samples between every two drivers all have a statistical difference, while some groups of the rest of the primitive samples between every two drivers have no statistically significant difference. Especially for primitive steering angle samples, the distribution differences for each pair of drivers is hard to statistically distinguish.

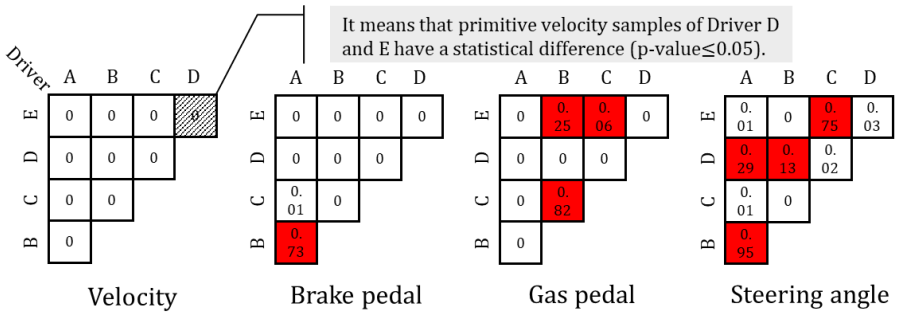

Fig. 5-5. Mann-Whiney U test results of original driving profile

Based on the results of Mann-Whiney U test, the independence factor is chosen to represent the performance of the original data by using all extraction methods. The extraction method with a higher independence factor provides better performance in terms of the significant difference results. Its definition is

$$I_i = \frac{Num_{\leq 0.05}}{Num_{all}} \quad , \qquad (5-25)$$

where, $Num_{\leq 0.05}$ is the number of p-values less than or equal to 0.05 of significant differences between each pair of drivers; Num_{all} is the number of all trials. Calculating by Eq. (5-25), the independence factor values of all involved extraction methods are presented in Table 5-2.

Table 5-2. Independence factor of using involved extraction methods

	Original	**Time**	**Frequency**	**SFFE-4**	**SFFE-5**	**SFFE-6**
$Num_{\leq 0.05}$	32	118	113	120	120	120
Num_{all}	40	120	120	120	120	120
I_i	0.80	0.98	0.94	1.00	1.00	1.00

Notes: the SFFE-4, -5, and -6 denote using the Feature 4, 5, and 6 as different spectral signals to guide extraction respectively.

By comparing the independence factor value, all extraction methods have a certain degree of improvement in stripping the driver's characteristics from the original driving data. Compared to time or frequency domain methods, the proposed SFFE can be more robustly implemented for these test drivers following the same road scenario. Through adaptively adjusting the size of sampling windows, this method can capture driving characteristics more accurately under relatively harsh conditions. Moreover, types of features collected may limit their significant difference. To evaluate the contribution of existing driving characteristics to driver identifiability is another interesting and independent topic that could be studied in future work.

5.4.2. IDENTIFICATION PERFORMANCE COMPARISON

In Table 5-3, the contribution of the extracted feature (training material) types to driver identification is investigated. An initial experiment was conducted on every single feature of using different extraction methods (Target groups). As [38] considered, the ablation validation was performed for features other than selected single features (Non-target groups). The training process, which uses each feature extracted from the training cycles, has been repeated 20 times and the best testing results for each feature and network structures is recorded respectively. After investigation, the training parameters of networks are set at 100 hidden units, 0.01 initial learn rate and 80 maximum epochs that are convergent and efficient.

Table 5-3. Identifiability comparison from view of features and networks

Feature		Forward LSTM		Bidirectional LSTM		Average identifiability	
Type	**Num.**	**Target**	**Non-target**	**Target**	**Non-target**	**Each num.**	**Each type**
Original	0	0.590	0.590	0.593	0.593	0.592	0.592
Time	1	0.579	0.653	0.749	0.726	0.677	
domain	2	0.599	0.714	0.622	0.833	0.692	0.719
	3	0.76	0.655	0.836	0.800	0.788	
Frequency	4	0.604	0.514	0.651	0.804	0.643	
domain	5	0.621	0.645	0.618	0.829	0.678	0.680
	6	0.565	0.764	0.785	0.754	0.717	
	7	0.745	0.758	0.773	0.806	0.771	
SFFE-4	8	0.776	0.906	0.733	0.909	0.806	0.798
	9	0.796	0.749	0.756	0.863	0.766	
	10	0.798	0.793	0.906	0.861	0.840	
SFFE-5	11	0.835	0.870	0.939	0.961	0.8940	0.855
	12	0.723	0.817	0.878	0.920	0.825	
	13	0.763	0.765	0.818	0.891	0.809	
SFFE-6	14	0.783	0.838	0.738	0.853	0.778	0.803
	15	0.761	0.721	0.797	0.914	0.748	
Average identifiability		0.706	0.762	0.735	0.832		0.759

It is seen that all three methods have a certain improvement in the characterization of the original data (59.2%), in which SFFE-5 method realize the highest identifiability of 96.1% by using Bi-LSTM networks without Feature 2. Obviously, the method proposed by Wijnands et al. used non-extracted data for training purposes is not applicable for this case [39]. From the perspective of extraction methods, the proposed SFFE ranks first with the 80.4% average identifiability compared to those of time domain (71.9%) and frequency domain (68.0%) extraction methods. From the perspective of network structure, the Bi-LSTM network has 78.6% average identifiability and the forward one has 71.7% average identifiability. With the double feature dimensions of training, the identifiability generally has an upward trend (average 9.35% up), whereas it does not work for the original data.

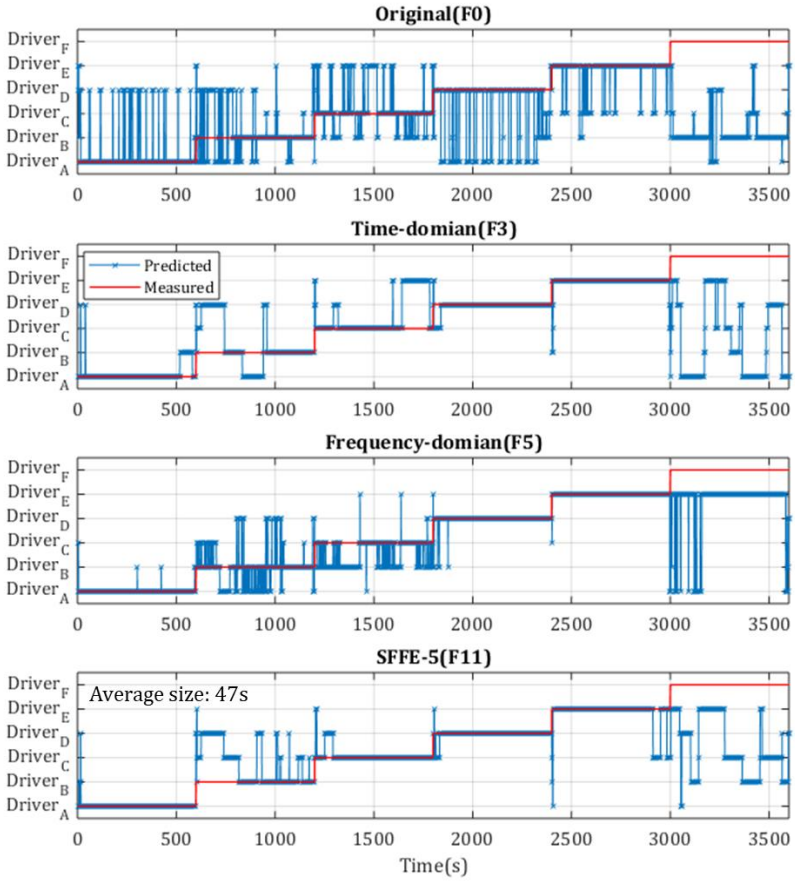

Fig. 5-6. Real-time performance of driver identification

Fig. 5-6 shows real-time driver identification that compares the best performance of each type of extraction methods, which includes the original (Feature 0), time-domain (Feature 3), frequency-domain (Feature 5) and the proposed SFFE (Feature 11). During real-time driving, the original data driven driver recognizer cannot identify the driver from their driving operation signal. Training by using time domain or frequency domain data improves the recognition accuracy of the driver recognizer, especially for Drivers A, D, and E. Training by using data extracted by the proposed SFFE can further improve recognition accuracy of Driver C and reduce the size of sampling windows from 60 s to 47 s, but there still is a defect in identifying Driver B. It may be caused by Driver B having many behavioural similarities to Driver C and D. This factor is related to the driving geography and the environment, wherein the feature homogenization could reduce the classification performance of the proposed method. Like Driver F, Driver B's data does not participate in the training process so that his driving fragments are assigned to other drivers. Then the DP-based supervisory controller calls a control policy corresponding to the driver for energy distribution to minimize the influence of the defect.

5.4.3. VEHICLE ADAPTABILITY PERFORMANCE

This section discusses the fuel economy of the driver-identified control supervisory system and examines vehicle adaptability under different control strategies. Fig. 5-7 shows fuel consumption comparison over different human drivers, in which each driving cycle in this case is of 60min duration and formed by six 10 min testing fragments from each driver. The data clearly indicates that fuel consumption over different human drivers has significant

differences, in which fuel consumption of Driver D (the highest in all testing drivers) is nearly twice that of Driver E. Compared to the baseline and FL-based schemes, the LSTM+DP control strategy always maintains the lowest fuel consumption for all of the drivers. From the perspective of the drivers, the higher the baseline fuel consumption, the greater the energy-saving potential of the LSTM+DP control strategy. Moreover, the gender of human drivers is not considered in the chapter but may also affect the energy-saving performance of the developed system, especially, in the way they apply pressure to gas and brake pedals. [8]

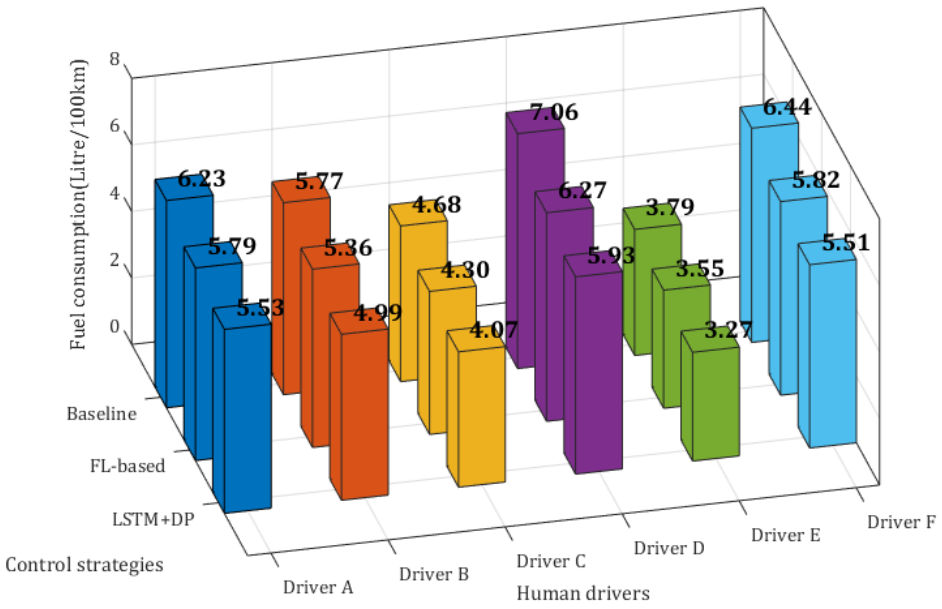

Fig. 5-7. Fuel consumption comparison over different human drivers

In Fig. 5-8, the driver-identified supervisory control system is further compared with the FL-based (fuzzy logic system) and baseline (charge depleting and charge sustaining control strategy) schemes under real-world driving conditions. These two widely-used strategies considered in the comparison group both have been employed and verified in the author's past work. [8, 9] Differing from FL-based control systems, the SFFE driven system has the unique ability to identify the driver and offer a personalized control policy. The fuel

consumption under the proposed control system is significantly lower than other control systems while maintaining the relatively higher SoC value. Compared to the baseline control system, both the FL-based and the proposed schemes have stronger robustness in adapting to the driving styles of differing drivers. Differing from the fuzzy control strategy, the DP algorithm considers fuel consumption of HEVs from a global perspective to balance the flow of electricity usage and maximize the fuel economy of HEV systems. The Bi-LSTM helps supervisory control systems to identify target drivers to ensure the effectiveness of optimized control policies. It is worth mentioning that for Driver F (no his knowledge in the network), the proposed system has excellent adaptability that continues to operate in the last period (3000 - 3600 s) with the lowest energy consumption. However, the conventional baseline control system has no ability to counter the change of drivers and even driving styles.

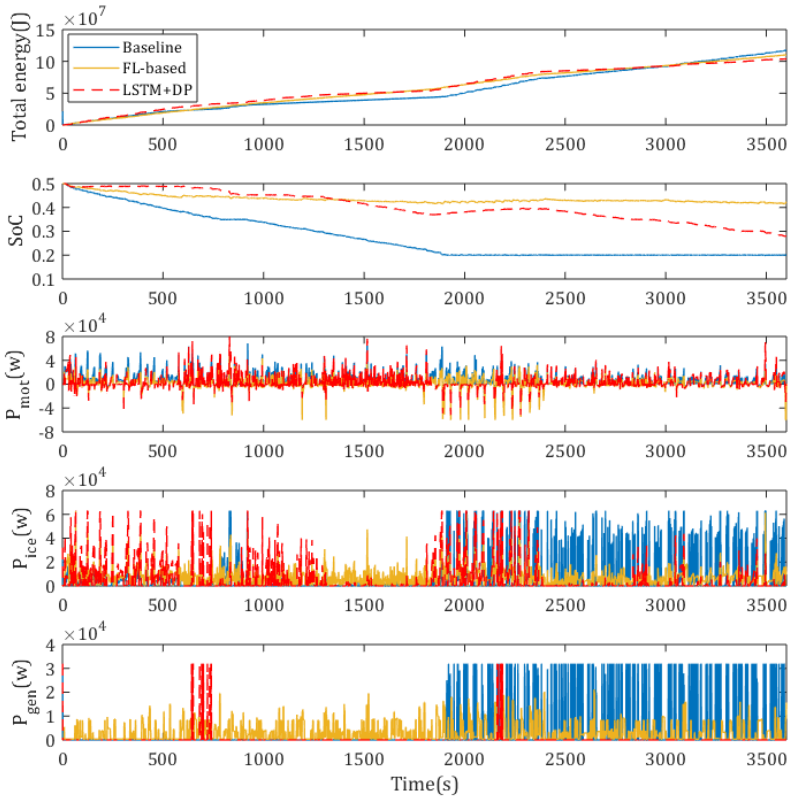

Fig. 5-8. Real-time performance comparison over different control strategies

The vehicle performance with different control strategies is summarized in Table 5-4. From the results, the LSTM+DP control strategy significantly reduces fuel consumption to $5.2\ \mathrm{liter}/100\ \mathrm{km}$, and saves 11.31% energy over the baseline (FL-based one saves 5.53%).

Table 5-4. Vehicle performance comparison over real-world driving

Control strategy	**Final SoC**	**Fuel consumption** ($\mathrm{liter}/100\ \mathrm{km}$)	**Total energy** (J)	**Energy saving** (%)
Baseline	0.2014	6.141	1.1715e+08	-
FL-based	0.4252	5.762	1.1031e+08	5.53%
LSTM+DP	0.2809	5.207	1.0389e+08	11.31%

5.5. SUMMARY

This chapter proposes a driver-identified supervisory control system of hybrid electric vehicles (HEVs), wherein an improved method of spectrum-guided fuzzy feature extraction (SFFE) is developed for improving the recognition accuracy and efficiency of this control system. The comparative study including involved extraction methods and their identification system performance as well as its application to HEV systems has been carried out. The contributions drawn from the investigation are as follows:

1) With help of the spectrum-guided fuzzy feature extraction, recognition accuracy of both forward and bi-directional LSTM networks rises 7% and 6% from other extraction methods (time or frequency domain).
2) Compared to forward LSTM networks, bi-directional LSTM networks have a better performance with an average of 7% higher accuracy in driver identification performance.

3) For each human driver, the driver-identified supervisory control system can save more fossil fuel, compared to fuzzy logic-based and rule-based them, especially for driver D (saving up to 16%).

4) Driven by a human driver whose data was not in the training set, this proposed system shows strong robustness and provides excellent energy-saving performance, compared to the baseline (11.31%) and FL-based (5.53%) schemes.

REFERENCES

[1] J. Li, Q. Zhou, Y. He, H. Williams, and H. Xu, “Driver-identified Supervisory Control System of Hybrid Electric Vehicles based on Spectrum-guided Fuzzy Feature Extraction,” *IEEE Transactions on Fuzzy Systems*, vol. 6706, no. c, pp. 1–1, 2020.

[2] Q. Zhou, Y. Zhang, Z. Li, J. Li, H. Xu, and O. Olatunbosun, “Cyber-Physical Energy-Saving Control for Hybrid Aircraft-Towing Tractor Based on Online,” *IEEE TRANSACTIONS ON INDUSTRIAL INFORMATICS*, vol. 14, no. 9, pp. 4149–4158, 2018.

[3] C. M. Martinez, M. Heucke, F. Wang, B. Gao, and D. Cao, “Driving Style Recognition for Intelligent Vehicle Control and Advanced Driver Assistance : A Survey,” *IEEE Transactions on Intelligent Transportation Systems*, vol. 19, no. 3, pp. 666–676, 2018.

[4] C. Miyajima et al., "Driver Modeling Based on Driving Behavior and Its Evaluation in Driver Identification," in Proceedings of the IEEE, vol. 95, no. 2, pp. 427-437. 2007.

[5] L. A. H. Zad, “A fuzzy-algorithmic approach to the definition of complex or imprecise concepts,” *International Journal of Man-Machine Studies*, pp. 249–291, 1976.

[6] M. Schuster and K. K. Paliwal, “Bidirectional Recurrent Neural Networks,” vol. 45, no. 11, pp. 2673–2681, 1997.

[7] R. Bellman, “Dynamic Programming,” *Science*, vol. 153, no. 3731, pp. 34–37, 1966.

[8] A. Wahab, C. Quek, C. K. Tan, and K. Takeda, “Driving profile modeling and recognition based on soft computing approach,” *IEEE Transactions on Neural Networks*, vol. 20, no. 4, pp. 563–582, 2009.

[9] J. Li *et al.*, “Dual-loop online intelligent programming for driver-oriented predict energy management of plug-in hybrid electric vehicles,” *Applied Energy*, vol. 253, no. November, p. 113617, 2019.

[10] J. Li, Q. Zhou, H. Williams, and H. Xu, “Back-to-back Competitive Learning Mechanism for Fuzzy Logic based Supervisory Control System of Hybrid Electric Vehicles,” *IEEE Transactions on Industrial Electronics*, vol. 2, no. c, pp. 1–1, 2019.

CHAPTER 6

REAR-HORIZON-BASED ONLINE ENERGY MANAGEMENT USING BACK-TO-BACK COMPETITIVE LEARNING MECHANISM

The content presented in the Chapter 6 is based on the author's published article, 'Back-to-back Competitive Learning Mechanism for Fuzzy Logic based Supervisory Control System of Hybrid Electric Vehicles' in IEEE transactions on Industrial Electronics. [1] This chapter proposes a novel back-to-back competitive learning mechanism (BCLM) for a fuzzy logic (FL) supervisory control system for hybrid electric vehicles (HEVs). This mechanism allows continuous competition between two fuzzy logic controllers during real-world driving. The leading controller will have the regulatory function of the supervisory control system. Firstly, the configuration of the HEV model and its FL-based control system are analysed. Secondly, the algorithm of chaos-enhanced accelerated particle swarm optimization (CAPSO) is developed for back-to-back learning of the membership function. Thirdly, based on fuel-prioritized cost functions, the regulation of competitive assessment is designed to select a controller with a better fuel economy. Finally, the competitive performance of using the CAPSO algorithm is contrasted with other swarm-based methods and the BCLM-driven control system is validated by a hardware-in-the-loop test. The results demonstrate that the BCLM control system significantly reduces fuel consumption, at least 9% from charge sustaining and charge depleting based, and at least 7% from conventional FL-based systems.

6.1. FL-BASED SUPERVISORY CONTROL SYSTEM

In order to rationally assign the vehicle's power demand, P_d, which has a corresponding torque demand (measured at the reducer input), T_d, to the three machines, it is paired with the state of charge, SoC, of the battery pack (BP) to make up the input to the FL-based supervisory control system that chooses between the two modes of pure electric traction, $Mode_{EV}$, and FL-based traction, $Mode_{FLC}$, and is expressed as follows:

$$\left.\begin{array}{ll}\left(T_{mot}, P_{ice}, P_{gen}\right) = Mode_{EV}(P_d, SoC), & SoC > 0.5, \\ \left(n_{mot}, P_{ice}, P_{gen}\right) = Mode_{FLC}(P_d, SoC), & SoC \leq 0.5,\end{array}\right\} \qquad (6-1)$$

where: T_{mot} is the trans-motor torque; n_{mot} is the trans-motor speed; P_{ice} is the ICE power; and P_{gen} is the ISG power.

The electric traction system has the capacity to completely satisfy the torque demand, enabling deactivation of the ICE and the ISG in the electric mode. The power distribution in this state is therefore given by

$$\left(T_{mot}, P_{ice}, P_{gen}\right) = (T_d, 0, 0). \qquad (6-2)$$

In the fuzzy logic control mode, FLCs are used to perform energy management. This structure supplies power to propel the vehicle while maintaining the BP's SoC between safe limits. The design of the FLCs is described below.

A. Fuzzification

The fuzzy sets with linguistic terms are regulated with standard triangular membership functions (MFs), where the degree of membership is expressed as a function of normalized values in the interval, $[0,1]$. The values of the MFs in the FLC are set at 3 levels: Low, Medium, and High. These functions fuzzify the crisp inputs.

The power demand may take both positive and negative values and is bounded by the maximum (accelerative) power, P_d^+, and the minimum (powertrain braking) power, P_d^-, which is negative. The "knee point" of the corresponding input, $Input_1$, is not set at the midpoint between the power demand boundaries: it is set via

$$Input_1 = \begin{cases} \frac{1}{2} + \frac{P_d}{P_d^+} \cdot \frac{1}{2}, & P_d \geq 0. \\ \frac{1}{2} - \frac{P_d}{P_d^-} \cdot \frac{1}{2}, & P_d < 0. \end{cases} \qquad (6-3)$$

Sensitivity homogenization is used in this paper to correct the correspondence between the value of the power demand and its rule of inference. However, since the FLC is not used in the EV mode, the BP's SoC also needs to be sensitively scaled to satisfy the boundaries of the $Mode_{FLC}$ working area. They are formulated mathematically through the relationship:

$$Input_2 = \frac{SoC - SoC_{min}}{SoC_{max} - SoC_{min}} \qquad (6-4)$$

where $SoC_{min} = 0.2$ and $SoC_{max} = 0.5$ are the value of SoC boundary positions when the FLC is engaged.

B. Inference

The rule base, as shown in Table 1, determines the control outputs C and D with the inputs states A and B, by applying a 'if A and B then C and D' policy. A mathematic expression of the 'if A and B then C and D' policy is:

$$[C \quad D] = (A \times B) \circ R \qquad (6-5)$$

where: 'A' denotes the fuzzy set of power demand; 'B' denotes the fuzzy set of SoC value; 'C' denotes the crisp value of the normalized motor rotational speed; 'D' denotes the crisp value of the normalized ISG power; and 'R' denotes the fuzzy relationship matrix indexed by the cross-product of 'A' and 'B'. The reasoning process is based on Eq. (6-5) with the Sugeno fuzzy set as described in the following table:

Table 6-1. Fuzzy logic based decision system inference

Rule	Demand power	SoC value	Motor speed Ref.	ISG power Ref.
1	Low	Low	High	High
2	Medium	Low	Low	High
3	High	Low	Low	High
4	Low	Medium	High	Medium
5	Medium	Medium	Medium	Medium
6	High	Medium	Low	Medium
7	Low	High	High	Low
8	Medium	High	High	Low
9	High	High	Medium	Low

C. Defuzzification

In inference mechanism, the implied fuzzy sets are produced using the max–min composition. In defuzzification, these implied fuzzy sets are combined to provide a crisp value of controller outputs. There are several approaches to accomplish the defuzzification process and here the centroid of area method has been adopted because it is relatively simple and has good information preserving properties [6]. The final output is then expressed as the mean of the individual membership values weighted by the corresponding centroids as follows:

$$\left.\begin{aligned} Output_1 &= \frac{\sum_{i=1}^{n} Out1_i \cdot O_i}{\sum_{i=1}^{n} O_i}, \\ Output_2 &= \frac{\sum_{i=1}^{n} Out2_i \cdot O_i}{\sum_{i=1}^{n} O_i}, \end{aligned}\right\} \qquad (6-6)$$

where, Out_i is the output of rule base i, and O_i is the centroid of the ith output MF. Based on Eq. (6-6), the rotational speed of the traction motor and the power ref. of the ISG can be calculated separately. From these outputs, the power distribution under the FLC mode is calculated as follows:

$$\left.\begin{aligned} n_{mot} &= Output_1 \cdot n_{mot}^{*}, \\ P_{gen} &= Output_2 \cdot P_{gen}^{*}, \\ T_{mot} &= T_d, \\ P_{ice} &= \begin{cases} P_d - n_{mot} \cdot T_{mot} - P_{gen}, & P_d \geq 0, \\ -P_{gen}, & P_d < 0, \end{cases} \end{aligned}\right\} \qquad (6-7)$$

where, n_{mot}^{*} is the maximum speed of the traction motor, and P_{gen}^{*} is the maximum power of the ISG.

6.2. PROPOSED SOLUTION

The back-to-back competitive learning mechanism (BCLM) that is proposed in this research is shown in Fig. 6-1. The concept of the BCLM comprises two main modules: back-to-back learning; and competitive assessment. In the back-to-back learning module, two FLCs with the same structure were adopted. The first FLC is trained by an intelligent swarm optimizer, while the second serves the supervisory control system. In the competitive assessment module, there is an evaluator that competitively assesses the two controllers, and its assessment result decides both the control assignment to the supervisory controller system and the target of the optimizer. During the real-world driving, if better MF scalar parameters in the controller being trained are detected, both selectors (shown on Fig. 6-1) will be switched to their opposite side in order to concurrently exchange the current tasks of the two controllers. The controller being trained will take over the supervisory control system and the execution controller will hand over the optimization task. The main advantage of this parallel control structure is that it can ensure strong robustness and high efficiency of the supervisory control system whether before or after each update takes effect.

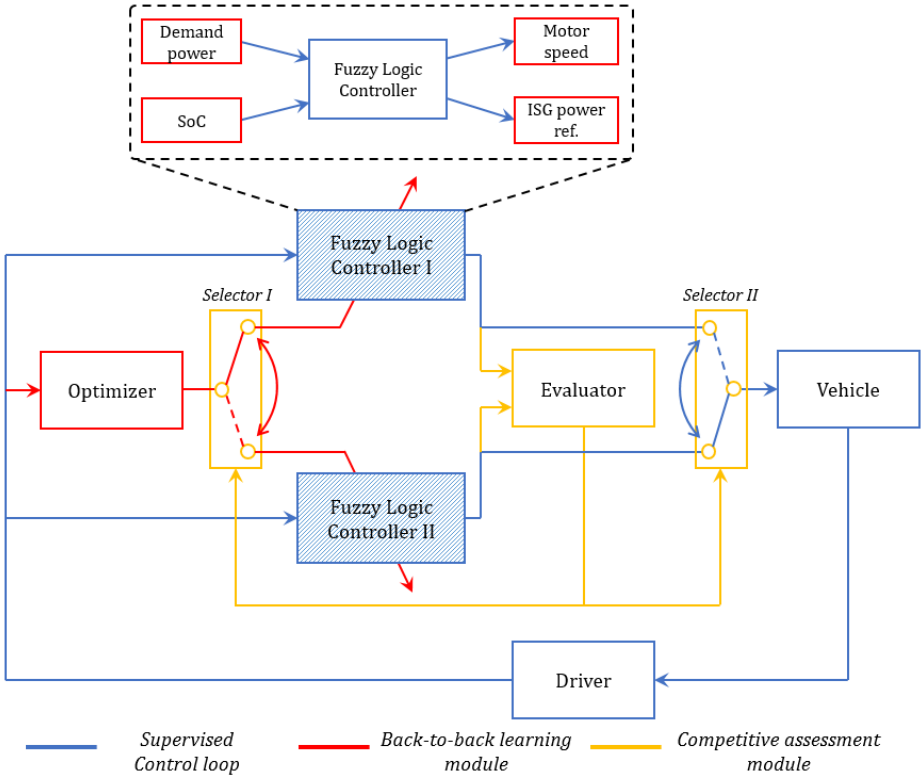

Fig. 6-1. Concept of back-to-back competitive learning mechanism

6.2.1. CAPSO-DRIVEN BACK-TO-BACK LEARNING

A. Search area and constraints

According to structure of the FLC, the boundary condition of the inputs and outputs are fixed at predetermined intervals. There is also no change to the fuzzy rules and the triangular MFs. The intelligent swarm optimizer is applied to each output. Here, the search variables in the multi-objective optimization problem are labelled in bold type shown in Fig. 6-2.

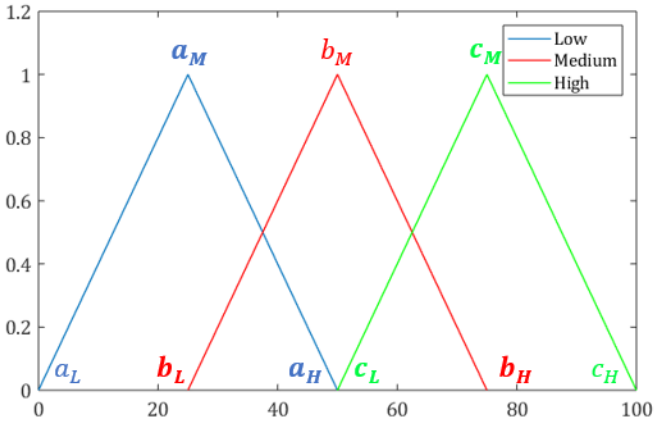

Fig. 6-2. Representation of triangular MFs

To simplify the implementation of optimization algorithms it is assumed here that the parameters a_M, b_L, a_H, c_L, b_H, and c_M are fixed for each input and output. In this way, 24 scalar parameters of the MFs need to be optimized, and the structure of the generic particle for each input and output is given by

$$|a_M \quad b_L \quad a_H \quad c_L \quad b_H \quad c_M| \qquad (6-8)$$

Considering the structure of the FLC shown in Fig. 6-1, it is supposed that the six parameters to optimize each input and output must obey the following order criteria:

$$\left.\begin{array}{ll} a_L < a_M < a_H, & a_L < b_L < c_H, \\ a_L < a_H < b_M, & b_M < c_L < c_H, \\ b_M < b_H < c_H, & b_M < c_M < c_H. \end{array}\right\} \qquad (6-9)$$

For each iteration of algorithm optimization, it is necessary to check the constraints in Eq. (6-9).

B. Cost functions and CAPSO algorithm

This chapter considers two principal targets, the first is the overall liquid fuel consumption, and the second is the BP's SoC at the end of test. These cost functions are defined by:

$$\left.\begin{aligned} J_1 &= \frac{1}{\rho_{gaso}} \int \dot{m}_f(t)dt \\ J_2 &= \frac{1}{SoC(t_{end})} \end{aligned}\right\} \qquad (6-10)$$

where, ρ_{gaso} is the density of gasoline (0.77 g/ml); $\dot{m}_f$ is the fuel consumption mass rate (g/s); and t_{end} is the final time of the driving cycle.

To convert the multi-objective optimization problem into a single objective optimization enabling the swarm-based algorithm, in the present work, the multi-objective optimization is formulated by using the weighted sum method. [2] Therefore, the optimal energy-flow control problem with constrains is expressed as: minimize the overall cost function, J, given by

$$\min J = w \cdot \frac{J_1}{J_1^*} + (1-w) \cdot \frac{J_2}{J_2^*} \qquad (6-11)$$

$$s.t. \begin{cases} SoC(k), & 0.8 \geq SoC(k) \geq 0.2 \\ n_{mot}(k), & n_{mot^*} \geq n_{mot}(k) \geq 0 \\ T_{mot}(k), & T_{mot^*} \geq T_{mot}(k) \geq -T_{mot^*} \\ P_{ICE}(k), & P_{ICE^*} \geq P_{ICE}(k) \geq 0 \\ P_{ISG}(k), & 0 \geq P_{ISG}(k) \geq -P_{ISG^*} \end{cases}$$

In Eq. (6-11), w is a weight coefficient; J_1^* and J_2^* are scaling constants for the cost functions, J_1 and J_2. The SoC contribution to the overall cost function ensures service life of the battery.

The CAPSO algorithm, which is an upgraded version of the accelerated particle swarm optimization (APSO) algorithm, is a computational algorithm inspired by animal swarms such

as ant colonies, bird flocks, fish schools, and other biological phenomena. [3] The standard APSO usually keeps the attraction parameters as a fixed value [4]; however, the solutions still change slightly as the optima are approached. In the chaos-enhanced algorithm, a dynamic attraction parameter in each iteration is used to create some 'accidents', which help the particles to jump out of any convergence to a local optimum proved by Refs. [5, 6] For the CAPSO, the particle's position updates with the following equation:

$$x^{(i+1,j)} = (1-\beta)\cdot x^{(i,j)} + \beta \cdot g^{(i,*)} + \alpha^{(i)} \cdot r^{(i,j)} \qquad (6-12)$$

In Eq. (6-12), $g^{(i,*)}$ is the best position in the ith iteration, β is the attraction parameter of CAPSO, α is the convergence parameters of CAPSO, and r is a $U[0,1]$ random variable. Here, α and β are updated in each iteration via:

$$\left.\begin{array}{c} \alpha^{(i)} = \alpha^{(0)} \cdot \gamma^{i}, \\ \beta^{(i+1)} = a \cdot \beta^{(i)} \cdot (1-\beta^{(i)}), \end{array}\right\} \qquad (6-13)$$

where, the settings, $\alpha^{(0)} = 0.9$ and $\gamma = 0.95$, were chosen; and the attraction parameter is mapped by the logistic map [3], in which the initial values $\beta^{(1)} = 0.6$ and $a = 4$ are used. When $\beta \to 0$ in any step, the algorithm may lead to slow changes. After the convergence has been achieved, the algorithm ends the main iteration and outputs the best position at the end iteration $g_{\max\ \_iter,*}$ as the global optimal solution.

6.2.2. FUEL-PRIORITIZED COMPETITIVE ASSESSMENT

A. Observation window for assessment

To evaluate the fuel-saving performance for both FLCs with back-to-back learning, a short-term moving window H is introduced. The observation window ensures that the competition between both controllers is fair and that the reference driving profiles for CAPSO-driven back-to-back learning are equal. Short-term speed and acceleration profiles are expected to be strongly influenced by variables with fast dynamics such as traffic congestion and driving style. This chapter examines the impact of the length of observation windows in the fuel-prioritized competitive assessment on the vehicle's fuel consumption. Different lengths of short-term windows are studied in the control system driven by the proposed mechanism.

B. Competitive assessment procedure

Fig. 6-3 sets out the competitive assessment procedure for electing the controller with the better fuel-saving performance. In each time-step, the optimizer calls the CAPSO algorithm to search the global best solution for the controller being trained based on the short-term driving profile restricted by the observation window. The best scalar parameters for the MFs are used in the controller being trained then the evaluator calculates the fuel-saving performance of both controllers.

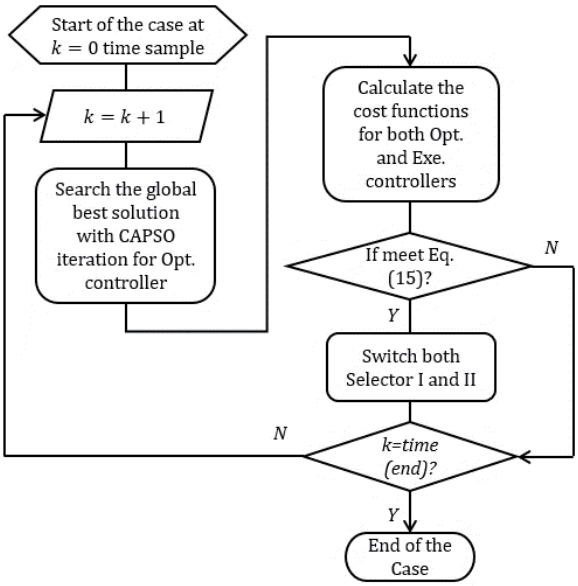

Fig. 6-3. Flowchart of competitive assessment procedure

Considering the impact of length of observation windows on the vehicle's fuel consumption, the cost function from Eq. (6-11) for each controller is modified as follows:

$$\left.\begin{aligned} csn_{exe} &= w \cdot \frac{J_1'}{H \cdot J_1^*} + (1-w) \cdot \left(\frac{J_2'}{H \cdot J_2^*}\right)^2, \\ csn_{opt} &= w \cdot \frac{J_1''}{H \cdot J_1^*} + (1-w) \cdot \left(\frac{J_2''}{H \cdot J_2^*}\right)^2, \end{aligned}\right\} \qquad (6-14)$$

where, H is length of the observation window; csn_{exe} and csn_{opt} are, respectively, the cost functions of the execution controller and the controller being trained; J_1' and J_2' are the evaluation objects for the execution controller; and J_1'' and J_2'' are the evaluation objects for the controller being trained. It should be noted that the introduced observation window would increase the sensitivity to the change of J_1 and reduces that for J_2. To ensure sufficient service life of the battery, the order of penalty J_2 should be increased when SoC value is low. Fig. 6-4 investigates the average value of cost function with different orders of penalty during

real world driving with the initial SoC value of 0.2. The cost functions of both objectives are scaled to the same range of $[0,1]$ with w fixed at 0.5 in Eq. (6-7). Compared to other investigated orders, the quadratic penalty J_2 gives the only positive differential related to J_1.

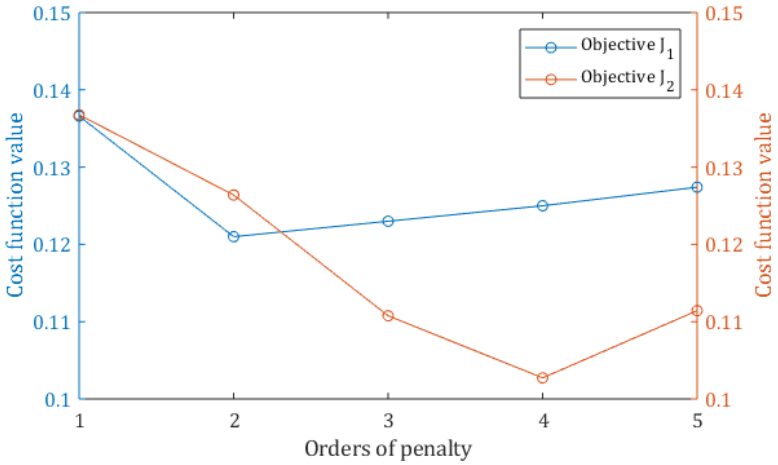

Fig. 6-4. Statistical results of cost function with different orders' penalty

In real time driving, cost functions of the execution controller are considered as a learning target to motivate another. At each time-step, the BCLM will calculate the cost functions of both controllers. If the current state meets the following conditions:

$$\left.\begin{array}{c} csn_{opt}(k) - csn_{exe}(k) < 0, \text{and} \\ \dfrac{csn_{opt}(k) - csn_{exe}(k)}{csn_{opt}(k-1) - csn_{exe}(k-1)} < 1. \end{array}\right\} \qquad (6-15)$$

where, errors and its derivatives between two cost function values as the main factors in this chapter affect the final decision. If $csn_{opt}(k-1) - csn_{exe}(k-1) = 0$, then only the first condition of Eq. (6-15) needs to be satisfied and the proposed mechanism takes action to switch both selectors to the other side, exchanging the current tasks and roles between the two controllers. Otherwise, the two controllers will continue to operate their current tasks

and the mechanism will explore the MF scalar parameters searching for better fuel-saving performance for the next time step.

6.3. EXPERIMENTAL PLAN

6.3.1. REAL-WORLD DRIVING CYCLES

As the goal of this work is to develop a supervisory control system that learns and adapts to human driving style the previously discussed HEV model was implemented in a driving simulator. Five human drivers were invited as experimental subjects to participate in 8000 seconds of real-world driving. The road map model used was a mixture of highway and local roads with traffic, multiple stop signs, traffic lights, and speed limit changes: it was provided by IPG CarMaker and is shown in Fig. 6-5. The human driver was instructed to follow the speed limits, stop signs, traffic lights, and other traffic regulations. The specification of the real-world driving cycle is listed in Table 6-2.

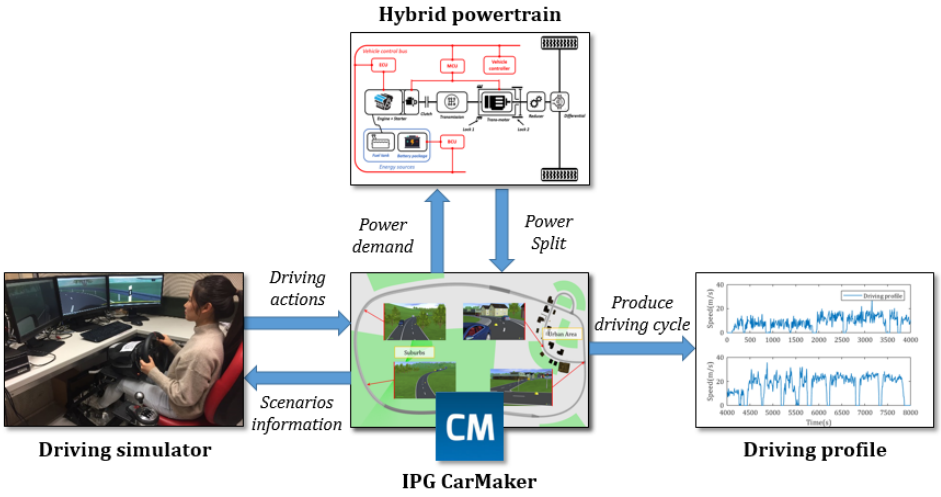

Fig. 6-5. Data collection of driving profiles

Table 6-2. Specification of real-world driving cycle

Human driver	Traffic type	Driving time(s)	Driving distance(km)
A	Urban	1880	11.6
B	Urban	1590	17.8
C	Urban	940	8.1
D	Highway	1350	22.5
E	Highway	2240	40.0

6.3.2. HARDWARE-IN-THE-LOOP EXPERIMENT

The work was carried out using the industry standard real-time testing equipment sourced from the ETAS Group. [7] The configuration of the HiL testing system is shown in Fig. 6-6. Firstly, the HEV model and its FL-based control system were compiled as MATLAB® code. Secondly, through the host PC, they were imported into the integration platform, which is the user interface through which the HiL system is configured, in preparation for creating signal paths between the models and the hardware, and generating code for the LABCAR simulation target LABCAR-RTPC. Thirdly, the whole vehicle system was downloaded to the DESK-LABCAR using the ETAS experimental environment (EE) via Ethernet protocol. In the experiment, vehicle performance was entirely supervised by the ETAS EE in the host PC. From the recorded results, the average computational time for CAPSO algorithm to complete an iterative convergence is 0.225 seconds so the computing resource still has a surplus for the current version given the fact that its capacity will continue to increase. As indicated by Moore's Law, it is anticipated the BCLM can perform on the actual on-board controller of HEVs for real-time energy saving.

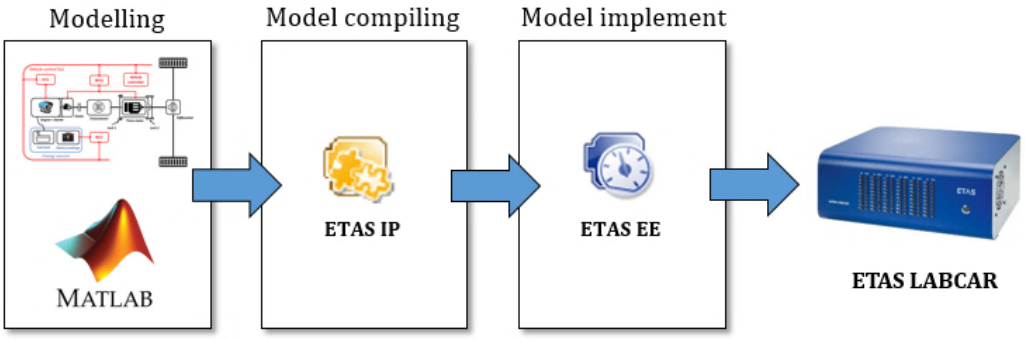

Fig. 6-6. Hardware-in-the-loop testing system

6.4. RESULT AND DISCUSSION

6.4.1. BACK-TO-BACK LEARNING PERFORMANCE

In this section, the evaluation of the back-to-back learning is presented in two parts as a performance comparison of optimization algorithms and the MF evolution process. Fig. 6-7 shows the cost function values achieved by the different swarm-based optimization algorithms averaged over 30 runs for 15 iterations.

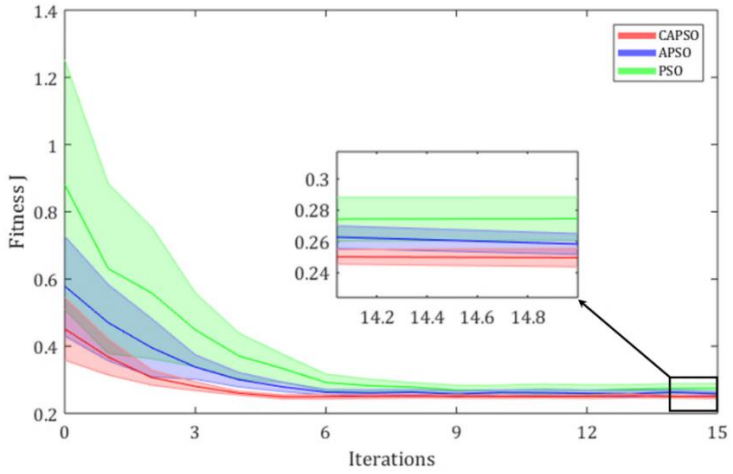

Fig. 6-7. Performance comparison of optimization algorithms

In each run: 20 particles for each variable in the swarm-based algorithms were initialized randomly; the weight coefficient of the cost function was set to $w = 0.7$; and the termination criterion was 15 iterations. From the results, all swarm-based algorithms realize fitness function convergence within 15 iterations. Especially at the fifth iteration, the CAPSO algorithm has reached the best global solutions while others are still in convergence. Therefore, the CAPSO algorithm enhanced by the chaos mapping strategy is more ambitious in expanding the exploration area for the global solution search.

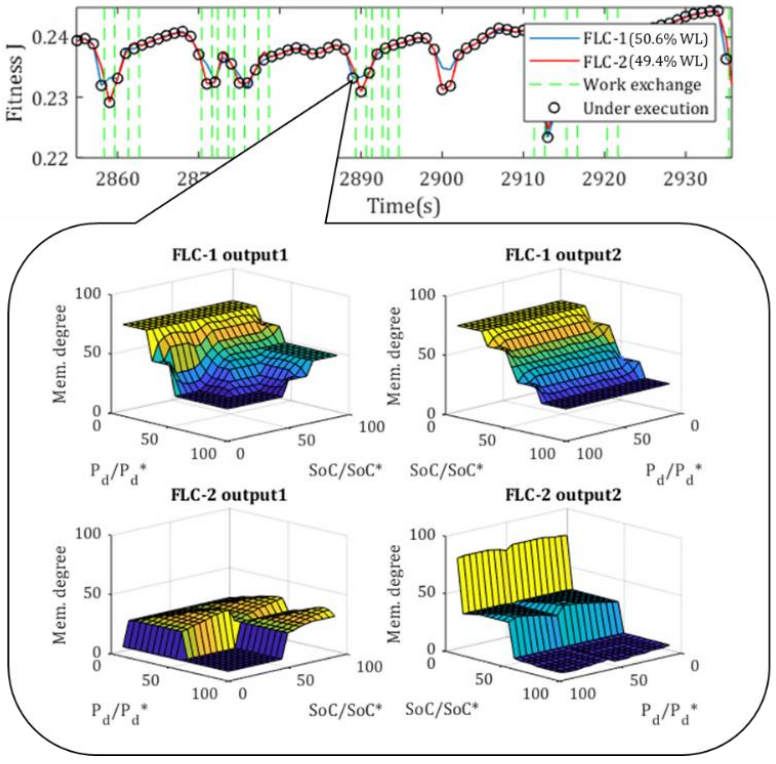

Fig. 6-8. Real-time performance of two FLCs boosted by the BCLM

Fig. 6-8 shows a fragment of real-time performance of two FLCs, wherein the green dotted line indicates the timing of two controllers' work exchange and the black circle indicates the fitness in the execution controller of HEV systems. From the results of the top subfigure, two controllers are alternately updated by the BCLM and their work exchanges frequently at

protruding spikes, which are caused by the dramatic changing in human driving behaviours. Although the working time and training time between two controllers cannot exactly equal in each optimization fragment, the BCLM can schedule them in relative balance to make both controllers have fair workloads (50.6% and 49.4%) during the long-term driving. The bottom subfigure dissects output surface evolution process between two FLCs at the 2889th seconds. It can be seen that the BCLM will abandon a relatively smooth output surface used for most driving scenarios and replace to an aggressive one for targeting higher fuel economy.

6.4.2. VEHICLE PERFORMANCE COMPARISON

In Fig. 6-9, the FL-based supervisory control system with the proposed mechanism is further compared with the conventional FL-based one during real-world driving. The fuel consumption under the FL-based control system with the proposed mechanism is significantly lower than the conventional one, while maintaining the higher SoC value. Boosted by the BCLM, the ICE initially tends to compensate for the total power demand to avoid the potential danger of a rapid drop in the BP's SoC. The ISG maintains a higher workload compared to that supervised by the conventional FL-based control system.

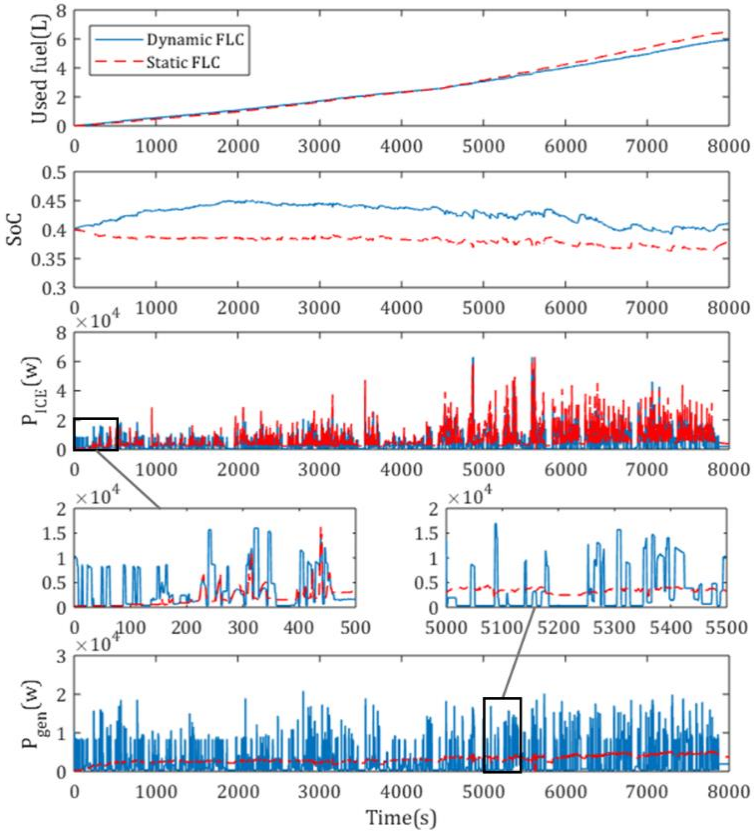

Fig. 6-9. Vehicle performance comparisons at initial SoC=0.4

The vehicle performance with different control strategies is summarized in Table 6-3. An analogous result can also be observed for initial SoCs of 0.5 and 0.3. The classic rule-based control strategies of charge depleting (CD) and charge sustaining (CS) were considered and used as a baseline for comparison with the FL-based strategies. As the decrease of initial SoC values, the space for freely distributing energy is narrowed. Compared to the CD/CS strategy, the static FL-based system after offline optimization can adaptively adjust energy distribution in the narrow SoC range but its improvement is not significant. Relatively, the dynamic FL-based system with the help of the BCLM always selects a controller with better cost-function value in real time to counter driving scenario change. The result shows the improved system

has the lowest fuel consumption while maintaining the highest SoC value, compared to the performance of others.

Table 6-3. The vehicle performance with different control strategies

Control strategy	Initial SoC	Final SoC	Used Fuel (L)	Saving (%)
CD/CS	0.5	0.353	6.41	-
Static FLC	0.5	0.379	6.24	2.7%
Dynamic FLC	0.5	0.408	5.44	15.1%
CD/CS	0.4	0.351	6.63	
Static FLC	0.4	0.379	6.48	2.3%
Dynamic FLC	0.4	0.412	5.88	11.3%
CD/CS	0.3	0.352	6.89	-
Static FLC	0.3	0.379	6.75	2.0%
Dynamic FLC	0.3	0.408	6.26	9.14%

6.4.3. HORIZON SENSITIVITY ANALYSIS

As discussed earlier, the observation window was introduced into the BCLM to regulate the learning range of the optimizer. In this section, the impact of the length of the observation window on the input-output signals of the controller is investigated, following which the sensitivity of the length of the observation window to the average applicable time for one set of MFs is analysed.

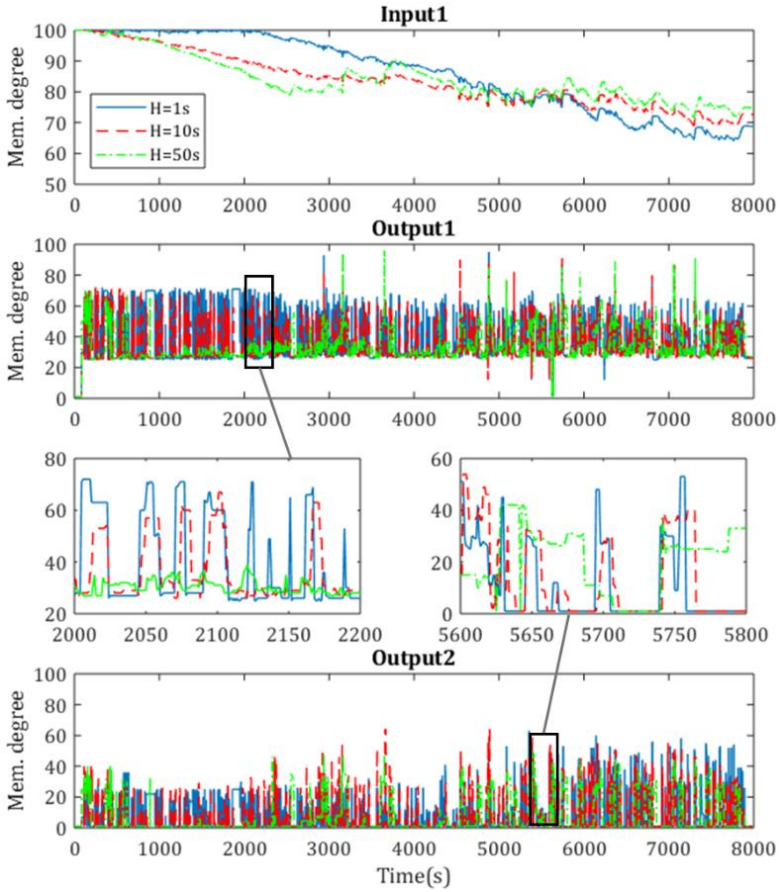

Fig. 6-10. The signal comparison over observation window lengths

Fig. 6-10 presents the signal comparison with different lengths of the observation window ($H = 1\ \mathrm{s}/10\ \mathrm{s}/50\ \mathrm{s}$) when the initial SoC=0.5. As the length of the observation window increases, the early-cycle power provided by the motor rises, and the number of occurrences of peak trans-motor rotational speed increases gradually. For the improved control system, the aggressive braking power can be better absorbed when the observation window, H, is $50\ \mathrm{s}$ than when it is $1\ \mathrm{s}$ or $10\ \mathrm{s}$. This leads to the signal of SoC value dropping fast at an early stage, after which the signal is stable within a small range of oscillation.

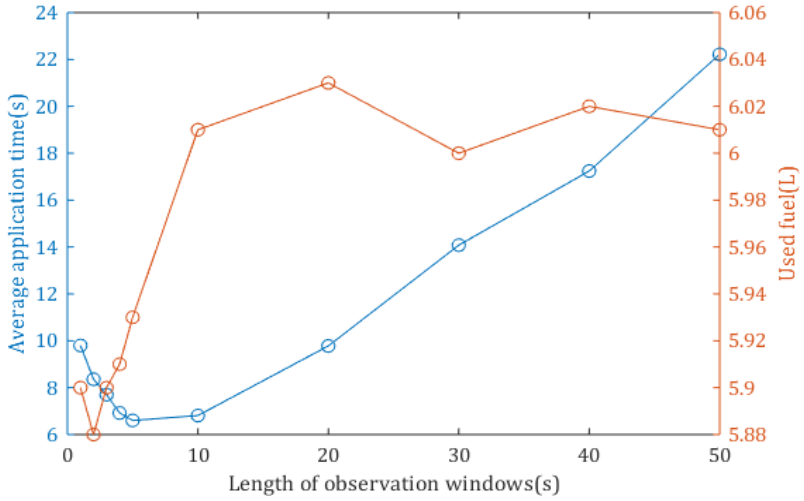

Fig. 6-11. Computational efficiency over backward horizons

Figure 6-11 shows the average application time and the fuel consumption over backward horizons, wherein the tests with the initial SoC=0.4 in each scenario were each repeated 10 times. As the length of observation windows shorten (< 5 s), the rules in the fuzzy inference to be called lessen, and involved scalar parameters of corresponding MFs to be optimized are relatively limited and fixed. Therefore, optimized scalar parameters have longer average application time. The average application time troughs at 6.60 seconds at which the length of observation windows is 5 seconds. After that, as the length of observation windows increases (> 5 s), the rules in the fuzzy inference to be called increases and even some single rules are called multiple times. It results in that involved scalar parameters of corresponding MFs to be optimized need to balance under multiple scenarios. Therefore, optimized scalar parameters with stronger adaptability can handle more driving scenarios thereby average application time is longer. The lowest fuel consumption (on the second y-axis) occurs when the length of observation windows is 2 seconds. As the most suitable observation duration of driving events, this result is consistent with the view of Clara Marina and Cao. [8] After which the fuel

consumption rises rapidly to $6.03\ \mathrm{L}\ (at\ H = 20\ \mathrm{s})$ then remains at a high level on further increase of H. Regarding balancing the computational resource usage and the accuracy of the real time prediction, the author has found computational resource usage is mainly affected by the sizes of state information i.e. size of the observation window. Comparing the various sizes of observation windows from 1 to 50 s, the 2-second observation window appears to be the best for learning from backward horizons as opposed to the longest one.

6.5. SUMMARY

This chapter proposes a back-to-back competitive learning mechanism for a FL-based supervisory control system to improve the fuel-saving efficiency of HEV energy management. The back-to-back learning performance is evaluated and compared with that optimized by other swarm-based algorithms. The contributions drawn from the investigation are as follows:

1) The proposed mechanism has demonstrated abilities to adapt to the change of driving behaviours and to ensure the effectiveness of the FL-based control system by real-time MF parameter updates (957 times) in the case study.
2) Under different initial SoC conditions ($SoC = 0.3/0.4/0.5$), the FL-based control system driven by the proposed mechanism can significantly improve the fuel consumption when compared to CD/CS and conventional FL-based control strategies.
3) The improved FL-based control system reduces fuel consumption over the testing real-world cycle, at least 9% from CD/CS-based and at least 7% from conventional FL-based systems.

4) Comparing the various size of observation windows from 1 to 50 s, the 2-second observation window appears to be the best for learning from backward horizons achieving the lowest fuel consumption of $5.88\ \text{litres}/100\ \text{km}$.

REFERENCES

[1] J. Li, Q. Zhou, H. Williams, and H. Xu, "Back - to - back Competitive Learning Mechanism for Fuzzy Logic based Supervisory Control System of Hybrid Electric Vehicles," *IEEE Transactions on Industrial Electronics*, no. Early Access, 2019.

[2] R. T. Marler and J. S. Arora, "The weighted sum method for multi-objective optimization : new insights," *Structural and multidisciplinary optimization*, vol. 41, no. 6, pp. 853–862, 2010.

[3] A. Hossein, G. Jin, X. Yang, and S. Talatahari, "Chaos-enhanced accelerated particle swarm optimization," *Communications in Nonlinear Science and Numerical Simulation*, vol. 18, no. 2, pp. 327–340, 2013.

[4] Kennedy, James, and Russell Eberhart. "Particle swarm optimization." *Proceedings of ICNN'95-International Conference on Neural Networks*. Vol. 4. IEEE, 1995.

[5] Q. Zhou, W. Zhang, S. Cash, O. Olatunbosun, H. Xu, and G. Lu, "Intelligent sizing of a series hybrid electric power-train system based on Chaos-enhanced accelerated particle swarm optimization," *Applied Energy*, vol. 189, pp. 588–601, 2017.

[6] Q. Zhou, Y. Zhang, Z. Li, J. Li, H. Xu, and O. Olatunbosun, "Cyber-Physical Energy-Saving Control for Hybrid Aircraft-Towing Tractor Based on Online," *IEEE TRANSACTIONS ON INDUSTRIAL INFORMATICS*, vol. 14, no. 9, pp. 4149–4158, 2018.

[7] "ETAS products," *ETAS Group*, 2018. [Online]. Available: https://www.etas.com/en/index.php?langS=true.

[8] C. M. Martinez and D. Cao, *IHorizon-Enabled Energy Management for Electrified Vehicles*. Butterworth-Heinemann, 2018.

CHAPTER 7

FRONT-HORIZON-BASED ONLINE ENERGY MANAGEMENT USING DUAL-LOOP ONLINE INTELLIGENT PROGRAMMING

The content presented in the Chapter 7 is based on the author's published article, 'Dual-loop Online Intelligent Programming for Driver-oriented Predict Energy Management of Plug-in Hybrid Electric Vehicles' in Applied Energy. [1] This chapter investigates an online predictive control strategy for series-parallel plug-in hybrid electric vehicles (PHEVs), resulting in a novel online optimization methodology named the dual-loop online intelligent programming (DOIP) that is proposed for velocity prediction and energy-flow control. By reconsidering the change of driving behaviours at each look-ahead step, this methodology guarantees the effectiveness of optimal control sequence in the energy-saving efficiency of online predictive energy management. The design procedure starts with the simulation of a series-parallel PHEV using a systematic control-oriented model and the definition of a cost function. Inspired by fuzzy granulation technology, a deep fuzzy predictor is created to achieve driver-oriented velocity prediction, and a finite-state Markov chain is exploited to learn transition probabilities between vehicle speed and acceleration. To determine the optimal control behaviours and power distribution between two energy sources, chaos-enhanced accelerated swarm optimization is developed for the DOIP algorithm. The prediction capability of the deep fuzzy predictor is evaluated by comparing with two existing predictors over the WLTP-based driving cycle, both of which have an excellent accuracy. The proposed control strategy is contrasted with short-sighted and dynamic programming based counterparts, and validated by a driver-

in-the-loop simulation platform. The results demonstrate that the deep fuzzy predictor can effectively recognize driving behaviour and reduce at least 19% errors compared to involved Markov chain based predictors. Online predictive control strategy using the DOIP algorithm is able to significantly reduce 9.37% fuel consumption from the baseline and shorten computational time.

7.1. PROBLEM STATEMENT

7.1.1. SEARCH AREA AND CONSTRAINS

The rotation speed of the motor (the relative speed of the rotor to the stator) and the power of the ISG are two optimization variables involved in this research, their boundary conditions need to be constrained as given by:

$$\begin{cases} 0 < n_{mot}(k) < n_{mot^*} \\ -P_{ISG^*} < P_{ISG}(k) < 0 \end{cases} \quad (7-1)$$

Due to the limitation of peak powers and the layout of the HEV powertrain, it is necessary to constrain for ICE, ISG and the traction motor during the optimization, which are formulated as:

$$\begin{cases} T_{mot} = T_d(k), \quad 0 < T_{mot}(k) < T_{mot^*} \\ T_{ICE} = T_d(k), \quad 0 < T_{ICE}(k) < T_{ICE^*} \\ n_{ICE} = \left(P_d(k) - \dfrac{T_{mot}(k) \cdot n_{mot}(k)}{9550} - P_{ISG}(k) \right) \cdot \dfrac{9550}{T_{ICE}(k)}, \quad 0 < n_{ICE}(k) < n_{ICE^*} \\ P_{bra} = \dfrac{T_d(k) \cdot n_d(k) - T_{mot}(k) \cdot n_{mot}(k)}{9550}, \quad P_{bra}(k) < 0 \end{cases} \quad (7-2)$$

where, T_{mot} is the torque of the motor; T_{ICE} is the torque of the engine; n_{ICE} is the rotation speed of the engine; P_{bra} is the braking torque; n_d is the demand speed. To ensure the BP is performing in proper condition and protect the BP from over discharge, the battery's state of charge should obey [2]:

$$0.2 \leq SoC(k) \leq 0.8 \qquad (7-3)$$

The total power generated by the powertrain needs to meet:

$$P_d = \frac{T_{mot}(k) \cdot n_{mot}(k) + T_{ICE}(k) \cdot n_{ICE}(k)}{9550} + P_{bra}(k) \qquad (7-4)$$

7.1.2. COST FUNCTION

Two main targets are mainly concerned in this chapter, one is the final fuel consumption from the fuel tank and the BP, and another is the BP's SoC. These optimization targets are defined as:

$$\begin{cases} J_1 = \sigma_{sfc} \int \dot{m}_f(t)dt \\ J_2 = SoC(t_{end}) \end{cases} \qquad (7-5)$$

where, σ_{sfc} is the specific energy of gasoline ($46kJ/g$); $\dot{m}_f$ is the fuel mass flow rate (g/s); t_{end} is the ending time of the driving cycle.

To convert the multi-objective optimization problem into a single objective optimization for CAPSO algorithm, in the present work, the multi-objective optimization is formulated by using the weighted sum method. [3] Therefore, the optimal energy-flow control problem is described as:

$$\min J = w \cdot J_1 \cdot \frac{1}{J_1^*} + (1-w) \cdot J_2^* \cdot \frac{1}{J_2} \qquad (7-6)$$

$$s.t. \begin{cases} 0 < n_{mot}(k) < n_{mot^*} \\ -P_{ISG^*} < P_{ISG}(k) < 0 \\ T_{mot} = T_d(k), \quad 0 < T_{mot}(k) < T_{mot^*} \\ T_{ICE} = T_d(k), \quad 0 < T_{ICE}(k) < T_{ICE^*} \\ n_{ICE} = \left(P_d(k) - \dfrac{T_{mot}(k) \cdot n_{mot}(k)}{9550} - P_{ISG}(k) \right) \cdot \dfrac{9550}{T_{ICE}(k)}, \quad 0 < n_{ICE}(k) < n_{ICE^*} \\ P_{bra} = \dfrac{T_d(k) \cdot n_d(k) - T_{mot}(k) \cdot n_{mot}(k)}{9550}, \quad P_{bra}(k) < 0 \\ 0.2 \le SoC(k) \le 0.8 \\ P_d = \dfrac{T_{mot}(k) \cdot n_{mot}(k) + T_{ICE}(k) \cdot n_{ICE}(k)}{9550} + P_{bra}(k) \end{cases}$$

where, w is a weight coefficient; J_1^* and J_2^* are scaling coefficients of optimization targets J_1, J_2. Here, the optimization target J_2 is formulated as the penalty function in the cost function.

7.2. PROPOSED SOLUTION

Dual-loop online intelligent programming (DOIP) involves one driver-oriented velocity predictor and one intelligent power splitter, which takes over the real-time optimal control system of the vehicle. Real pedal actions $\boldsymbol{S}_{vel}$ by the human driver and the vehicle state data are sent to the DOIP algorithm for online optimization, then a real optimal control signal will be sent back to the powertrain for the energy distribution. 0.1 seconds is chosen according to Ref. [4] as the sampling time k, which is approved to be able to track the system dynamics while reserving enough time slot for algorithm computing. The mechanism of the DOIP for the PHEV system is shown in Fig. 7-1.

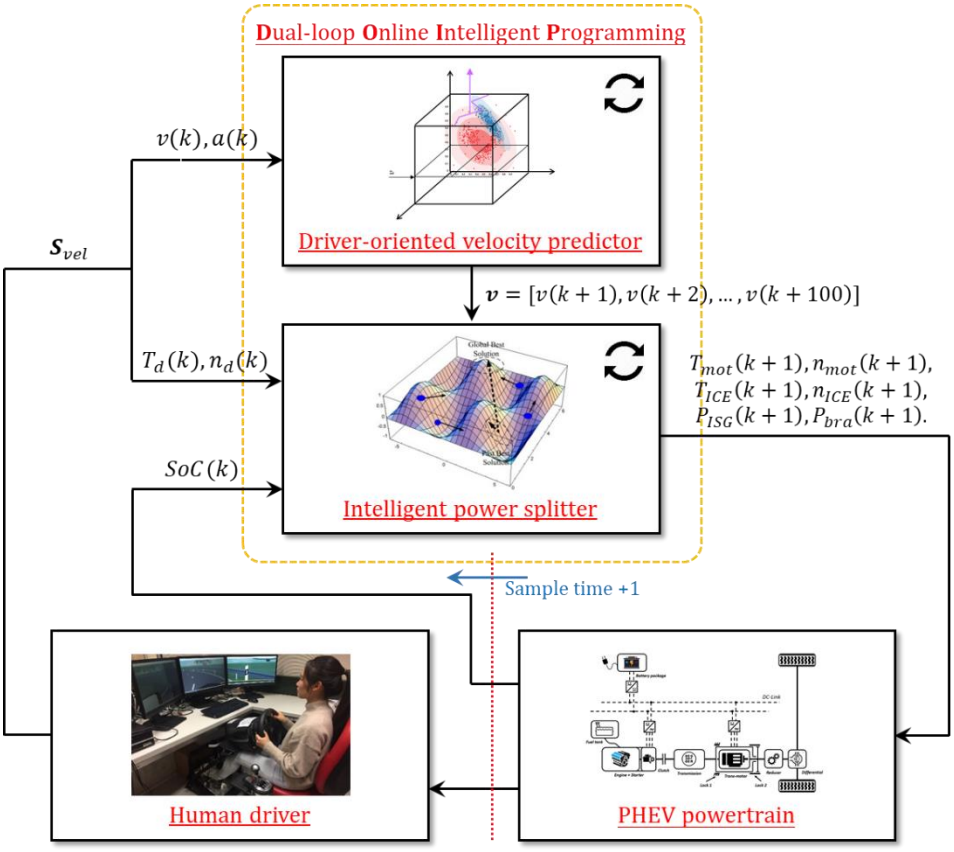

Fig. 7-1. Mechanism of dual-loop online intelligent programming

7.2.1. INTERVAL FUZZY PREDICTOR

In this chapter, the vehicle velocity and acceleration are described as a finite-state MC, [5] its state space is denoted as $V = v_i \mid i = 1, \dots, M \subset X \subset R$, and $W = a_j \mid j = 1, \dots, N \subset Y \subset R$. The transition probabilities may be estimated from the frequencies of observed transitions as given by

$$\begin{cases} p_{ij} = P(a^+ = a_j | v = v_i) = \dfrac{H_{ij}}{H_i} \\ H_i = \sum_{j=1}^{N} H_{ij} \end{cases} \quad (7-7)$$

where, v is the present velocity; a^+ is the next step acceleration; p_{ij} is the transition probability from v_i to a_j; H_{ij} indicates the transition counts from v_i to a_j; H_i is the total transition counts initiated from v_i; the transition probability matrix $\prod$ is filled with elements p_{ij}. Motivated by Eq. (7-7), the probability vector of the next state is defined as

$$\left(\lambda^+(a)\right)^T = \left(\lambda(v)\right)^T \prod = \prod_j^T \qquad (7-8)$$

where, $\lambda^T(v) = [0 \dots 1 \dots 0]$ is an N-dimensional probability vector with the jth element, to indicate a discrete state a_j in disjoint intervals $I_j, j = 1, \dots, N$; $\prod_j^T$ denotes the jth row of the transition probability matrix $\prod$. In the fuzzy encoding technique, X and Y are divided into finite sets separately with fuzzy subsets $\Phi_i, i = 1, \dots, M$ and $\Phi_j, j = 1, \dots, N$. The fuzzy subset Φ_i and Φ_j are pairs of $(X, \mu_i(\cdot))$ and $(Y, \mu_j(\cdot))$, where $\mu_i(\cdot)$, $\mu_j(\cdot)$ are Lebesgue measurable membership functions that satisfy the following property:

$$\begin{cases} \mu_i : X \to [0,1]\ s.t. \forall v \in X, \exists i, 1 \le i \le M, \mu_i(v) > 0 \\ \mu_j : Y \to [0,1]\ s.t. \forall a \in Y, \exists j, 1 \le j \le N, \mu_j(a) > 0 \end{cases} \qquad (7-9)$$

where, $\mu_i(v)$ reflects the degree of membership of $v \in X$ in μ_i; $\mu_j(a)$ reflects the degree of membership of $a \in Y$ in μ_j. Based on the theory of approximate reasoning, [6] the transformation with normalization allocates an M-dimensional probability vector for each $v \in X$ as follows:

$$\left(O(v)\right)^T = \left[\frac{\mu_1(v)}{\sum_{i=1}^M \mu_i(v)}, \frac{\mu_2(v)}{\sum_{i=1}^M \mu_i(v)}, \dots, \frac{\mu_M(v)}{\sum_{i=1}^M \mu_i(v)}\right] \qquad (7-10)$$

This transformation is used to do normative fuzzification and map velocity in the space X to vector in M-dimensional probability vector space $\bar{X}$, and the sum of the elements in the probability vector $\sim O(v)$ equals to 1. The probability distribution of the next state in $\bar{Y}$ is

computed based on Eq. (7-10), then aggregated with membership function $\mu(a)$ to decode vectors in $\overline{Y}$ back to the space Y as given by:

$$z^{+}(a) = \left(O^{+}(v)\right)^{T}\mu(a) = \left(O(v)\right)^{T}\prod\mu(a) \qquad (7-11)$$

where, the element p_{ij} in the transition probability matrix Π is interpreted as a transition probability between Φ_i and Φ_j. The membership function $\mu(a)$ is used to encode the probability vector of the next state in the space Y.

In this chapter, it is assumed that membership functions have the same volume from which it follows that $\sum_{j=1}^{N} p_{ij} = 1$ and $\sum_{i=1}^{M} O_i(v) = 1$, and the next one-step-ahead velocity is calculated and simplified to

$$\begin{cases} a^{+} = \dfrac{\sum_{i=1}^{M} O_i(v) \sum_{j=1}^{N} p_{ij}\overline{V}_j\,\overline{c}_i}{\sum_{i=1}^{M} O_i(v) \sum_{j=1}^{N} p_{ij}V_j} = \left(O(v)\right)^{T}\prod\overline{c} \\ v^{+} = v + a^{+} \end{cases} \qquad (7-12)$$

where, $\overline{c}_i$ and $\overline{V}_j$ are the centroid and volume of the membership function $\mu_j(v)$.

7.2.2. DEEP FUZZY PREDICTOR

As driver-oriented predict models, the deep fuzzy predictor (DFP) is created with multi-dimensional fuzzification to improve the precision of future velocity predictions by reconsidering driving behaviours for each look-ahead step. Unlike a single MC model with fuzzy encoding, the DFP involves five driver-oriented MC models, which are classified by fuzzy C-mean clustering algorithm. A membership criterion vector solved by clustering is utilized as weighted sum coefficients to aggregate the predicted accelerations of the five driver-oriented

MC models. The fuzzy granulation evolution for the MC models is drawn in Fig. 7-2 and the production process of the DFP is presented as follows.

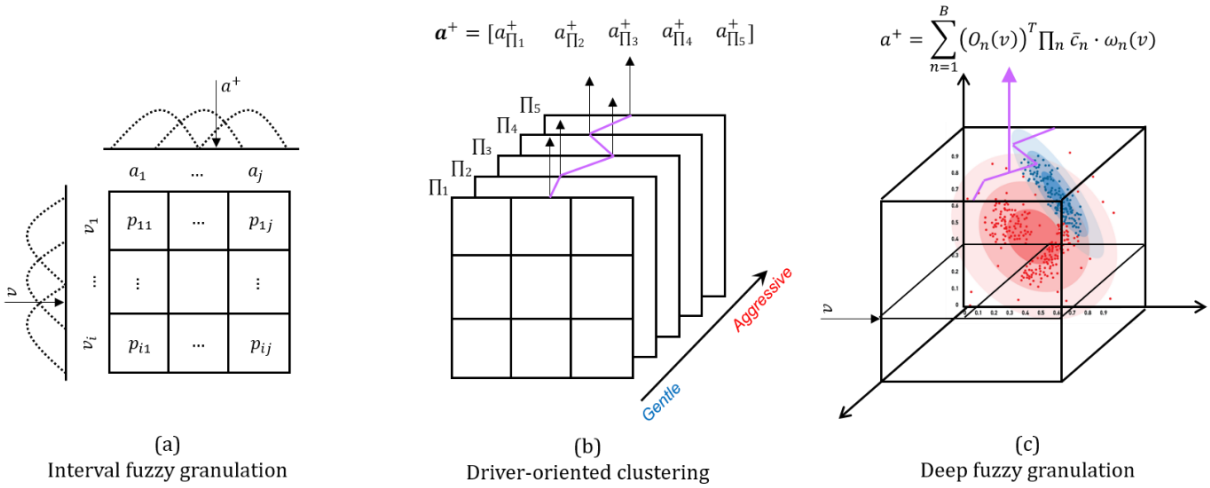

Fig. 7-2. Fuzzy granulation evolution for MC models

The auto-regression (AR) model is a proven tool for generalizing the signal's average time regressive pattern and predicting by following the dynamic. The AR model used in this study follows the structure described in [7]:

$$v(k) = \sum_{r=1}^{K} \vartheta_r v(k-r) + \varepsilon_k \qquad (7-13)$$

where, ϑ_r are the AR coefficients; K is the order of AR model; ε_k refers to the i.i.d noise; $v(k)$ is the vehicle speed at time step k, with sample period $\tau = 0.1s$ in this study.

Due to real-world driving involving frequent transitions in the driver behaviour, the AR model is used in the moving horizon way to extract driver-oriented velocity information, in which parameters of past measurement horizon length and the AR model order R need to be investigated. AR models of horizons ranging from 10 to 500 seconds and with orders from 1st to 4th have been tested on 9000s WLTP-based driving cycles. Second order AR models with

200 seconds horizons show consistent advantage judged by the Corrected Akaike Information Criterion. [8] Its result is described as data vector $\boldsymbol{\gamma}_r$ of speed interval samples, which contains four sets of information as given by

$$\boldsymbol{\gamma}_r = [\vartheta_{r1} \quad \vartheta_{r2} \quad a_{r\_avg} \quad a_{r\_maxR}] \tag{7-14}$$

where, the AR coefficient set ϑ provides the trend of sampling speed change; average acceleration rate a_{r_avg} marks the average state and the maximum acceleration range a_{r_maxR} marks the range of acceleration changes.

Considering the computation efficiency and prediction accuracy, 5-layer Markov-chain model is reliable for training purpose as has been proved by Ref. [7]. In this chapter, the AR model coefficient sets are classified into 5 clusters representing different acceleration states to label the estimated AR models to some specific driver states. The five clusters are fuzzified to reflect the acceleration range relationship among different driving behaviours, the driving behaviours are noted as 1. Very Gentle, 2. Gentle, 3. Normal, 4. Aggressive, 5. Very Aggressive. As there is no prior information on the predicted vehicle's performance or the driver's preference, the fuzzy C-mean method with unsupervised learning process is recommended for dividing information with less strict internal borders and unpredictable external borders. It is more sensitive to the isolated point i.e. dramatic driving state. The method uses a membership criterion $\omega_{k,n}$ and the Euclidean distance from data x_k ($k \in \{1,\cdots,A\}$) to identify multiple cluster centres C_n ($n \in \{1,\cdots,B\}$). The cluster centers C_n are iterated till the total distance is minimized [9]:

$$J = \sum_{k=1}^{A}\sum_{n=1}^{B} \omega_{k,n}^{m} \parallel x_k - C_n \parallel^2 \tag{7-15}$$

$$\begin{cases} \omega_{k,n} = \dfrac{1}{\sum_{k=1}^{B} \left(\dfrac{\| x_k - C_n \|}{\| x_k - C_n \|} \right)^{\frac{2}{m-1}}} \\ C_n = \dfrac{\sum_{k=1}^{B} {\omega_{k,n}}^m \boldsymbol{\gamma}_k}{\sum_{k=1}^{B} {\omega_{k,n}}^m} \end{cases} \quad (7-16)$$

where, parameter m (m > 1) controls the fuzziness of cluster overlapping, which is set at $m = 2$ in this study. The classification results provide data's membership distributions with respect to all of the clusters. According to driving behaviour classification, the transition probability matrix $\prod$ in Eq. (7-8) is expanded into five transition probability matrixes as given by

$$|\prod_1 \quad \prod_2 \quad \prod_3 \quad \prod_4 \quad \prod_5| \quad (7-17)$$

where, the transition probability matrix with customized division can more accurately reflect the probability distribution of acceleration under different driving behaviours. Therefore, the next one-step-ahead accelerations by driver-oriented clustering (Fig.7-2 b) can be translated to

$$a_n^+ = \left(O_n(v)\right)^T \prod_n \bar{c}_n \quad (7-18)$$

Here, the membership criterion is utilized as weighted sum coefficient to aggregate predict acceleration of five driver-oriented MC models. Based on Eq. (7-18), the next one-step-ahead velocity is calculated as given by

$$\begin{cases} a^+ = \sum_{n=1}^{B} \left(O_n(v)\right)^T \prod_n \bar{c}_n \cdot \omega_n(v) \\ v^+ = v + a^+ \end{cases} \quad (7-19)$$

where, the membership criterion vector $\omega_n(v)$ corresponds to the data vector $\boldsymbol{\gamma}_r$ of the speed interval sample.

7.2.3. INTELLIGENT POWER SPLITTER AND DOIP WORKFLOW

In this section, an intelligent power splitter is designed based on CAPSO algorithm, which has three main procedures, namely, initialization, main iteration, and optimal position retrieving. The details and principle of the CAPSO algorithm working procedure are discussed in the author's previous work. [10] To solve the optimization problem in Eq. (7-6) online, the algorithm is customized and modified in the following aspects. At the initialization procedure, the position of each particle is defined as:

$$x^{(i,j)} = \begin{bmatrix} n_{mot}^{(i,j)} & P_{ISG}^{(i,j)} \end{bmatrix} \tag{7-20}$$

Here, the superscript i is an index of iterations, for a swarm intelligent algorithm that has $M = 15$ iterations, $i = [1,2,3 \dots M]$. The superscript j is the index of the particle, for swarm that has $N = 20$ particles, $j = [1,2,3 \dots N]$. $n_{mot}^{(i,j)}, P_{ISG}^{(i,j)}$ are the rotation speed of motor and the demand power of an ISG in the jth agent and ith iteration. For the CAPSO, the particles position updates with the following equation:

$$x^{(i+1,j)} = (1-\beta) \cdot x^{(i,j)} + \beta \cdot g^{(i,*)} + \alpha^{(i)} \cdot \epsilon^{(i,j)} \tag{7-21}$$

In Eq. (24), $g^{(i,*)}$ is the best position in the ith iteration, β is the attraction parameters of CAPSO, α is the convergence parameters of CAPSO and ϵ is the $[0,1]$ random number. Here, α and β could be updated respectively in each iteration as:

$$\begin{cases} \alpha^{(i)} = \alpha^{(0)} \cdot \gamma^{i} \\ \beta^{(i+1)} = a \cdot \beta^{(i)} \cdot (1-\beta^{(i)}) \end{cases} \tag{7-22}$$

where, the setting range of $\alpha^{(0)}$ and γ are $\alpha^{(0)} = 0.9$, $\gamma = 0.95$ in this chapter; the attraction parameter is mapped by the logistic map [11], in which the initial value $\beta^{(1)} = 0.6$ and $a = 4$

are used. When $\beta \to 0$ in any step, the algorithm may lead to slow changes. After the convergence has been achieved, the algorithm ends the main iteration and outputs the best position at the end iteration $g_{\max\ \_iter,*}$ as the global optimal solution.

The proposed DOIP has two online iteration loops for updating predict model and optimizing control sequence, which can obtain a real-time optimal control signal for energy flow distribution. Inspired by fuzzy granulation technology, the DOIP algorithm improves the precision of future velocity by reconsidering driving behaviours for each look-ahead step to guarantee the effectiveness of the optimal control sequence solved by CAPSO algorithm. The DOIP workflow (at k sampling time) is shown in Fig 7-3.

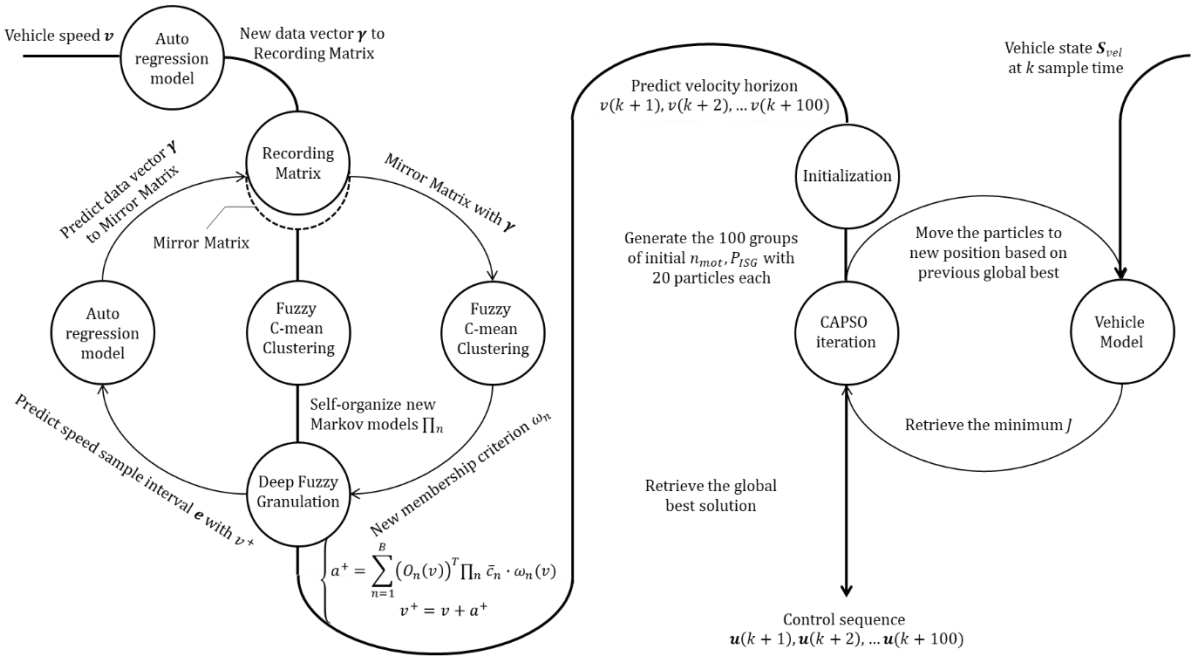

Fig. 7-3. Workflow of dual-loop online intelligent programming

In the prediction process of the DOIP algorithm, a recording matrix and its mirror matrix are involved and used as short-term length moving windows for driving data collection. Although the size of the training data is limited by length of moving windows, the DOIP algorithm will

continuously motivate the training data to keep fresh all the time. It can be described as given by:

$$\boldsymbol{R} = \boldsymbol{R}_{mirror} = [\boldsymbol{\gamma}_k, \boldsymbol{\gamma}_{k-1}, \cdots, \boldsymbol{\gamma}_{k-5000}]^T \quad (7-23)$$

where, $\boldsymbol{\gamma}_k$ indicates data vector of the moving memory horizon at sampling time k; the update frequency of recording matrix $\boldsymbol{R}$ is 5 seconds; the update frequency of mirror matrix $\boldsymbol{R}_{mirror}$ is consistent with the communication frequency of the real-time PHEV system (0.1s).

Between two updates of the record matrix $\boldsymbol{R}$, the mirror matrix $\boldsymbol{R}_{mirror}$ will participate in the iterative calculation of multi-step prediction and its procedure is as follows. Based on Eq. (22), the new data vector $\boldsymbol{\gamma}_{k+1}$ related to the next one-step-ahead velocity $v(k+1)$ is calculated and used to squeeze out the last data vector $\boldsymbol{\gamma}_{k-5000}$ in the mirror matrix. Therefore, the mirror matrix $\boldsymbol{R}_{mirror}$ is replaced to $\boldsymbol{R}'_{mirror}$ as given by

$$\boldsymbol{R}'_{mirror} = [\boldsymbol{\gamma}_{k+1}, \boldsymbol{\gamma}_k, \cdots, \boldsymbol{\gamma}_{k-4999}]^T \quad (7-24)$$

Based on the new mirror matrix $\boldsymbol{R}'_{mirror}$, the membership criterion of the next one-step-ahead $u_n(\boldsymbol{\gamma}_{k+1})$ is calculated as the weighted sum coefficient to aggregate the next two-step-ahead velocity from predict results of five driver-oriented Markov models. The next-two-step velocity $v(k+2)$ can be calculated as given by

$$\begin{cases} a(k+2) = \sum_{n=1}^{B} \left(O_n\big(v(k+1)\big)\right)^T \prod_n \bar{c}_n \cdot \omega_n\big(v(k+1)\big) \\ v(k+2) = v(k+1) + a(k+2) \end{cases} \quad (7-25)$$

After iterative calculation, the future horizon velocity $v(k+1), v(k+2), \ldots, v(k+100)$ is obtained, then used in the second iteration loop for optimizing the control sequence via the CAPSO algorithm. Finally, the first fifty elements of the control sequence $\boldsymbol{u}(k+1), \boldsymbol{u}(k+$

$2), \ldots, \boldsymbol{u}(k+100)$ will be sent back to the powertrain of the PHEV system for real-time energy management. Once the next updating trigger comes, the recording matrix $\boldsymbol{R}$ and the mirror matrix $\boldsymbol{R}_{mirror}$ will both be updated following which the driver-oriented MC models $\prod_n$ will be re-learned respectively.

7.3. EXPERIMENTAL PLAN

7.3.1. REAL-WORLD DRIVING CYCLES

In this research, experimental studies are conducted on the cockpit package with the same PHEV model, in which five human drivers are invited as experimental objects to participate in 8000 seconds real-world driving. The road map model used with traffic is a mixture of highway and local roads with multiple stop signs, traffic lights, and speed limit changes provided by IPG CarMaker as Fig. 7-4. The human driver is required to follow the speed limits, stop signs, traffic lights, and other traffic regulations. It should be noted that the driver's pedal behaviour may be dependent on the vehicle, the pedal to its torque map, and even the physical pedal resistance feedback. This dependence is not studied in this research. The proposed model in this chapter is for generating/learning the drivers' behaviour for a given vehicle. The specification of the real-world driving cycle is shown in Table 7-1.

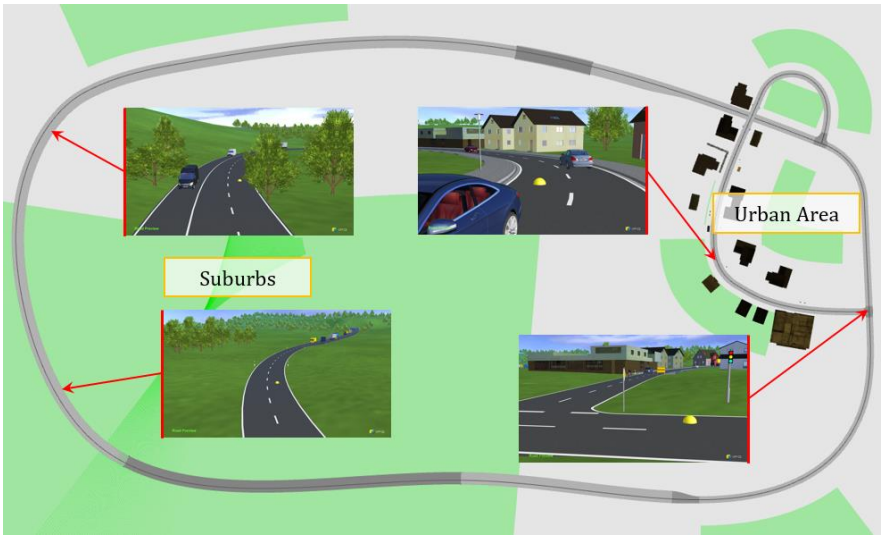

Fig. 7-4. Driving scenario with traffic provided by IPG CarMaker

Table 7-1. Specification of real-world driving cycle

Human driver	Traffic type	Driving time(s)	Driving distance(km)
A	Urban	1880	11.6
B	Urban	1590	17.9
C	Urban	940	8.1
D	Highway	1350	22.5
E	Highway	2240	40.0

7.3.2. DRIVING SIMULATION PLATFORM

A static system experience platform driving simulator is involved in this work as shown in Fig. 7-5, which is the ideal tool for subjectively testing vehicle functions through direct experience. It makes the most of the advantages offered by the combination of a detailed and realistic human machine interface simulation and a real-world driving experience, coupled with the CarMaker open integration and test platform. [12] There is one cockpit package supported by a Thrustmaster T500RS and one host PC with I5-6500 3.2GHz processor and 8GB RAM. Their

communication relies on a 3.0 USB cable, in which sampling frequency of the PHEV system and pedal data acquisition are both 10 Hz.

Fig. 7-5. Driving simulator used in this research

7.4. RESULT AND DISCUSSION

7.4.1. VELOCITY PREDICTION COMPARISON

Existing MC-based predictors including the nearest neighbour predictor (NNP) [13] and the fuzzy encoding predictor (FEP) i.e. the interval fuzzy predictor [14] is considered in this chapter and compared with the proposed DFP. As the unique ability, the DFP can efficiently differentiate driving behaviours at each driving state using fuzzy C-mean clustering algorithm. In Fig. 7-6, it can be seen that five-level driving behaviours are clearly discriminated through deep fuzzy granulation, in which the driver with more aggressive actions have more wide operation range. Especially at deceleration range [-6,-3], the DFP differentiates the operation border of each driving behaviour.

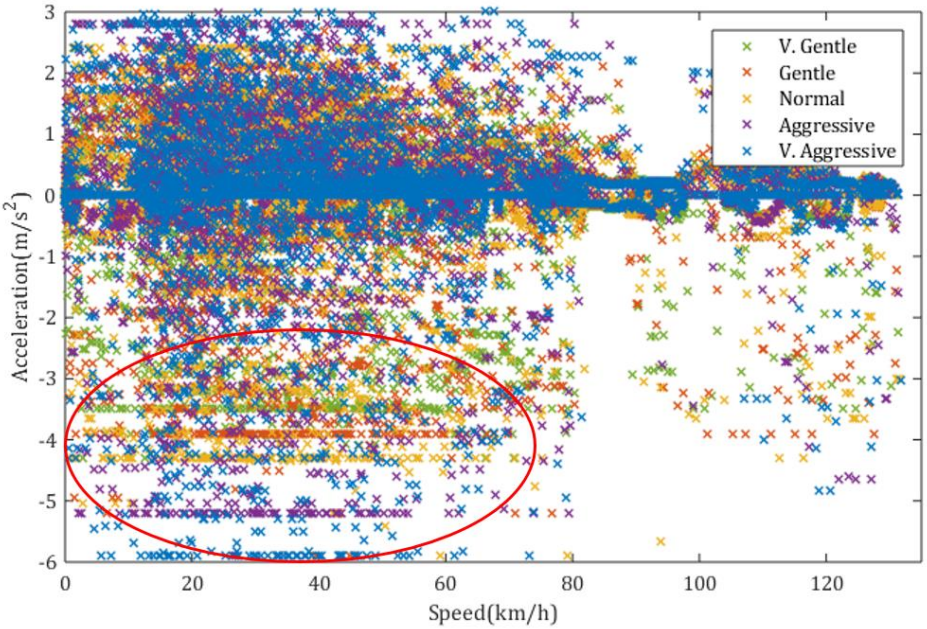

Fig. 7-6. Clustering results of driving behaviour by the DFP

Fig. 7-7 presents 5-second velocity prediction result of three predictors on the personalized WLTP-based cycles. In conjunction with the fragment of real-time delta-v comparison of using three predictors, it is very hard for the NNP to make a good prediction in the low-speed area because the transition probability of this area is very small by using one discrete MC model. Through fuzzy granulation, the FEP fixes the problem from the low-speed area but to treat different driving habits in a unified way makes its prediction performance in the medium-high-speed area still unsatisfied. Compared with both MC-based predictors of the NNP and the FEP, it is apparent that the DFP can achieve more excellent accuracy because the training database of the predictive model is continuously updating during real-world driving. The prediction model can realize more personalized prediction in time-series through driver-oriented continuous adjusting among 5-layer Markov-chain models. The integral time absolute error (ITAE) in DFP (2.4237×10^5) is less than that in NNP (3.3412×10^5) and FEP (2.7074×10^5),

in which the maximum error in DFP decreases 2.59% compared to that in FEP. More comparison detail is shown in Table 7-2.

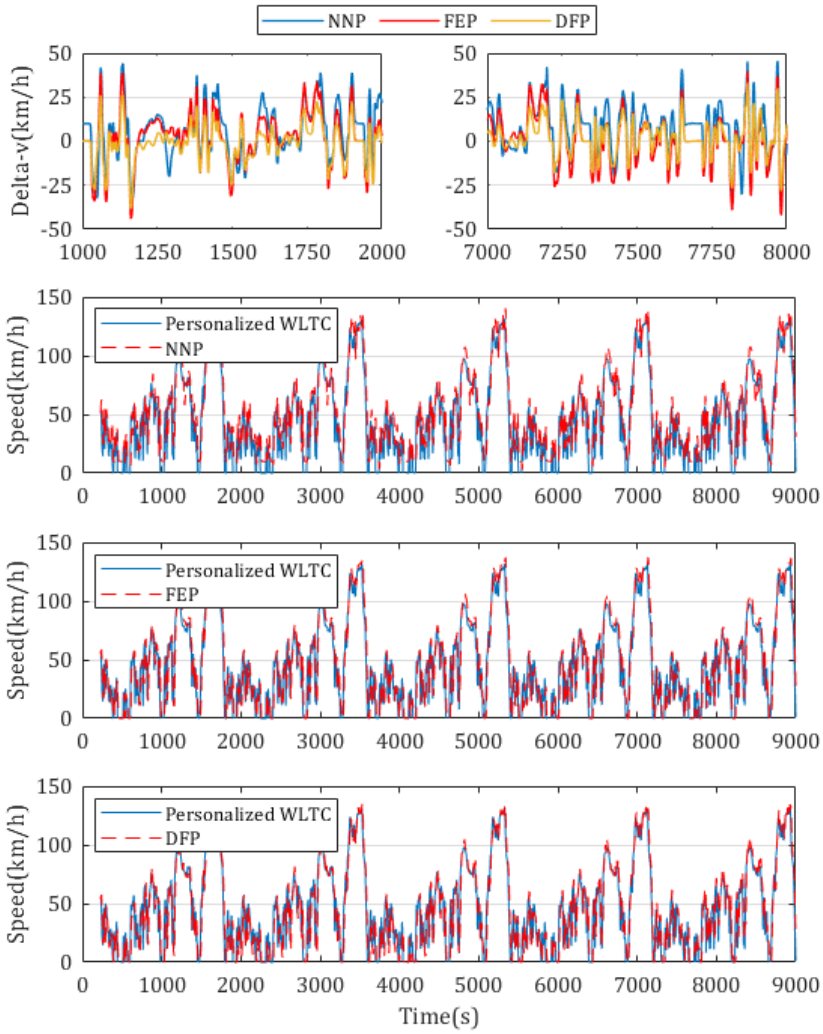

Fig. 7-7. Velocity prediction result of three MC-based predictors

Table 7-2. Velocity prediction comparison of three MC-based predictors

Predictor	Driving behaviour recognition	Maximum error	ITAE(10^5)	Reduce (%)
NNP	NA	14.81%	3.3412	-
FEP	NA	4.81%	2.7074	18.97%
DFP	Yes	2.22%	2.4237	27.46%

7.4.2. PERFORMANCE OVER CYCLE-BASED DRIVING

Here, the DOIP-based online control strategy using the DFP (10-second look ahead) is further compared with DP-based one and a rule-based control strategy over the WLTP-based driving cycle. Fig. 7-8 illustrates the vehicle system performance comparison when initial SoC=0.8. It can be discerned that the power split trajectory in the DOIP-based online control strategy is close to that of DP-based control strategy and clearly differs from the rule-based control. Especially during the hybrid mode, the rule-based control strategy more often let the engine work at maximum power. Relatively, the DP and DOIP based control strategies let engine keep working in a high-efficiency region for fuel saving.

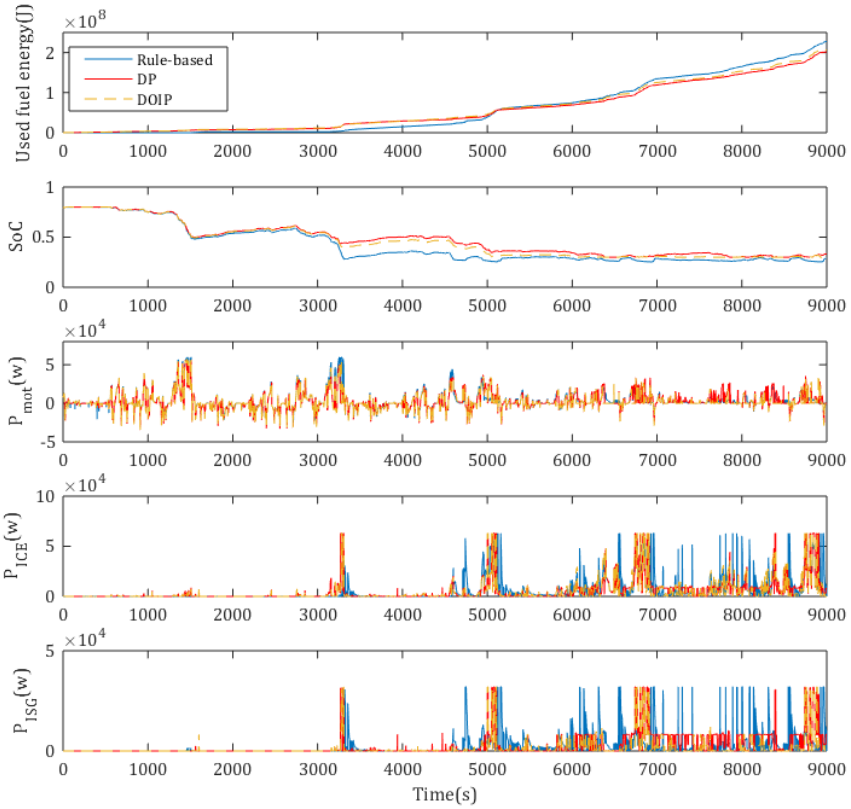

Fig. 7-8. Vehicle system performance comparison when initial battery SoC=0.8

An analogous result also can be observed in Fig. 7-9 when initial SoC=0.2. Obviously, the fuel consumption under the DOIP-based online control strategy is closest to that of the DP-based control, 9.18% and 11.8% energy-saving from the rule-based control strategy at SoC=0.8 and SoC=0.2. Compared to the rule-based control strategy, the DP and DOIP based them have a higher SoC level during the entire journey as backup energy for the potential high power requirements. Compared with when the initial battery SoC=0.2, energy-saving performance of productive control strategies is more significant when the initial battery SoC=0.8. The vehicle performance with different control strategies is summarized in Table 7-3.

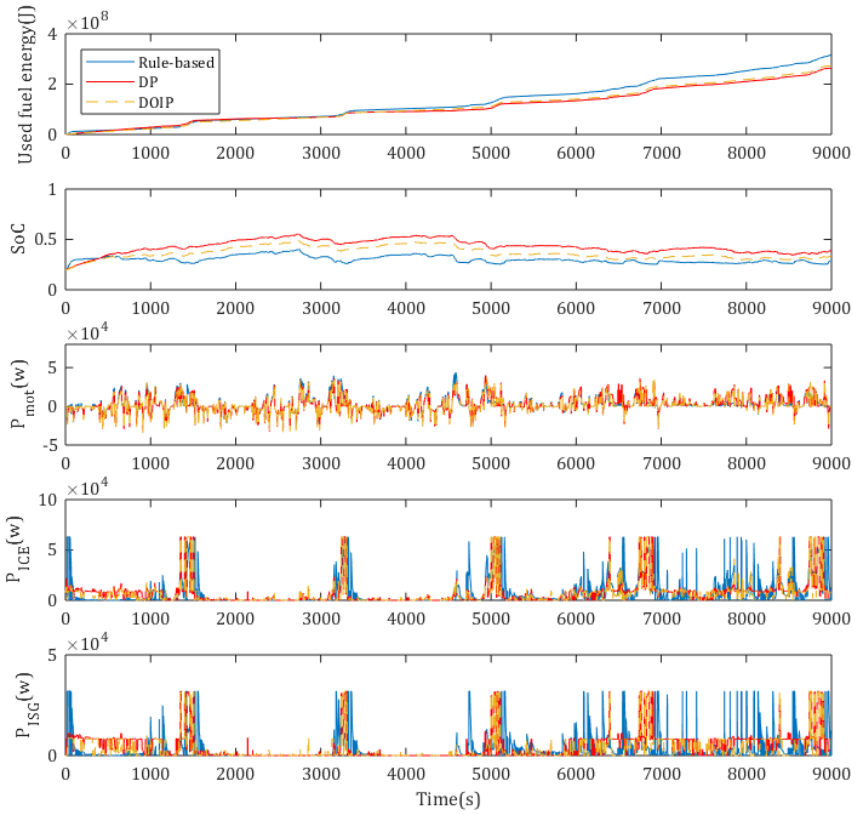

Fig. 7-9. Vehicle system performance comparison when initial battery SoC=0.2

Table 7-3. Vehicle system performance over WLTP-based driving

Optimization strategy	Initial SoC	Final SoC	Used fuel energy (10^8J)	Savings (%)
Rule-based	0.8	0.2893	2.2730	-
DP	0.8	0.3339	2.0146	11.37%
DOIP	0.8	0.3093	2.0644	9.18%
Rule-based	0.2	0.2893	3.0951	-
DP	0.2	0.3891	2.6383	14.76%
DOIP	0.2	0.3348	2.7300	11.80%

7.4.3. PERFORMANCE OVER REAL-WORLD DRIVING

All the experiments here were conducted on the driving simulation platform. Fig. 7-10 shows the DiL experiment result operated by five human drivers in simulation driving scenarios, where each driver's independently driven section is separated by a black dotted line. After 600-second initialization of the recording matrix, the DFP starts to produce 10s look-ahead horizon and its prediction models are real-time updating per five seconds. The predicted velocity feature relies on last-one-step driving behaviour not related to the driver's change. This means that if the driving behaviour of a single driver has changed dramatically, its predicted velocity will be adjusted adaptively according to a new pedal action (shown in magnified views). It is emphasized that the recording matrix of the DFP will be completely replaced within 600 seconds so that to relearn a new driver behaviour takes up to 10 minutes whenever the driver changes.

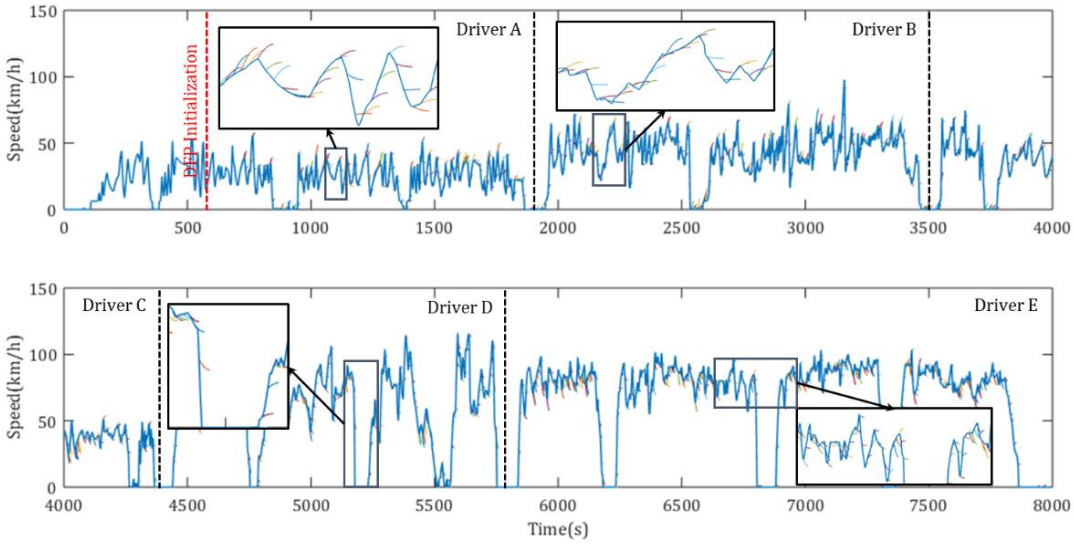

Fig. 7-10. Online prediction results over real-world driving

Fig. 7-11 indicates when BP's SoC is high, the DOIP-based control strategy allows the engine to compensate for the total power demand for low power. Fig. 7-12 indicates when BP's SoC is low, this control strategy will give the engine a priority in compensating the total power demand compared to the generator to compensate the BP. Compared with the rule-based strategy, Up to 9.37% total energy can be saved while maintain the higher SoC value by the DOIP-based control strategy. During the real-world driving, the DOIP algorithm breaks the bondage of conventional rule-based strategy and freely explore the more efficient way for the PHEV's energy-split. Due to no prior information on the predicted vehicle's performance or the driver's preference, global optimal algorithms i.e. the DP-based control strategy is no longer suitable for online optimization of the HEV energy management. More specification comparison over real-world driving is reported in Table 7-4.

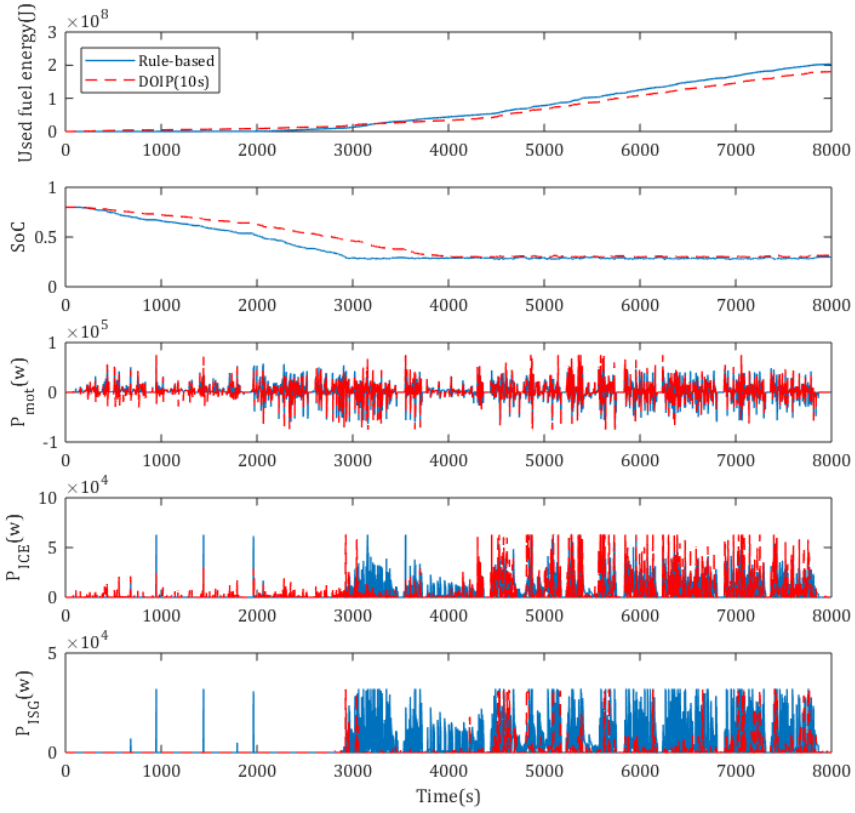

Fig. 7-11. Vehicle performance over real-world driving when initial battery SoC=0.8

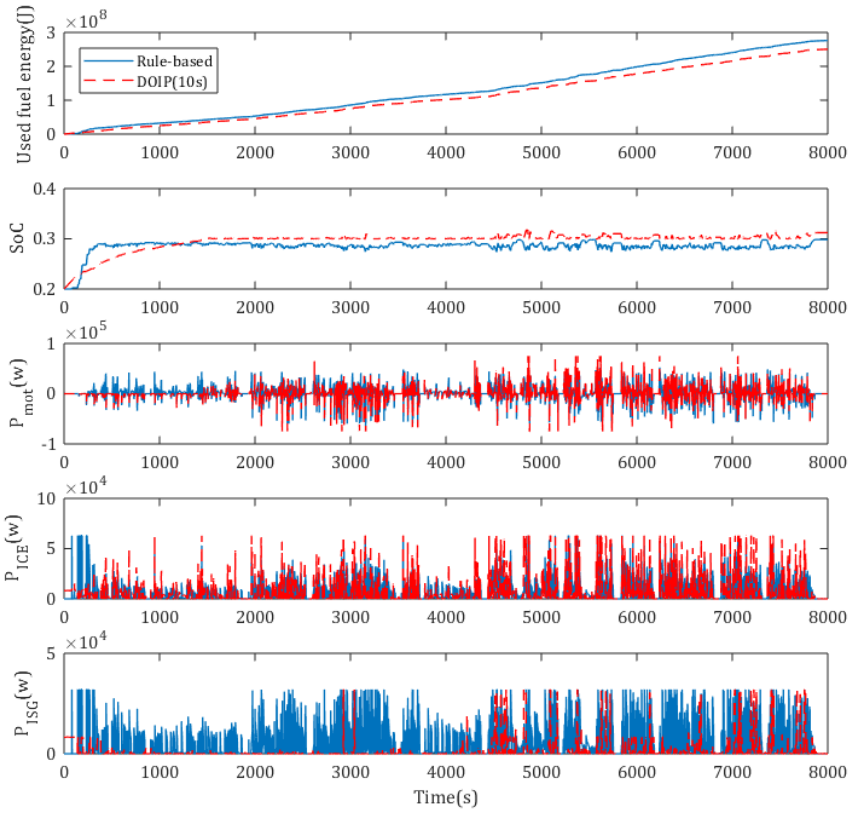

Fig. 7-12. Vehicle performance over real-world driving when initial battery SoC=0.2

Table 7-4. Online performance comparison over real world driving

Optimization strategy	Initial SoC	Final SoC	Used fuel energy (10^8J)	Saving (%)
Rule-based	0.8	0.2985	2.0217	-
DOIP	0.8	0.3144	1.8668	7.66%
Rule-based	0.2	0.2985	2.7638	-
DOIP	0.2	0.3123	2.5049	9.37%

The computational time of the DOIP algorithm in the DiL experiment is investigated and contrasted in Table 7-5. The solving speed of the DOIP algorithm is affected by look-ahead horizon length and computational efficiency of the processor, where the latter will not be

discussed in this chapter. As an increase of look-ahead horizon length, iterative calculations in this algorithm increase and its computational time appears a linear upward trend. When the look-ahead horizon is 20 seconds, the computational time increases to 0.79s per second but computing resources still have a surplus depending on its concise solving frame. As the rapid development of computer science, it is feasible to operate the DOIP algorithm on the actual on-board controller of HEVs for real-time energy saving.

Table 7-5. Computational time in different look-ahead horizon length

Optimization strategy	Look-ahead horizon	Time (per second)	Relative increase (%)
DOIP	5s	0.54s	-
DOIP	10s	0.67s	24.07%
DOIP	20s	0.79s	46.30%

7.5. SUMMARY

This chapter develops an online predictive control strategy using the proposed DOIP algorithm for series-parallel PHEVs. Its prediction performance is demonstrated and compared with existing MC-based predictors. Cycle-based driving (WLTP) and real-world driving are conducted on the driving simulator experimental platform for vehicle performance validation. The conclusions drawn from the investigation are as follows:

1) The proposed DFP has the ability to differentiate driving behaviours at each driving state in real time. Its prediction result shows excellent accuracy with the lowest maximum error (2.22%), compared with the NNP (14.81%) and the FEP (4.81%).

2) From the cycle-based driving results, energy management efficiency of the DOIP-based control strategy is close to DP-based control strategy. It is clearly superior to the rule-based one over the WLTP-based driving cycle with up to 11.80% reduction in fuel consumption.
3) During real world driving, up to 9.37% total energy can be saved compared with the rule-based control strategy. The DP-based control strategy cannot work in this online environment.
4) Whether cycle-based driving or real-world driving scenarios, the energy-saving performance of the DOIP-based control strategy is more outstanding when the initial SoC is low (SoC=0.2).
5) The computational time of the DOIP algorithm is investigated. It is feasible to operate the DOIP algorithm for 20s look-ahead horizon and computing resources still have a surplus.

REFERENCES

[1] J. Li *et al.*, "Dual-loop online intelligent programming for driver-oriented predict energy management of plug-in hybrid electric vehicles," vol. 253, no. July, 2019.

[2] Z. Chen, R. Xiong, C. Wang, and J. Cao, "An on-line predictive energy management strategy for plug-in hybrid electric vehicles to counter the uncertain prediction of the driving cycle," *Applied Energy*, vol. 185, pp. 1663–1672, 2017.

[3] R. T. Marler and J. S. Arora, "The weighted sum method for multi-objective optimization : new insights," *Structural and multidisciplinary optimization*, vol. 41, no. 6, pp. 853–862, 2010.

[4] X. Zeng, J. Wang, and S. Member, "A Stochastic Driver Pedal Behavior Model Incorporating Road Information," *IEEE TRANSACTIONS ON HUMAN-MACHINE SYSTEMS*, vol. 47, no. 5, pp. 614–624, 2017.

[5] D. P. Filev and I. Kolmanovsky, "Generalized Markov Models for Real-Time Modeling of Continuous Systems," *IEEE TRANSACTIONS ON FUZZY SYSTEMS*, vol. 22, no. 4, pp. 983–998, 2014.

[6] L. Johannesson, M. Åsbogård, and B. Egardt, "Assessing the Potential of Predictive Control for Hybrid Vehicle Powertrains Using Stochastic Dynamic Programming," *IEEE TRANSACTIONS ON INTELLIGENT TRANSPORTATION SYSTEMS*, vol. 8, no. 1, pp. 71–83, 2007.

[7] J. Jing, D. Filev, A. Kurt, E. Özatay, J. Michelini, and Ü. Özgüner, “Vehicle Speed Prediction using a Cooperative Method of Fuzzy Markov Model and Auto-regressive Model,” in *Intelligent Vehicles Symposium (IV), 2017 IEEE*, 2017, no. Iv, pp. 881–886.

[8] H. Akaike, “Information theory and an extension of the maximum likelihood principle,” in *Selected papers of hirotugu akaike*, Springer, 1998, pp. 199–213.

[9] J. C. Bezdek, “Objective function clustering,” in *Pattern recognition with fuzzy objective function algorithms*, Springer, 1981, pp. 43–93.

[10] Q. Zhou, Y. Zhang, Z. Li, J. Li, H. Xu, and O. Olatunbosun, “Cyber-Physical Energy-Saving Control for Hybrid Aircraft-Towing Tractor Based on Online,” *IEEE TRANSACTIONS ON INDUSTRIAL INFORMATICS*, vol. 14, no. 9, pp. 4149–4158, 2018.

[11] Q. Zhou, W. Zhang, S. Cash, O. Olatunbosun, H. Xu, and G. Lu, “Intelligent sizing of a series hybrid electric power-train system based on Chaos-enhanced accelerated particle swarm optimization,” *Applied Energy*, vol. 189, pp. 588–601, 2017.

[12] IPG Carmaker, “System Experience Platform,” *IPG Automotive, Karlsruhe, Germany*, 2014. [Online]. Available: https://ipg-automotive.com/products-services/test-systems/driving-simulators/#system-experience-platform.

[13] C. Lin, H. Pengl, and J. W. Grizzle, “A Stochastic Control Strategy for Hybrid Electric Vehicles,” in *American Control Conference*, 2004, pp. 4710–4715.

[14] T. Liu, X. Hu, S. E. Li, and D. Cao, “Reinforcement Learning Optimized Look-Ahead Energy Management of a Parallel Hybrid Electric Vehicle,” *IEEE/ASME TRANSACTIONS ON MECHATRONICS*, vol. 22, no. 4, pp. 1497–1507, 2017.

CHAPTER 8

CONCLUSION AND FUTURE WORK

Interdisciplinary research has been carried out for the past four years to shape the idea of developing a series of human-machine interactive systems for series-parallel hybrid electric vehicles using computational intelligence. This thesis demonstrates a new methodology for solving emerging engineering problems with the help of cutting-edge technologies of computational intelligence. This chapter draws the conclusions and highlights from the doctoral research, summarises the innovation and impact, and discusses possible future research directions.

8.1. CONCLUSIONS AND HIGHLIGHTS

This research exploits emerging 'mediums', computational intelligence, and the Internet of Things to establish an accessible human-machine interaction system. The impact of drivers on the hybrid system is first exposed and exhaustively studied. Computational intelligence (including fuzzy logic, evolutionary algorithms, and deep learning) and cyber-physical control technologies have been applied to this research. The conclusions of this thesis are drawn as follows, corresponding to the relevant chapters:

a) **Adaptability - the proposed driver-oriented supervisory control system with personalized non-stationary inference significantly enhances the robustness of hybrid electric vehicles.**

According to the work carried out in Chapter 4, a cyber-physical control approach of using personalized non-stationary inference is proposed to enhance energy economy and robustness of the rule-based vehicle control system by real-time monitoring driving behaviour. Specified conclusions drawn from this research are:

- Compared to the CD/CS strategy with stationary inference, up to 9% total energy can be saved over the WLTP-based cycle by using personalized non-stationary inference, especially for very gentle drivers.
- Compared to driven by type-1 fuzzy sets, driving style recognizer driven by type-2 fuzzy sets helps save a further 2.35% of total energy for stochastic changes in driving style.
- When the control signal is completely lost, energy-saving performance of the improve vehicle system is still higher than that of the ECMS (1.11%) and the CD/CS strategy (4.31%).

b) Global optimality - the proposed spectrum-guided fuzzy feature extraction helps accurately identify the human driver from natural operating signals, and provides driver-identified globally optimal control policies, as opposed to mere control actions.

Chapter 5 carries out the research concerning a new concept of the driver-identified supervisory control system, wherein an improved method of spectrum-guided fuzzy feature extraction (SFFE) is developed for improving the recognition accuracy and efficiency of this control system. The findings from this research are as follows:

- With the help of the spectrum-guided fuzzy feature extraction, the recognition accuracy of both forward and bi-directional LSTM networks rises 7% and 6% respectively from other extraction methods (time or frequency domain).
- Compared to forward LSTM networks, bi-directional LSTM networks give an average of 7% higher accuracy in driver identification performance.
- Driven by a human driver whose data was not in the training set, this proposed system shows strong robustness and provides an excellent energy-saving performance, compared to the baseline (11.31%) and FL-based (5.53%) schemes.

c) Synergy - the proposed back-to-back competitive learning mechanism has the capability of synergistic promotion of robustness and efficiency of hybrid electric vehicle systems.

A novel back-to-back competitive learning mechanism (BCLM) for a fuzzy logic (FL) supervisory control system has been researched in Chapter 6. This mechanism breaks through the upper limit of heuristic system decisions and compensates the lower limit of optimization-based system decisions; and then makes the two systems complement each other. Specific conclusions drawn from the investigation are:

- The proposed mechanism has demonstrated abilities to adapt to the change of driving behaviours and to ensure the effectiveness of the FL-based control system by real-time MF parameter updates (957 times) in the case study.
- The improved FL-based control system reduces fuel consumption over the testing real-world cycle, by at least 9% from the CD/CS-based and at least 7% from the conventional FL-based systems.

- Comparing the various sizes of the observation windows from 1 to 50 s, the 2-second observation window appears to be the best for learning from backward horizons, achieving the lowest fuel consumption of $5.88\ \text{litres}/100\ \text{km}$.

d) Predictability - the proposed dual-loop online intelligent programming has an online self-updating predictor that guarantees the effectiveness of the optimal control sequence in the energy-saving efficiency of online predictive energy management.

Chapter 7 investigates an online predictive control strategy for series-parallel plug-in hybrid electric vehicles (PHEVs), resulting in a novel online optimization methodology that is proposed for velocity prediction and energy-flow control. Inspired by fuzzy granulation technology, a deep fuzzy predictor is created to achieve driver-oriented velocity prediction, and a finite-state Markov chain is exploited to self-learn transition probabilities between vehicle speed and acceleration. The findings from this research are as follows:

- The proposed DFP has the ability to differentiate driving behaviours at each driving state in real time. Its prediction result shows excellent accuracy with the lowest maximum error (2.22%), compared with the NNP (14.81%) and the FEP (4.81%).
- During real-world driving, up to 9.37% total energy can be saved compared with the rule-based control strategy. The DP-based control strategy cannot work in this online environment.
- The computational time of the DOIP algorithm is investigated. It is feasible to operate the DOIP algorithm for a 20-s look-ahead horizon, and the computing resources still have a surplus.

8.2. INNOVATION AND IMPACT

Through systematic research of driver-oriented intelligent control methodology for series-parallel HEVs, the substantial outcomes comprise: 1) control-oriented real-time models of a series-parallel hybrid powertrain and its components (Chapter 3); 2) a driver-oriented distributed control framework for series-parallel hybrid electric vehicles (Chapters 4 and 6); 3) a back-to-back competitive learning mechanism to allow competition of two fuzzy-logic-based supervisory controllers in a vehicle system (Chapter 5); 4) a spectral-guided fuzzy feature extraction method to self-adaptively reduce sampling windows (Chapter 6); 5) an online velocity predictor with real-time driving style adaptation (Chapter 7); 6) dual-loop online intelligent programming of the velocity predictor and power-split optimizer (Chapter 7).

Following the main chapter order, the research outcomes of Chapter 4 have been submitted with ***IEEE Transactions on Systems, Man, Cybernetics: Systems*** which is a top journal (IF=7.351, JCR Q1) in the field of human-computer interaction and control and systems engineering. The journal ***IEEE Transactions on Industrial Electronics*** (IF=7.503, JCR Q1) the number one journal in industrial engineering and a journal in the top four in automation and control systems, has published the research of Chapter 5. The journal ***IEEE Transactions on Fuzzy Systems*** has published the research results of Chapter 6, and is a leading journal (IF= 8.759, JCR Q1) in the field of applied mathematics and artificial intelligence. ***Applied Energy***, an eminent journal in the field of industrial and manufacturing engineering (IF= 8.426 JCR Q1), has recorded the research outcomes of Chapter 7.

In terms of application background of each individual control strategy in real cases, the first two of the driver-oriented supervisory control systems are more suitable for relatively fixed driving conditions e.g. bus routes and aircraft pushback routes. Because of offline optimization nature, they could maximize the system efficiency via route preview and global optimization algorithm implementation. The last two of the online energy management systems are more appropriate for relatively stochastic driving conditions e.g. taxi routes and family car routes. Because of online optimization nature, they could evaluate the system effectiveness in real time to acclimate to oncoming driving conditions via route prediction and real-time optimization algorithm implementation.

8.3. FUTURE RESEARCH DIRECTION

This section points out some of the suggested future paths of research.

Chapter 3: Research Methodology and Experimental Facilities

- Many components should be further refined, in particular the electronic components i.e. the induction motor and permanent magnet generator. The engine and battery models should be developed further, to allow the modelling of emissions and battery degradation.
- It would be useful to conduct X-in-the-loop testing involving both humans and hardware, or even implement control strategies in real vehicles.

Chapter 4: Driver-oriented Supervisory Control System with Personalized Non-stationary Inference

- Swarm driving behaviour in different regions should be considered, to expand the scope of personalization that would benefit the energy management of a large-scale intelligent transportation system.
- In the cyber-physical system, how to ensure the real vehicle system maintains high efficiency under condition of signal loss is an interesting topic.

Chapter 5: Driver-oriented Supervisory Control System based on Spectrum-guided Fuzzy Feature Extraction

- This research only involves six participants. To expand the diversity of samples, participants with various attributes, such as gender, age, ethnicity, even education level should be analysed.
- It is obviously impractical to increase the complexity of training networks in exchange for more driver segmentation. Transfer learning is a new favourite in machine learning that could be a good solution to handle driver-domain adaptation.

Chapter 6: Rear-view-based Online Energy Management using Back-to-back Competitive Learning Mechanism

- The function safety to embed the architecture of the back-to-back competitive learning mechanism into a real vehicle controller should be evaluated.

- Fuzzy logic controllers perform a synergistic promotion in robustness and efficiency of vehicles, but it is not clear that they are the best control architecture. Deep learning technologies, including a generative adversarial network, deep Q network, and neuro-evolution could be good candidates to replace them.

Chapter 7: Front-view-based Online Energy Management using Dual-loop Online Intelligent Programming

- Using data from the V2X and the near-field sensors should help to improve the prediction performance trade-off between length and accuracy. The difficulty is how to reduce the dimensionality of these data while maintaining the prediction performance.
- Dual-loop online intelligent programming should be developed for serving platoon energy management, especially for predictive adaptive cruise control.

Although there are already fully autonomous vehicles on the roads for testing purposes, a rollout is far away. Autonomous vehicles are still not able to handle everyday driving and remain reliant on the driver when they reach their system limitations. One suggested approach to resolve this problem is indirect shared control as an emerging shared control method, which is able to realize cooperative driving through input complementation instead of haptic guidance. The big challenge is how to model human drivers' trust in cooperative driving. This means if the driver has confidence in cooperative driving, he/she could focus more on relaxing himself than pursuing the desired path. Besides, driving behaviour modelling is an indispensable task for deploying autonomous driving. How to compromise the trade-off between energy economy, safety, and passenger acceptance during driving behaviour modelling is another big challenge. As a meaningful attempt towards applications of the man-

machine system on HEVs, the proposed driver-oriented intelligent control methodology will continue to provide technical support and inspire more insights for future connected and autonomous vehicles.